

UNIVERSITÄTSKLINIKUM HAMBURG-EPPENDORF

Klinik und Poliklinik für Augenheilkunde, Experimentelle Ophthalmologie,
Universitätsklinikum Hamburg-Eppendorf

Prof. Dr. Martin Spitzer

**Analysis of the retinal phenotype and comparative evaluation
of the efficacy of two enzyme replacement strategies for the
treatment of the retinal dystrophy in a mouse model of CLN10
disease.**

Dissertation

zur Erlangung des Doktorgrades PhD
an der Medizinischen Fakultät der Universität Hamburg.

vorgelegt von:

Junling Liu
aus Guizhou

Hamburg 2021

**Angenommen von der
Medizinischen Fakultät der Universität Hamburg am: 23.06.2021**

**Veröffentlicht mit Genehmigung der
Medizinischen Fakultät der Universität Hamburg.**

Prüfungsausschuss, der/die Vorsitzende: Prof. Dr. Udo Bartsch

Prüfungsausschuss, zweite/r Gutachter/in: Prof. Dr. Christian Hagel

Table of contents

1 Introduction	1
1.1 Neuronal ceroid lipofuscinosis, a neurodegenerative lysosomal storage disorder	1
1.2 Therapeutic approaches to treat neuronal ceroid lipofuscinosis	4
1.2.1 Enzyme replacement therapy	4
1.2.2 Gene therapy- and cell-based enzyme replacement strategies	5
1.2.3 Cell-based neuroprotective approaches	9
1.2.4 Corrective gene therapy	9
1.2.5 Immunomodulatory therapy	10
1.3 Cathepsins	13
1.3.1 Cathepsins family	13
1.3.2 Cathepsin D	13
1.4 CLN10 disease	14
2 Materials and Methods	18
2.1 Animals	18
2.2 Generation of neural stem cell lines	18
2.3 AAV vector production	19
2.4 In vitro differentiation of NSCs and primary retinal cell culture	20
2.5 CTSD uptake experiment	21
2.6 Intravitreal NSCs transplantations and intravitreal AAV injections	21
2.7 Western Blot and enzyme activity assay	21
2.8 Immunocytochemistry and Immunohistochemistry	22
2.9 Statistical analysis	24
3 Results	25
3.1 Expression of CTSD in undifferentiated and differentiated NSCs and cellular uptake of CTSD in vitro.	25
3.2 scAAVshH10 transduces RPE cells and Müller cells	28
3.3 Correction of the biochemical phenotype of Ctsd ko retinas after intravitreal injections of NSCs or AAV vectors.	30
3.4 Attenuation of neuroinflammation in treated Ctsd ko retinas	36

3.5 CTSD supplementation via CTSD-NSCs did not rescue retinal neurons in Ctsd ko mice.	37
3.6 CTSD supplementation via scAAVshH10-CTSD rescued retinal neurons in Ctsd ko mice.	39
4 Discussion	43
4.1 Enzyme replacement strategies	43
4.2 A hallmark of NCL: accumulation of storage material.....	47
4.3 Storage material and neurodegeneration	48
4.4 Lysosomal and autophagic dysfunction	49
4.5 The role of neuroinflammation in disease progression in NCL	51
4.6 The impact of enzyme replacement strategies on neuroinflammation .	52
4.7 Loss of photoreceptors and bipolar cells	53
5 Summary	58
6 Zusammenfassung.....	59
7 List of abbreviations	61
8 References	64
9 Publication 1	80
10 Publication 2	106
11 Declaration of personal contribution to the thesis and publications	113
11.1 Personal contribution in the main project of the thesis:	113
11.2 Personal contribution in Publication 1:.....	113
11.3 Personal contribution in Publication 2:.....	113
12 Acknowledgements.....	115
13 Curriculum vitae	116
14 Eidesstattliche Versicherung	117

1 Introduction

1.1 Neuronal ceroid lipofuscinosis, a neurodegenerative lysosomal storage disorder

The neuronal ceroid lipofuscinoses (NCLs) comprise a group of neurodegenerative lysosomal storage disorders (LSDs) mainly affecting children [1]. Patients suffering from this fatal disorder typically present with progressive decline of cognitive and motor capacities, epilepsy and vision loss, and die prematurely [2]. NCL is a rare neurodegenerative lysosomal storage disorder with an incidence of 1:100,000 worldwide, and 1:12,500 in the US and in Scandinavian countries [3]. The common hallmark of NCLs is the intracellular accumulation of autofluorescent storage material as a result of lysosomal dysfunction, termed ceroid [4].

The first description of NCL disease was published by Otto Christian Stenge in 1826. He described 6-year-old children that represented with a combination of severe symptoms including progressive vision loss, mental decline, epileptic seizure and died prematurely [5]. Thereafter, additional patients were identified which also presented with the characteristic clinical symptoms of NCL, but with a variable age at disease onset. As a result, NCLs were classified according to the age at disease onset in congenital, infantile, late infantile, juvenile, and adult onset NCLs [6]. During the last years, mutations in 13 genes have been identified that cause NCL. These genes encode soluble lysosomal enzymes, lysosomal membrane proteins, membrane proteins of the endoplasmic reticulum and soluble proteins [7]; Table 1). Based on these data, NCLs are now grouped according to the disease-causing gene (CLN1 to CLN8, CLN10 to CLN14), irrespective of the age at disease onset which can be highly variable between patients carrying mutations in the same gene [8].

All NCL patients except those suffering from congenital CLN10 disease have a normal psychomotor development prior to the appearance of the first symptoms. Disease usually starts at childhood, but in rare cases may also develop in patients aged 60 years or older [9]. All NCL patients suffer from a variable combination of characteristic neurological symptoms including

progressive mental deterioration, epilepsy and motor malfunctions, ultimately resulting in premature death [9]. Vision loss as a result of progressive retinal degeneration is another characteristic clinical symptom in most NCLs, including CLN1, CLN2, CLN3, CLN5, CLN6, CLN7, CLN8, CLN10, CLN11 and CLN14 disease [1, 10-15]. The recent identification of CLN3 and CLN7 patients presenting with non-syndromic retinal dystrophies [16, 17] is of particular interest in the context of the present thesis, as this finding highlights the particular susceptibility of the retina to lysosomal dysfunctions, at least in certain NCL variants.

In terms of pathological morphological alterations, cerebral atrophy, cerebellar atrophy, and a secondary enlargement of the ventricles as a result of the severe atrophy of the brain are characteristic features in most NCL patients [14]. Activation of microglia and astrocytes may precede neurodegeneration, and was therefore hypothesized to be a cause of neuron loss [18]. Retinal degeneration might precede neurodegeneration in the brain, or might become detectable only at late stages of the disease, depending on the NCL variant and the type of mutation [12, 19, 20]. Photoreceptor cells are usually the first affected cells, followed by interneurons in the inner nuclear layer, and finally by retinal ganglion cells [15].

A common feature of NCL is the accumulation of autofluorescent storage material as a result of lysosomal dysfunction. Subunit c of mitochondrial ATP synthase (SCMAS) and/or sphingolipid activator protein A and D (saposin A and saposin D) are major components of this material [15]. Storage material accumulates in diverse cell types such as neurons, macrophages, smooth muscle cells and vascular endothelial cells in all NCL forms [7, 9]. At the electron microscopic level, the storage material is classified according to its ultrastructural appearance into granular osmiophilic deposits (GRODs), fingerprint profiles (FPP), curvilinear profiles (CLP), and rectilinear complex (RLC) [21]. The type of ultrastructural aggregates or combinations thereof are to some extent characteristic for the different genetically defined NCL variants [22].

Diagnostically, a NCL disorder must be suspected when some “alert” symptoms, such as progressive and unexplained loss of acquired psychomotor or motor abilities, epilepsy or retinopathy occur in children or young adults [12].

Brain magnetic resonance imaging (MRI) will eventually reveal cerebral and cerebella atrophy, enzyme activity assays are available to identify dysfunctions of lysosomal enzymes, and ultrastructural examinations of skin biopsies or blood samples might reveal accumulation of storage material [9]. However, a final and defined diagnosis ultimately depends on genetic technologies.

A variety of naturally occurring and transgenic animal models of NCL are available, including mice, zebrafish or nematodes, but also larger species such as dogs, sheeps or cattles [23]. Many of these animal models faithfully recapitulate the brain pathology and the retinal dystrophy seen in patients with CLN1, CLN3, CLN4, CLN5, CLN6, CLN7, CLN10, CLN11 disease [11, 24-51]. Despite the availability of appropriate animal models for distinct NCL forms only a few preclinical studies have been published that have developed and evaluated experimental therapies for the treatment of retinal degeneration (see below).

Several therapeutic strategies are currently being developed for the treatment of various NCL variants, including gene therapy, stem cell therapy, enzyme replacement therapy (ERT), small molecule therapy, and immunoregulatory therapies [31, 52-61]. However, until now, only one clinical drug, cerliponase alfa (BrineuraTM, BioMarin Inc.), a recombinant human tripeptidyl peptidase 1 (TPP1) proenzyme, has been approved worldwide in 2017 for the treatment of patients with CLN2 disease [62]. In a phase I/II clinical trials, bi-weekly intracerebroventricular injections of cerliponase alfa have been shown to significantly delay progression of motor and language deterioration in CLN2 children (NCT01907087) [63]. A phase II study including presymptomatic, young patients (NCT02678689), a long-term extension of the phase I/II study (NCT02485899) and an expanded access program (NCT02963350) are in progress.

As detailed above, diverse animal models of NCLs faithfully recapitulate the common traits of the disease in humans, and are widely used to establish treatment options and to evaluate their efficacy in preclinical settings. Selected preclinical studies are described below.

1.2 Therapeutic approaches to treat neuronal ceroid lipofuscinosis

1.2.1 Enzyme replacement therapy

ERT is a promising therapeutic approach for the treatment of NCLs caused by dysfunctions of lysosomal enzymes, the cause of CLN1, CLN2, CLN10 and CLN13 disease [8]. “Classical” ERT aims at delivering functional lysosomal enzymes to diseased tissues by injections of recombinant proteins. The efficacy of ERT is related to the fact that lysosomal enzymes are mannose-6-phosphate- (M6P) modified. After injections of recombinantly produced enzymes into diseased tissues, affected cells take up the enzyme via M6P-receptor mediated endocytosis, eventually resulting in improved lysosomal functions [64]. Different injection routes are used to target different diseased tissues. For example, intraventricular and intrathecal injections are employed to target the brain, intravenous injections to target visceral organs, and intravitreal or subretinal injections to target the retina. Numerous preclinical studies have demonstrated the efficacy of this approach. For instance, intrathecal injection of recombinant human palmitoyl-protein thioesterase (rhPPT1) – the enzyme affected in CLN1 disease - extended the lifespan, delayed motor deterioration, and ameliorated the neuropathological phenotype of a PPT1-deficient mouse model [65]. Furthermore, intravenously injected rhPPT1 resulted in beneficial therapeutic effects in visceral organs such as spleen, liver, kidney and intestine as indicated by a clearance of autofluorescent storage material in these organs [66]. Similarly, injections of recombinant human TPP1 (rhTPP1) into the brain resulted in a reduction of the amount of storage material, delayed the progression of various neurological symptoms, reduced brain atrophy and neuroinflammation, and increased the lifespan of a mouse and a dog model of CLN2 disease [67-69]. Of note, administration of TPP1 into the cerebrospinal fluid (CSF) also delayed pupillary light reflex deficits, but did not attenuate loss of vision in a CLN2 canine model [70].

A CLN2 dog model with a TPP1 loss-of-function mutation shows progressive retinal degeneration and as a consequence loss of vision [71].

Intravitreal injection of rhTPP1 into post-symptomatic animals resulted in detectable amounts of TPP1 in the vitreous humor. However, TPP1 levels in the vitreous and plasma were hardly detected after a prolonged time after the injection. The detection of anti-TPP1 antibodies in the blood plasma of treated dogs demonstrated a systemic immune response to TPP1 after intravitreal injection [72]. However, the treatment effectively reduced storage material in the treated dog retinas [73], which is particularly evident in retinal ganglion cells of untreated animals [71]. Furthermore, intravitreal rhTPP1 injections resulted in attenuation of retinal degeneration, as indicated by a significant rescue of retinal cells in the inner and outer nuclear layer. The irregular arrangement of interfaces between the photoreceptor and the retinal pigment epithelium (RPE), the abnormal termination of axons of bipolar cells in the outer plexiform layer, and the loose organization of pigmented epithelium in the stroma of the ciliary body was ameliorated after intravitreal rhTPP1 injections of rhTPP1. Of note, the treatment also attenuated the decline of rod photoreceptor and cone photoreceptor responses in electroretinogram (ERG) recordings, indicating the efficacy of this therapeutic approach in preserving retinal function in the CLN2 dog model.

Together with numerous other successful preclinical ERT studies, the above outlined examples demonstrate the efficacy of this approach to treat NCL forms caused by dysfunctions of lysosomal enzymes. However, as further detailed in the discussion of this thesis, there is only one study until now that has tested the efficacy of a classical ERT approach to treat retinal degeneration[74]. Due to the limited half-life of recombinantly produced enzymes, repeated injections of the recombinant proteins are required in order to achieve significant and long-lasting therapeutic effects using ERT. A sustained delivery of enzymes through gene therapy- or cell-based strategies may represent a more effective treatment option.

1.2.2 Gene therapy- and cell-based enzyme replacement strategies

Adeno-associated virus (AAV)-based enzyme replacement strategy is a promising strategy to treat different NCLs caused by defects in soluble

lysosomal proteins, as it represents a strategy to continuously deliver lysosomal enzymes to diseased tissues. “Cross correction” makes this AAV-based enzyme replacement strategy an effective treatment option, because the enzyme of interest secreted by the genetically modified endogenous cells is subsequently endocytosed by neighboring non-modified cells via the mannose-6-phosphate pathway, potentially correcting lysosomal dysfunction also in these cells [64]. A robust transgene expression by AAVs in distinct cell populations depends on the virus titer, the serotype, the promoter, and on the injection route of the viral particles.

The efficacy of AAV mediated gene therapy approaches was tested in presymptomatic and symptomatically animal models of NCL. These studies demonstrated attenuation of the progression of the neuropathology and the neural dysfunctions in various NCL animal models. For instance, an AAV-mediated gene transfer of PPT1 via intracranial administration of various AAV serotypes resulted in partial correction of the neuropathology, decrease of storage material accumulation in cortical, hippocampal, and cerebellar neurons, increase of brain mass, improvement of motor function, and extension of lifespan in PPT1-deficient mice [75-77]. In addition, a combination of injections into different tissues has been shown to further improve therapeutic outcomes. Injections of AAV2/9 encoding hPPT1 either intrathecally or intracranially resulted in only limited therapeutic effects in only localized areas of the central nervous system of a CLN1 mouse model. However, combining intrathecal and intracranial injections yielded better benefits, including complete correction of pathological features, synergistic improvements of motor deterioration, and an unprecedented extension of lifespan [78]. For CLN2 disease, intracranial injection of AAV1-hCLN2 prior to the onset of symptoms prevented storage material accumulation, protected neurons from degeneration, and extended the lifespan of treated CLN2 mutant mice by a factor of two when compared to untreated controls [79]. The efficacy of an AAV-mediated enzyme replacement strategy was also confirmed when the treatment was started in post-symptomatic CLN2 dogs. Intraventricular AAV2-hTPP1 administrations resulted in expression of TPP1 in ependymal cells which secreted the enzyme into the cerebrospinal fluid from where it diffused in wide areas of the diseased brain parenchyma. In the treated dogs, disease progression was slowed as

indicated by a delayed appearance of neurological symptoms, a delayed decline of cognitive dysfunctions, and a significantly prolonged life span [80]. Similarly, pre- and post-symptomatic CLN5 sheep that received AAV9-hCLN5 injections showed therapeutic benefits, with more slowly progressing neuropathological alterations and a less pronounced dysfunction of motor and behavioral abilities. Of note, onset of vision loss was significantly delayed in treated CLN5 sheep, likely because of a preservation of visual brain areas rather than because of therapeutic effects on the retina [81]. Of particular interest in the context of the present thesis is a study that has analyzed the effects of an AAV-mediated gene transfer of cathepsin D (CTSD) to the brain and/or visceral organs of a mouse model of CLN10 disease. By expression of CTSD via an AAV1/2 vector in the brain, neurological and visceral pathologies were prevented, including the accumulation of storage material and attenuation of microgliosis in the brain, and the maintenance of the gastro-intestinal system, liver, and spleen integrity. The therapeutic effect on peripheral organs after treatment of the brain was demonstrated to be mediated by CTSD secreted from neurons in the brain and delivered via lymphatic routes to the viscera. Through this lymphatic drainage, CTSD expressed in the central nervous systems (CNS) played an important role on retaining the immune system and the homeostasis of peripheral organs. It was also shown that the rescue of phenotype of *Ctsd*^{-/-} mice was related to the enzymatic activity of CTSD rather than to ligand-receptor interactions [82]. In conclusion, AAV mediated gene therapy has been demonstrated to be well-tolerated, and to be effective in attenuating the neurological phenotype of NCL animal models [75-77, 80, 81, 83].

In addition to the neurodegeneration in the brain, retinal degeneration can also be attenuated by enzyme supplementation through an AAV-mediated enzyme replacement strategy. PPT1-deficient mice are affected by a severe retinal dysfunction starting as early as at postnatal day 45 (P45). The retinal dystrophy is accompanied by reactive microgliosis and astrogliosis, accumulation of storage material, dysregulation of various lysosomal proteins, and autophagic dysfunction. A significant loss of different retinal nerve cell types started at advanced stages of the disease, characterized by degeneration of ganglion cells, photoreceptor cells, and bipolar cells [26, 84]. After intravitreal

administration of AAV2-hPPT1, PPT1 activity in the treated eyes was approximately five times higher than in untreated healthy wild-type eyes. PPT1 immunoreactivity was largely refined to the retinal ganglion cells (RGCs) as a result of the AAV2 serotype used in this study. The light-adapted pure cone responses and dark-adapted mixed rod/cone responses in ERG recordings were significantly improved in treated retinas when compared to control retinas, indicating the benefits of intravitreal AAV2-hPPT1 injections on retinal function in this CLN1 mouse model. At the morphological level, treated retinas had a thicker and better organized outer nuclear layer (ONL) when compared to untreated control retinas. Survival of photoreceptor cells was, however, not significantly improved through the treatment, possibly due to the limited amount of PPT1 released by the ganglion cells or a limited distribution of PPT1 in the host retinas. Interestingly, enzymatic PPT1 activity was also detected in some brain regions near the trajectory of retinal ganglion cell axons, suggesting axonal transport of the enzyme from the retina to the brain. Of note, neurodegeneration was reduced in brain regions at or near the retinal projection [26].

A cell-based enzyme replacement strategy is another possibility to achieve a continuous supply of a lysosomal enzyme to diseased nervous tissue. For instance, transplantations of genetically non-modified human neural stem cells into the brain of a PPT1-deficient mouse resulted in sufficient levels of PPT1 in the host brain to correct the neuropathology, including reduction of autofluorescent storage material, delaying the loss of motor function and attenuating the loss of cortical and hippocampal neurons [85].

In the context of retinal degeneration in NCL, intravitreally transplanted stem cells have been shown to survive well in the vitreous, without exerting adverse effects to the host retina [86]. Stem cells have also been genetically modified to express a gene of interest for the treatment of retinal degeneration in NCL. For instance, bone marrow-derived mesenchymal stem cells (MSCs) that were modified to overexpress TPP1 have been grafted intravitreally into a CLN2 canine model, where they continuously released the enzyme which then diffused into the mutant retina. The transduced cells significantly prevented the development of the characteristic disease-related retinal detachments in this CLN2 animal model, and attenuated the thinning of all retinal layers and the

disorganization of photoreceptor inner and outer segments. Functional deficits were also partially corrected in the retinas treated with TPP1 overexpressing MSCs, as indicated by increased ERG amplitudes compared to the contralateral control retinas. This protective effect of TPP1-MSCs on retinal structure and function in CLN2 canine model was dose-dependent [87].

In summary, AAV-based and stem cell-based enzyme replacement strategies have both been shown to represent effective strategies to treat pathological changes in either the brain or the retina of various NCL animal models.

1.2.3 Cell-based neuroprotective approaches

In some studies, stem cell-based neuroprotective approaches resulted in attenuation of retinal degeneration in certain NCL forms. For instance, intravitreal transplantations of ciliary neurotrophic factor (CNTF)-overexpressing neural stem cells resulted in delivery of CNTF to the dystrophic retinas for at least six weeks, and in preservation of photoreceptors in a mouse model of CLN6 disease [88]. Additionally, after intravitreal administration of neuralized embryonic stem cells into motor neuron degeneration (mnd) mice, an animal model of CLN8 disease, donor cells integrated into the host retina. The treatment reduced the amount of lysosomal storage material and promoted the survival of host photoreceptor cells by a yet unknown mechanism [89].

1.2.4 Corrective gene therapy

Corrective gene therapy attempts to supplement each affected cell with a functional variant of the defective gene, and is thus among the potential treatment options for NCL forms caused by dysfunctions of lysosomal transmembrane proteins. Specific cell populations can be targeted by the use of appropriate AAV serotypes showing a tropism for these cells and/or by the use of AAV vectors containing cell type-specific promoters. Bosch and colleagues generated two self-complementary AAV vectors (serotype 9; scAAV9) encoding CLN3 driven by either the methyl-CpG-binding protein 2

(MeCP2) promoter or the ubiquitously active chicken β -actin (CAG)/cytomegalovirus (CMV) enhancer promoter to assess the effect of different CLN3 dosages in Cln3ex7/8 mice. After intravenous injection, CLN3 expression levels in the brain were significantly higher in mutant mice injected with the vector containing the CAG promoter than with the vector containing the MeCP2 promoter. However, the correction of motor deficits and the attenuation of neuroinflammation and lysosomal pathology were more pronounced in scAAV9/MeCP2-hCLN3 treated mice. This might result from differences between the cell types successfully transduced using these two AAV vectors, as scAAV9/MeCP2-hCLN3 mainly transduced neurons whereas scAAV9/CAG-hCLN3 mainly transduced astrocytes [90].

In the Cln6^{nclif} mice model, retinopathy is characterized by early-onset reactive gliosis and apoptotic degeneration of photoreceptors, accompanied by accumulation of storage material, dysregulation of lysosomal proteins, and activation of microglia [42]. Unexpectedly, AAV2/8-mediated expression of CLN6 in photoreceptors neither promoted photoreceptor survival nor preserved photoreceptor function in Cln6^{nclif} mice. CLN6 is strongly expressed in bipolar cells which degenerate only after photoreceptor cells in Cln6^{nclif} mice. Targeting bipolar cells with an AAV2/2 variant 7m8 and a promoter that is active in a subpopulation of bipolar cells resulted in robust CLN6 expression in these interneurons. Of note, CLN6 expression in bipolar cells preserved the morphology and function of photoreceptors, indicating that defects in bipolar cells are the cause of the photoreceptor cell loss observed in the CLN6 mouse model [91].

1.2.5 Immunomodulatory therapy

Early onset neuroinflammation as indicated by activated microgliosis and astrogliosis is a characteristic pathological feature of NCL. Efforts have been made to identify reagents that modulate or suppress neuroinflammation [92, 93], but treatment effects were mostly limited. However, some immune suppression therapies achieved promising benefits in attenuating neuron loss

and microgliosis, and in improving motor functions in CLN1 or CLN3 animal models [94, 95].

The therapeutic potential of immunomodulatory approaches has also been tested for the treatment of retinal dystrophies. By using the immunomodulatory compounds fingolimod and teriflunomide, retinal ganglion cell loss and retinal thinning were significantly attenuated in a CLN1 mouse model [95]. Furthermore, dietary supplementation of either docosahexaenoic acid or curcumin reduced reactive microgliosis and partially protected retinal function in the *Cln6^{ncif}* mouse model [42].

Table 1. Human neuronal ceroid lipofuscinoses

Mutated genes	Name of disease	Protein and location	Age of onset
palmitoyl protein thioesterase 1 (PPT1)	CLN1 disease	soluble lysosomal enzyme	infantile, late infantile, juvenile, adult
tripeptidylpeptidase 1(TPP1)	CLN2 disease	soluble lysosomal enzyme	infantile, late infantile, juvenile
CLN3	CLN3 disease	lysosomal membrane protein	juvenile, adult
DNAJC5	CLN4 disease	synaptic vesicle	adult
CLN5	CLN5 disease	soluble lysosomal enzyme	late infantile, juvenile, adult
CLN6	CLN6 disease	membrane protein endoplasmic reticulum	late infantile, juvenile, adult
MFSD8	CLN7 disease	lysosomal membrane protein	late infantile, juvenile, adult
CLN8	CLN8 disease	membrane protein endoplasmic reticulum	late infantile
unknown	CLN9 disease	unknown	juvenile
cathepsin D (CTSD)	CLN10 disease	soluble lysosomal enzyme	congenital, infantile, late infantile, juvenile
progranulin (GRN)	CLN11 disease	soluble lysosome enzyme	adult
ATPase Type 13A2 (ATP13A2)	CLN12 disease	lysosomal membrane protein	juvenile
cathepsin F (CTSF)	CLN13 disease	soluble lysosomal enzyme	adult
potassium channel tetramerization domain-containing protein 7 (KCTD7)	CLN14 disease	soluble intracytoplasmic protein	infantile

1.3 Cathepsins

1.3.1 Cathepsins family

The cathepsin family of proteolytic enzymes consists of cathepsin A-H, cathepsin K-L, cathepsin O, cathepsin S, cathepsin V-W, and cathepsin Z [96]. According to their proteolytic functions, cathepsins are classified into cysteine proteases, serine proteases, and aspartyl proteases [97]. Although cathepsins are generally expressed in various cell types throughout the body, certain cathepsins are expressed in a cell-specific manner [96]. The enzymes are vital for a wide range of normal physiological functions such as autophagy, apoptosis, vesicular trafficking, proliferation, and for the processing and activation of various proteins and hormones, [98-100]. Any dysregulated expression or dysfunction of a member of the cathepsin family may result in various diseases, including neurodegeneration, macular degeneration, cardiovascular diseases, cancer and metastasis, inflammation, or obesity [101].

1.3.2 Cathepsin D

Cathepsin D (CTSD) is the major lysosomal aspartic protease [98, 102]. It is initially synthesized as an inactive pre-pro-cathepsin D in the rough endoplasmic reticulum (RER), then transported to the Golgi complex (GC), and subsequently targeted to endosomes via the mannose-6-phosphate receptor pathway or an alternative pathway. In the endosomes, pro-cathepsin D undergoes the first maturation step through proteolytic removal of the N-terminal propeptide, leading to the intermediate form. Upon reaching the lysosomes, the mature CTSD is formed, consisting of a heavy chain and a light chain that are interlinked by disulfide bridges [103, 104]. The CTSD protein is ubiquitously expressed in most mammalian tissues and organs. In the retina, it is most abundant in the RPE, iris epithelium, ciliary body, retinal ganglion cells, and Müller cells [102, 105, 106]. CTSD performs multiple physiological functions, including general protein degradation and turnover [107], activation and degradation of polypeptide hormones and growth factors [108-112], activation of enzyme precursors [113-116], antigen processing [117-119],

degradation of cytoskeletal proteins [120-122], monocyte-mediated fibrinolysis [123, 124], regulation of apoptosis [125], and processing of enzyme activators and inhibitors [126]. In addition, CTSD enzymatic activity is essential for maintenance of the homeostasis in postnatal tissues, including tissue renewal, tissue remodeling and regulation of aging and programmed cell death. In the retina, CTSD in the RPE plays an important role in the degradation of the shed photoreceptor outer segments and of rhodopsin [127-129].

1.4 CLN10 disease

CLN10 disease, also known as congenital NCL, is the most severe NCL form. Since the 1940s, only a few patients with congenital NCL have been reported. The classification as congenital NCL was based on the clinical presentation, and not on a genetic diagnosis. In 2006, a mutation in the gene encoding CTSD was detected in a NCL patient and linked to CLN10 disease [130]. Depending on the mutation, CLN10 patients with infantile, late infantile, juvenile and adult disease onset have been identified, demonstrating the broad clinical spectrum of this NCL form. CTSD enzymatic activity is either completely or severely abolished in patients with congenital CLN10, or partially reduced in patients with a later-onset type of CLN10. Newborns with congenital CLN10 present with microcephaly, respiratory failure, rigidity, seizures, and early death, whereas patients with late-onset CLN10 disease present with cognitive dysfunction, ataxia, motor deterioration and vision loss [130, 131].

To date, fifteen different pathogenic mutations have been identified in the CTSD gene, including missense mutations, nonsense mutations, deletions, insertion and splicing defects [130-135].

Disease onset of congenital CLN10 is in utero. Around the third trimester, some affected fetuses showed abnormal fetal movements. Pathological changes were found through ultrasound examination and included ventriculomegaly with a dilated third ventricle, corpus callosum agenesis, abnormally developed gyri of the brain, choroid plexus cysts and arachnoidal cysts [133, 136]. After birth, all reported congenital CLN10 cases shared similar clinical features such as spasticity, intractable seizures, and respiratory

insufficiency [132, 133, 136]. Other morphological abnormalities of patients include microcephaly, receding forehead, overriding sutures and obliterated fontanelles [132, 133]. Abnormal facial morphologies like external ear malformations (low-set ear and/or rudimentary external ear) and a broad nasal bridge, were observed in some neonates [133]. The lifespan of congenital CLN10 patients is limited to several days, or in rare cases to a few weeks.

One patient with infantile onset of CLN10 showed an early and dramatically decreasing rate of head growth with brain atrophy and microcephaly [130]. Patients with juvenile CLN10 disease presented with milder symptoms, starting at school age, or even later at an age up to 15 years. Patients showed motor deterioration and ataxia, visual disturbances leading to blindness, progressively developing cognitive decline, and eventually hypertrophic cardiomyopathy [130, 131]. Some of these juvenile CLN10 patients had a life expectancy of more than 30 years.

Similar to other subtypes of NCL, final diagnosis of CLN10 requires the identification of a pathogenic mutation in the *CLN10* gene [5]. However, during the gestation period, cardiotopography (CTG) and ultrasound examination can identify intrauterine growth retardation and abnormal brain morphology. Neonates who meet the following conditions should be suspected as congenital CLN10: consanguineous parents, congenital microcephaly, external ear malformation, respiratory failure, seizures and hypertonia. Patients with a later onset of microcephaly, ataxia, vision loss, and progressively developing neurological abnormalities should undergo brain MRI and electroencephalogram (EEG) recordings. Pathologic examination of skin or muscle biopsies may demonstrate deposits of storage material (e.g. GRODs and lamellar structures) or hypertrophic cardiomyopathy as further indications of a NCL disease [131, 135]. Of note, CTSD enzyme activity assays are critical for the diagnosis of CLN10 disease, and estimation of the residual CTSD activity is important for the prognosis of disease severity. For patients with visual impairment, fundus examinations are necessary for the diagnosis of a retinopathy.

Various naturally occurring or transgenic animal models of CLN10 are available such as sheeps, dogs and mice. Based on the specific mutation, the

amount of residual enzymatic CTSD activity varies, resulting in a phenotypic diversity between the different animal models. A CTSD-deficient mouse was generated by interrupting the open reading frame of the *Ctsd* gene in exon 4, resulting in the complete absence of the CTSD enzyme in C57BL/6J mice [137]. In the first two weeks after birth, *Ctsd* ko mice develop normally. However, this period is followed by a rapid loss of body weight, progressive intestinal atrophy, and profound lymphoid cells destruction in thymus and spleen. *Ctsd* ko mice manifest progressive neurological symptoms, including repetitive seizures, tremor, and reductions of escape reactions at the end stage of the disease [48, 137]. In the last a few days, *Ctsd* ko mice have closed eyelids, and fail to react to light [48]. Death occurs around postnatal day 26 ± 1 [48, 137]. Similar to animal models of other NCL forms, pathological characteristics of *Ctsd* *-/-* mice include accumulation of autofluorescent storage material displaying the ultrastructure of GRODs and fingerprint profiles in neurons, brain atrophy, widespread neuron loss and activation of microglia and astrocytes [48, 138, 139].

Table 2. Experimental therapeutic approaches for the treatment of retinal dystrophies in NCL diseases

Diseases	Protein	Animal model	Therapeutic approaches	Treatment effect	Reference
CLN1	PPT1	Mouse (knock-out)	Intravitreal injections of AAV-PPT1	Improved retinal function (ERG)	Griffey et al. (2005)
CLN1/CLN3	PPT1/CLN3	Mouse (knock-out)/ Mouse (knock-out)	drinking water supplemented with fingolimod and teriflunomide	Attenuated retinal thinning, prevented the loss of retinal ganglion cells	Groh et al. (2017)
CLN2	TPP1	Dog (spontaneous mutation)	Intravitreal injections of recombinant TPP1	Delayed retinal degeneration, improved retinal function (ERG)	Whiting et al. (2020)
CLN2	TPP1	Dog (spontaneous mutation)	Intravitreal injections of autologous MSCs with overexpression of TPP1	Delayed retinal degeneration, improved retinal function (ERG)	Tracy et al. (2016)
CLN6	CLN6	Mouse (spontaneous mutation)	Dietary supplementation with the immune-regulatory compounds curcumin and docosahexaenoic acid	Ameliorated microgliosis and reduced retinal degeneration	Mirza et al. (2013)
CLN6	CLN6	Mouse (spontaneous mutation)	intravitreal transplantation of NSCs overexpressing CNTF	delayed degeneration of photoreceptor cells	Jankowiak et al. (2015)
CLN6	CLN6	Mouse (spontaneous mutation)	Intravitreal injections of AAV-CLN6	Improved retinal function (ERG), delayed degeneration of photoreceptor cells	kleine Holthaus et al. (2018)
CLN8	CLN8	Mouse (spontaneous mutation)	Intravitreal transplantation of neuralized embryonic stem cells	Reduced accumulation of storage material, improved survival of retinal neurons	Meyer et al. (2006)
CLN10	CTSD	Mouse (knock-out)	Intravitreal injections of recombinant CTSD	Partial correction of lysosomal protein dysregulation, attenuation of reactive microgliosis	Marques et al. (2019)

Abbreviations: AAV: Adeno-associated virus; CLN6: ceroid lipofuscinoses neuronal protein 6; CNTF: ciliary neurotrophic factor; CTSD: Cathepsin D; ERG: electroretinogram; MSCs: mesenchymal stem cells; NSCs: neural stem cells; PPT1: palmitoyl protein thioesterase 1; TPP1: tripeptidyl peptidase 1.

2 Materials and Methods

2.1 Animals

Cathepsin D knockout (*Ctsd* ko) mice[137] were derived from heterozygous breeding pairs maintained on a C57BL/6J genetic background. Genotypes of animals were determined by polymerase chain reaction (PCR) using forward primer 5'-GTC ACC TGC AGC TTT GGT A -3' and reverse primer 5'-TCA GCT GTA GTT GCT CAC ATG-3'. Wild-type (wt) littermates were used as a control. All animals were housed under standard conditions with ad libitum access to food and water. All animal experiments were approved by the local ethic committee (077/2019) and were carried out in accordance with the EU directive guidelines for animal experiments.

2.2 Generation of neural stem cell lines

To generate CTSD overexpressing neural stem cells (CTSD-NSCs), the mouse full-length CTSD cDNA was cloned into a polycistronic lentiviral vector composed of a cytomegalovirus enhancer/chicken β -actin (CAG) promoter, the internal ribosome entry site (IRES) of the encephalomyocarditis virus, a tdTomato reporter gene and a blasticidin (BSD) resistance gene, giving rise to pCAG-CTSD-IRES-tdTomato-BSD. The same vector but lacking the CTSD cDNA (pCAG-IRES-tdTomato-BSD) was used to generate a wild-type neural stem cell (NS cell) line as a control for *in vitro* experiments (wt-NSCs). As a control for *in vivo* experiments, a clonal *Ctsd* ko NS cell line was established using a vector composed of the elongation factor1 α (EF1 α) promoter, an IRES sequence, a venus reporter gene and a puromycin resistance gene separated by a the P2A sequence of porcine teschovirus-1 (2A) (ko-NSCs). Lentiviral particles were prepared by transient transfection of human embryonic kidney (HEK) 293T cells as described (<http://www.LentiGo-Vectors.de>). Clonal NS cell lines were established and cultivated as described (Jung et al., 2013, Flachsbarth et al., 2014). Successfully transduced cells were expanded in the presence of either 4ug/ml blasticidin (Life Techonologies, Darmstadt, Germany)

or 0.6 µg/ml puromycin (Life Technologies), and single cells with high levels of reporter gene expression were sorted into 96 well plates by fluorescence activated cell sorting (FACS; FACS Arianllu, BD Bioscience, San Diego, CA), followed by clonal expansion.

2.3 AAV vector production

Productions of viral particles were performed in the Vector Facility at the University Medical Center Eppendorf, Hamburg, Germany as follows:

Production and titration of AAV particles. AAVshH10 pseudotyped vectors [140] were generated by co-transfection of HEK293-AAV cells (Cell Biolabs, San Diego, CA) with the AAV transfer plasmid scAAV-CMV-CTSD and the AAV packaging plasmid shH10 (shH10 was a gift from John Flannery & David Schaffer, Addgene plasmid # 64867) and pHelper (Cell Biolabs). HEK293-AAV cells (Cell Biolabs) were cultivated in Dulbecco's modified Eagle's medium (DMEM, High Glucose, Glutamax) supplemented with 10% (v/v) heat-inactivated fetal calf serum, 0.1 mM MEM Non-Essential Amino Acids (NEAA), 100 U/ml penicillin and 100 µg/ml streptomycin. Tissue culture reagents were obtained from Life Technologies. Briefly, 10^7 HEK293-AAV cells were seeded one day before transfection on 15-cm culture dishes and transfected with 7.5 µg packaging plasmid shh10, 10 µg pHelper (Cell Biolabs) and 6.4 µg pAAV plasmid scAAV-CMV-CTSD or 7.1 µg scAAV-CMV-CTSD-E2A-GFP per plate complexed with Polyethylenimine "Max" (PEI MAX, Polysciences, Warrington, PA, USA) at a PEI:DNA ratio (w/w) of 3:1 [141]. After 72 h cells were harvested and resuspended in 5 ml lysis buffer (50 mM Tris base, 150 mM NaCl, 5 mM MgCl₂, pH 8.5). After three freeze-thaw cycles, benzonase (Merk; final concentration 50 U/ml) was added and the lysates were incubated for 1 h at 37 °C. Cell debris was pelleted and vector containing lysates were purified using iodixanol step gradients. Finally, iodixanol was removed by ultrafiltration using Amicon Ultra Cartridges (10 mwco) and three washes with DPBS.

The genomic titers of DNase-resistant recombinant AAV particles were determined after alkaline treatment of virus particles and subsequent

neutralization by qPCR using the qPCRBIO SY Green Mix Hi-Rox (Nippon Genetics Europe GmbH, Düren, Germany) and an ABI PRISM 7900HT cycler (Applied Biosystems, Waltham, USA). Vectors were quantified using primers specific for the CMV promoter sequence (5'-GGGACTTTCCTACTTGGCA and 5'-ctaccgcccatttgcgctc). Real-time PCR was performed in a total volume of 10 µl with 0.3 µM for each primer. The corresponding scAAV transfer plasmid was used as a copy number standard. A standard curve for quantification was generated by serial dilutions of the respective plasmid DNA. The cycling conditions were as follows: 50 °C for 2 min, 95 °C for 10 min, followed by 35 cycles of 95 °C for 15 sec and 60 °C for 60 sec. Calculations were done using the SDS 2.4 software (Applied Biosystems).

2.4 *In vitro* differentiation of NSCs and primary retinal cell culture

Differentiation of CTSD-NSCs, wt-NSCs and ko-NSCs into astrocytes and neurons were performed as described previously [88]. For primary retinal cell cultures, eyes from P2 *Ctsd* ko mice were enucleated and immediately immersed in 80% ethanol for 10 seconds. Retinas were isolated, dissociated with accutase (Life Technologies) for 5-10 minutes at 37°C, and centrifuged at 1400rpm for 7 minutes. Cell pellets were suspended in DMEM/F12 (Life Technologies) containing 2 mM glutamine, 0.3% glucose, 5 mM hydroxyethyl piperazineethanesulfonic acid (HEPES), 3 mM sodium bicarbonate (all from Sigma-Aldrich, St. Louis, MO), 1% fetal calf serum (Life Technologies) and 2% B27 (Life Technologies; astrocyte differentiation (AD) medium). Cell suspensions were filtered through a 40 µm FALCON Cell Strainer (Life Sciences) and cultivated at a density of 220,000 cells/cm² on matrigel-coated coverslips in AD medium for 9 days.

2.5 CTSD uptake experiment

For CTSD uptake experiments, CTSD-NSCs and ko-NSCs were differentiated into astrocytes (CTSD-astrocytes, ko-astrocytes, respectively), and supernatants were collected every two days, filtered using 0.45µm filters (Sarstedt, Nümbrecht, Germany) and stored at -80°C. Ko-astrocytes derived from ko-NSCs and primary retinal cells from *Ctsd* ko mice were seeded onto coverslip and cultured in conditioned media from either CTSD-astrocytes or ko-astrocytes for 7 days. Conditioned media were changed every second day.

2.6 Intravitreal NSCs transplantations and intravitreal AAV injections

NSCs and AAV particles were intravitreally injected into 7 and 5 days old mice, respectively as described (Jung et al., Flachsbarth et al., Jankowiak et al). About 3.8×10^5 CTSD-NSCs in 1µl PBS or 1µl of scAAVshH10-CMV-CTSD (scAAVshH10-CTSD) was injected into the right eyes. The contralateral eyes served as a control and received injections of 3.8×10^5 ko-NSCs or scAAVshH10-CMV-GFP (scAAVshH10-GFP). Intravitreal injections of AAV particles were performed in the same manner as intravitreal transplantations of NS cells [88]. Animals were sacrificed at postnatal day 22.

2.7 Western Blot and enzyme activity assay

Cell pellets or retinas were homogenized in lysis buffer containing 50mM Tris-HCl, pH 7.5, 150mM NaCl, 0.5% Triton-X100 and protease inhibitors, and incubated on ice for 15 min. After centrifugation for 10 min at x20,000 g, supernatants were collected. For detecting SQSTM1/p62 and saposinD, retinas were sonified in radioimmunoprecipitation assay buffer (RIPA buffer) containing 50 mM Tris-HCl, pH 7.4, 150mM NaCl, 1% Triton-X100, 0.5% Sodium deoxycholate (Sigma-Aldrich Corp., St. Louis, MO, USA), 0.1% sodium dodecyl sulfate (SDS, Merck, Darmstadt, Germany), 1mM ethylenediaminetetraacetic acid (EDTA, Roth, Karlsruhe, Germany), 10mM

sodium fluoride (Naf, Merck), 1mM phenylmethylsulfonyl fluoride (PMSF, Roth) and protease inhibitors, centrifuged at 13,000g for 15 minutes at 4 °C and supernatants were collected. Protein concentrations were determined using the bicinchoninic acid assay (Roth). Samples were separated by SDS-PAGE, transferred onto nitrocellulose membranes and processed for immunoblotting as described [84]. Glyceraldehyde 3-phosphate dehydrogenase (GAPDH) was used as a loading control. Blots were visualized using the Odyssey® Fc Imaging System (LI-COR Biosciences, Lincoln, USA) and quantified using the Empiria Studio® Software 1.2.0.79 (LI-COR Biosciences). Chameleon Duo Pre-stained Protein Ladder (LI-COR Biosciences) was used to determine molecular masses. Each experiment was performed at least in triplicate.

For the determination of CTSD enzyme activity, pellets from the different cell cultures and untreated and experimentally treated retinas were lysed for 1 h in PBS containing 0.2% Triton X-100 on a shaker. Lysates were clarified by centrifugation, and protein concentrations were determined with the BCA Protein Assay (Thermo Fischer Scientific, Waltham, USA). 2.5 µg of cell lysates or 5 µg of retina lysates were incubated at 37°C in activity buffer (50 mM sodium acetate, pH 5.5, 0.1 M NaCl, 1 mM EDTA, and 0.2% Triton X-100) containing 10 µM of CTSD and E substrate (Enzo Life Sciences, P-145, Lörrach, Germany) and 25 µM leupeptin. The AMC released as a result of proteolytic activity was quantified with a Synergy™ HT Multi-Detection microplate reader (excitation: 360 nm; emission: 440 nm, band pass 40). 2 µl of purified enzymatically active CTSD was used as a positive control. 2µl enzymatically active CTSD in the presence of 1.4 µM Pepstatin A was used as a negative control.

2.8 Immunocytochemistry and Immunohistochemistry

For immunocytochemical analyses, cell cultures were fixed in PBS (pH 7.4) containing 4% paraformaldehyde (PA) for 10-15 min., blocked for 1 hour in PBS (pH 7.4) containing 0.1% bovine serum albumin (BSA) and 0.3% Triton X-100 (both from Sigma-Aldrich Corp.), and incubated with primary antibodies (Table 3) overnight, followed by incubation with Cy2-, Cy3- or Cy5-conjugated secondary antibodies (1:200; all from Jackson Immunoresearch Laboratories,

West Grove, PA, USA) for 4 hrs. Cell nuclei were stained with 4',6-diamidino-2-phenylindole (DAPI; Sigma-Aldrich).

Immunohistochemical analyses of retinal sections were performed as previously described [74]. At least six animals were analyzed for each antigen and experimental group. To allow for direct comparison of staining intensities, sections from treated and contralateral control eyes were processed in parallel in each experiment.

Images from immunostained cell cultures and retinal sections were taken with an AxioObserverZ.1 microscope equipped with an ApoTome.2 (Zeiss, Oberkochen, Germany) and ZEN2.3 software. Arrestin-, m+s opsin-, protein kinase C-alpha (PKC α)- and secretagogoin (SCGN)-positive cells were counted in 3 equidistant areas each with a width of 250 μ m in both the nasal and the temporal half of central retinal sections. The number of cluster of differentiation 68 (CD68)-positive cells was determined in 0.24 μ m thick optical sections of entire central retina sections. PKC α -, SCGN- and CD68-positive cells were counted in optical sections with a thickness of 0.24 μ m, while m + s opsin- or arrestin-positive cone photoreceptor cells were counted in z-stacks through the entire retina thickness.

Table 3. Primary antibodies.

Antigen	Dilution	Company/Reference	Catalog Number
arrestin	1:2000 (ICC) 1:5000 (IHC)	Millipore, Temecula, CA, USA	AB15282
β -tubulin III	1:1000 (ICC)	Sigma Aldrich, Deisenhofen, Germany	T2200
cathepsin D (CTSD)	1:2000 (ICC) 1:2000 (IHC) 1:500 (WB)	Santa Cruz Biotechnology, Inc.	Sc-6486
cathepsin D (CTSD)	1:4000 (IHC)	kind gift of Thomas Braulke, University Medical Center Hamburg-Eppendorf	n.a.
cathepsin X/ZP (CTSZ)	1:100 (IHC)	R&D Systems GmbH	AF1033
cluster of differentiation 68 (CD68)	1:1000 (IHC)	Bio Rad Laboratories, Kidlington, UK	MCA1957
glyceraldehyde 3-phosphate dehydrogenase (GAPDH);	1:20,000 (WB)	Sigma Aldrich, Deisenhofen, Germany	G3893
glial fibrillary acidic protein (GFAP)	1:500 (ICC) 1:500 (IHC)	Dako Cytomation GmbH, Hamburg, Germany	Z0334
green fluorescent protein (GFP)	1:10,000 (IHC)	Abcam, Cambridge, UK	Ab290

green fluorescent protein (GFP)	1:100 (IHC)	R&D Systems GmbH	AF4240
glutamine-synthetase (GS)	1:100 (IHC)	BD Biosciences, Heidelberg, Germany	610517
ionized calcium-binding adapter molecule 1 (IBA1)	1:500 (IHC)	Wako Chemicals GmbH, Neuss, Germany	019-19741
lysosomal-associated membrane protein 1 (LAMP1)	1:2000 (ICC) 1:2000 (IHC) 1:500 (WB)	Santa Cruz Biotechnology, Inc.	Sc-19992
lysosomal-associated membrane protein 2 (LAMP2)	1:200 (ICC) 1:200 (IHC) 1:500 (WB)	Developmental Studies Hybridoma Bank, Iowa City, IA, USA	Clone ABL93
Microtubule-associated protein 2 (MAP2)	1:200 (ICC)	Sigma Aldrich, Deisenhofen, Germany	M4403
m opsin	1:500 (IHC)	Millipore, Temecula, CA, USA	AB5405
protein kinase C alpha (PKC α)	1:500 (ICC) 1:500 (IHC)	Santa Cruz Biotechnology, Inc.	Sc-208
rhodopsin	1:1000 (ICC)	Sigma Aldrich, Deisenhofen, Germany	O4886
s opsin	1:200 (IHC)	Santa Cruz Biotechnology, Inc.	Sc-14363
saposin D	1:4000 (IHC)	Konrad Sandhoff, Bonn, Germany	n.a.
saposin D	1:500 (WB)	Synaptic Systems, Goettingen, Germany	2018-SA9052_06
secretagogin (SCGN)	1:1000 (ICC) 1:2000 (IHC)	BioVendor Research and Diagnostic Products	RD184120100
sequestosome 1/p62 (SQSTM1/p62)	1:1000 (IHC) 1:1000 (WB)	Enzo Life Sciences GmbH, Lörrach, Germany	BML-PW9860
subunit c of mitochondrial ATP synthase (SCMAS)	1:1000 (IHC)	Abcam, Cambridge, UK	Ab181243
Abbreviations: ICC: Immunocytochemistry, IHC: immunohistochemistry, WB: Western blot.			

2.9 Statistical analysis

Statistical analyses of retinal cell numbers were performed with the paired Student's t-test. Statistical analyses of immunoblots and CTSD activity assays were performed with the one-way ANOVA followed by the Newman-Keuls test using Prism 5.02 software (GraphPad Software, San Diego, CA, USA).

3 Results

3.1 Expression of CTSD in undifferentiated and differentiated NSCs and cellular uptake of CTSD *in vitro*.

To analyze the transgene expression in undifferentiated NSCs and NSC-derived neural cell types *in vitro*, immunocytochemical analyses were performed on *Ctsd* ko neural stem cells (ko-NSCs), wild-type NSCs (wt-NSCs), cathepsin D overexpressing NSCs (CTSD-NSCs), and astrocytes and neurons derived from these stem cells. Ko-NSCs (Figure 1Aa) and GFAP-positive astrocytes (Figure 1Ad) and MAP2-positive neurons (Figure 1Ag) derived from ko-NSCs (ko-astrocytes and ko-neurons, respectively) expressed the reporter

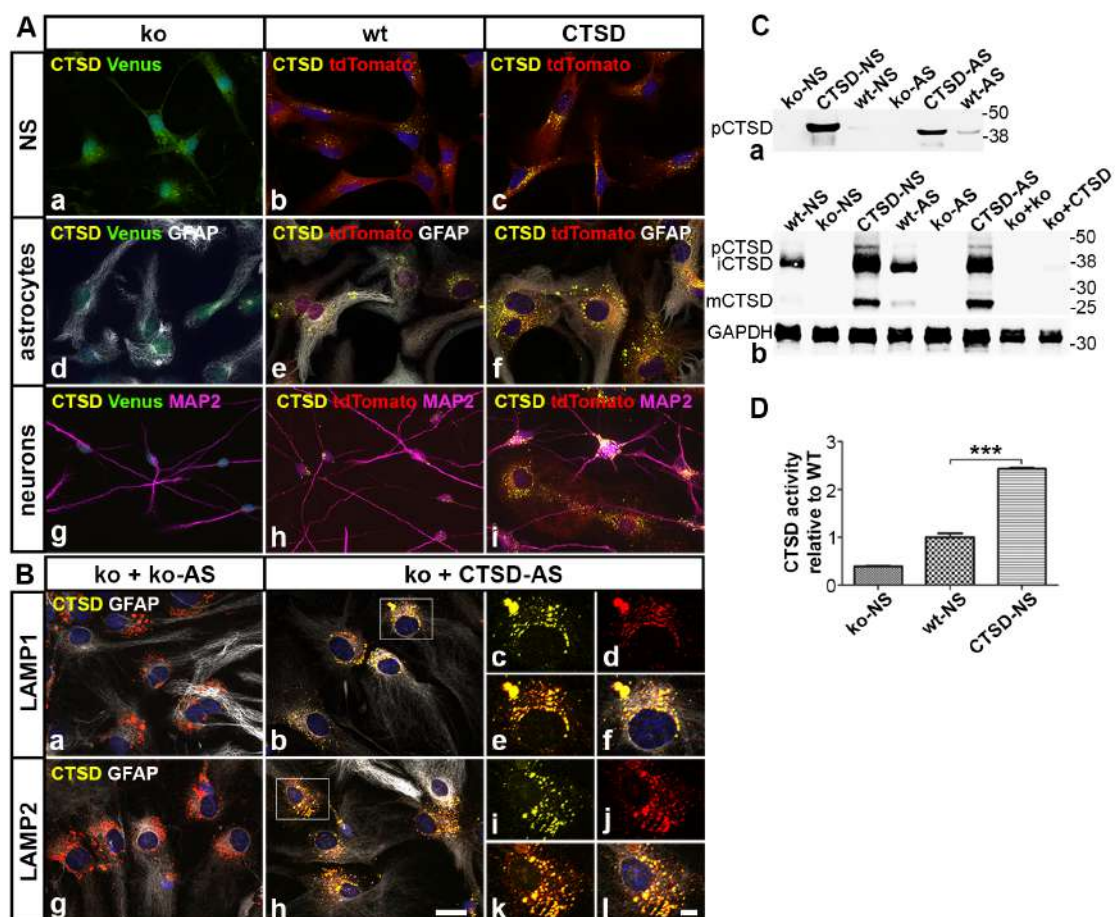


Figure 1. Expression and enzymatic activity of CTSD in undifferentiated and differentiated neural stem cell (NSC) cultures and uptake of CTSD by NSC-derived astrocytes. (A) CTSD immunocytochemical staining of undifferentiated NSC (a-c), NSC-derived GFAP-positive astrocytes (d-f) and NSC-derived MAP2-positive

neurons (g-i). **(B)** Localization of CTSD and LAMP1 (a-f) or CTSD and LAMP2 (g-l) in astrocytes derived from *Ctsd* ko-NSCs and cultured in the presence of conditioned medium from *Ctsd* ko (a, g) or CTSD overexpressing (b, h) astrocytes. The boxed areas in (b) and (h) are shown at higher magnification in (c-f) and (i-l), respectively. **(C)** CTSD immunoblot of supernatants from different NSC cultures and NSC-derived astrocytes (a) or cell pellets from different NSC cultures and NSC-derived astrocytes (b). **(D)** CTSD activity assay of *Ctsd* ko, *Ctsd* wt and CTSD overexpressing NSCs. Each bar represents the mean value (\pm SEM) of 4 independent cultures. ***, $p < 0.001$, one-way ANOVA. AS, astrocytes; CTSD, cathepsin D; NS, neural stem cells; GAPDH, glyceraldehyde-3-phosphate dehydrogenase; GFAP, glial fibrillary acidic protein; iCTSD, intermediate-CTSD; ko, knockout; ko + ko, *Ctsd* ko neural stem cell-derived astrocytes maintained in the presence of conditioned medium from *Ctsd* ko astrocytes; ko + CTSD, *Ctsd* ko neural stem cell-derived astrocytes maintained in the presence of conditioned medium from CTSD overexpressing astrocytes. LAMP1, lysosomal-associated membrane protein 1; LAMP2, lysosomal-associated membrane protein 2; MAP2, microtubule-associated protein 2; mCTSD, mature-CTSD; wt, wild-type; pCTSD, pro-CTSD. Scale bar in (h): 20 μm ; in (l): 5 μm .

gene Venus, but no detectable levels of CTSD. Wt-NSCs (Figure 1Ab), wt-astrocytes (Figure 1Ae) and wt-neurons (Figure 1Ah) expressed the reporter protein tdTomato and were CTSD-positive. tdTomato-positive CTSD-NSCs (Figure 1Ac) and astrocytes (Figure 1Af) and neurons (Figure 1Ai) derived from these stem cells (CTSD-astrocytes and CTSD-neurons, respectively) expressed significantly higher levels of CTSD when compared to corresponding wt cell types.

To analyze the cellular uptake of CTSD *in vitro*, ko-NSCs were differentiated into astrocytes and cultured for 7 days in conditioned medium from ko-astrocytes or CTSD-astrocytes. Immunocytochemical analysis revealed that ko-astrocytes cultured in conditioned medium from ko-astrocytes showed elevated LAMP1 (Figure 1Ba) and LAMP2 (Figure 1Bg) signals, both in number and in size, when compared to ko-astrocytes cultured in conditioned medium from CTSD-astrocytes (Figure 1Bb, Bh). Co-localization of CTSD and LAMP1 (Figure 1Bc-f) or CTSD and LAMP2 (Figure 1Bi-l) in ko-astrocytes cultured in conditioned medium from CTSD-astrocytes suggested uptake of CTSD into LAMP1- or LAMP2-positive endolysosomes.

Western blot analyses of culture supernatant (Figure 1Ca) demonstrated the presence of pro-CTSD (pCTSD) in the media from CTSD-NSCs and CTSD-astrocytes, and wt-NSCs and wt-astrocytes, indicating secretion of CTSD from these cells. No signal was detected in supernatants from ko-NSCs and ko-astrocytes. Western blot analyses of cell pellets (Figure 1Cb) showed that CTSD-NSCs, wt-NSCs and astrocytes derived from these stem cells expressed

pCTSD, intermediate-CTSD (iCTSD) and mature-CTSD (mCTSD), with iCTSD being the predominant form. Intensities of the CTSD signals in CTSD-NSCs and CTSD-astrocytes were significantly increased when compared to wt-NSCs and wt-astrocytes, respectively. No CTSD was detected in ko-NSCs and ko-astrocytes, as expected. An iCTSD signal was detected in ko-astrocytes cultured in conditioned medium from CTSD-astrocytes, indicating uptake of pCTSD by ko-astrocytes from the supernatant which was further processed into iCTSD form. CTSD was not detectable in ko-astrocytes cultured in conditioned medium from ko-astrocytes.

Analyses of CTSD enzymatic activity in cell pellets from NSC cultures (Fig 1D) revealed a 2.43-fold (± 0.03 ; mean \pm SEM) higher activity in CTSD-NSCs than in wt-NSCs. CTSD enzymatic activity in cell pellets from ko-NSCs was almost absent, as expected.

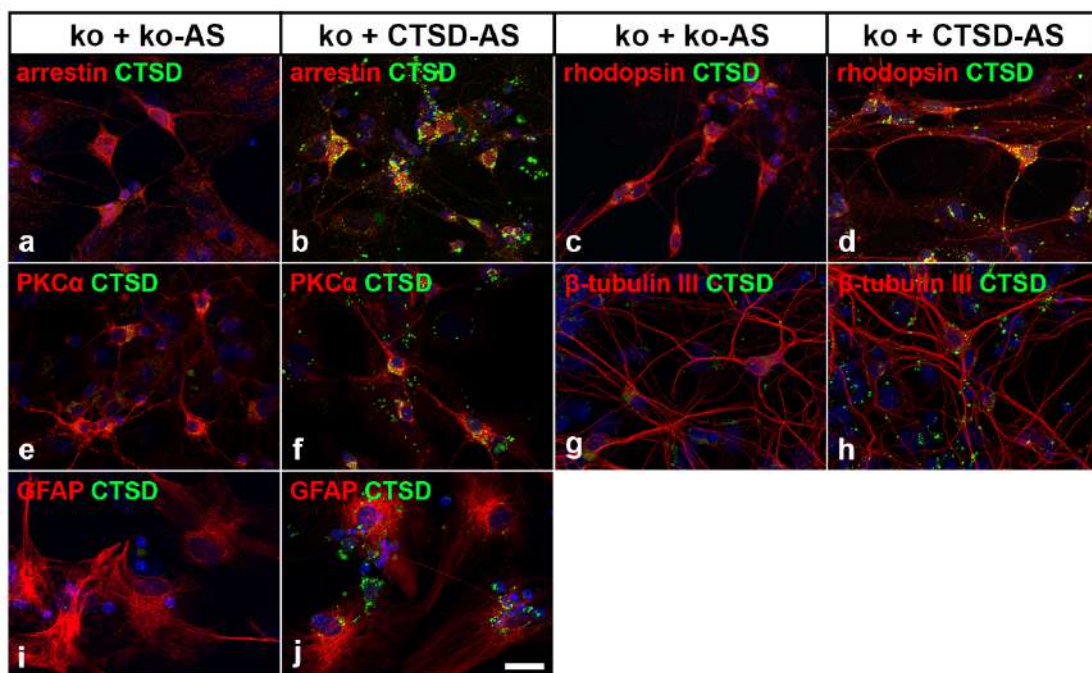


Figure 2. Uptake of CTSD in primary retinal cell cultures from *Ctsd* ko mice. Double-immunostainings of primary retinal cell cultures maintained in conditioned medium from *Ctsd* ko astrocytes (a, c, e, g, i) or CTSD overexpressing astrocytes (b, d, f, h, j) with antibodies to CTSD and either cone-arrestin (a, b), rhodopsin (c, d), PKC α (e, f), β -tubulin III (g, h) or GFAP (i, j). CTSD, cathepsin D; GFAP, glial fibrillary acidic protein; ko, knockout; ko + ko-AS, *Ctsd* ko primary retinal cell cultures maintained in the presence of conditioned medium from *Ctsd* ko astrocytes; ko + CTSD-AS, *Ctsd* ko primary retinal cell cultures maintained in the presence of conditioned medium from CTSD overexpressing astrocytes; PKC α , protein kinase C-alpha. Scale bar, 20 μ m.

To further analyze CTSD uptake by various retinal cell types, immunocytochemistry analyses were performed on primary retinal cells from *Ctsd* ko mice cultured either in conditioned media from ko-astrocytes or CTSD-astrocytes (Figure 2). CTSD labeling was observed in multiple retinal cell types maintained in conditioned medium from CTSD-astrocytes, including arrestin-positive cone photoreceptor cells (Figure 2b), rhodopsin-positive rod photoreceptor cells (Figure 2d), PKC α -positive rod bipolar cells (Figure 2f), β -tubulin III positive neurons (Figure 2h) and GFAP-positive astrocytes (Figure 2j). Retinal cells maintained in conditioned media from ko-astrocytes were CTSD-negative (Figure 2a, c, e, g, i).

3.2 scAAVshH10 transduces RPE cells and Müller cells

To investigate the tropism of an scAAVshH10 serotype in the murine retina, we injected scAAVshH10-GFP (1 μ l, CMV 2.47 \times 10¹² v.g./ μ l) intravitreally into *Ctsd* wt mice at postnatal day 5. Two weeks post-injection, we observed robust expression of GFP throughout the retina (Figure 3a, 3b). Immunostainings of

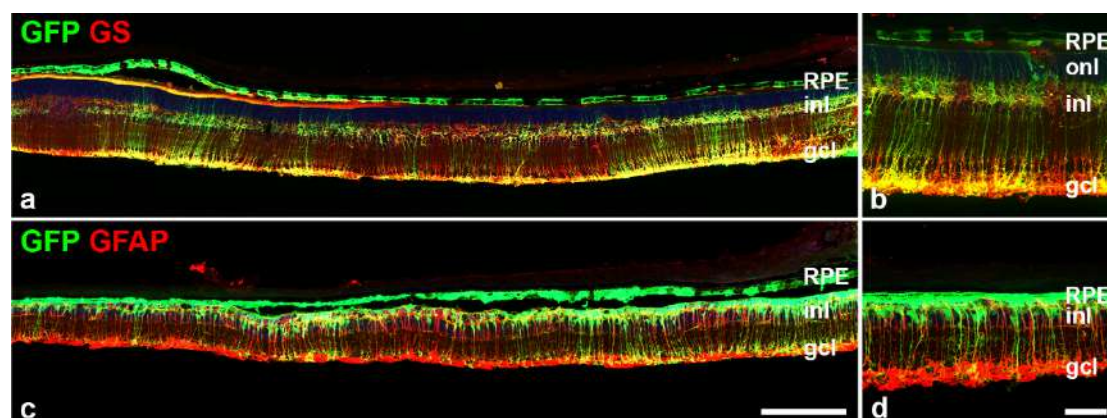


Figure 3. Transgene expression after intravitreal injections of scAAVshH10-GFP in RPE cells and Müller cells. scAAVshH10-GFP was intravitreally injected into *Ctsd* wt (a, b) and *Ctsd* ko (c, d) mice at P5, and retinas were double-stained with antibodies to GFP and GS (a, b) or GFP and GFAP (c, d) at P22. gcl, ganglion cell layer; GFAP, glial fibrillary acidic protein; GFP, green fluorescent protein; GS, glutamine-synthetase; inl, inner nuclear layer; onl, outer nuclear layer; RPE, retinal pigment epithelium. Scale bar in (c): 200 μ m; in (d): 50 μ m.

sections with antibodies to glutamine-synthetase (GS) revealed co-localization of GFP and GS, demonstrating efficient transduction of Müller glia. GFP expression was also found in RPE cells (Figure 3a, 3b). Similarly, intravitreal injections of scAAVshH-GFP (1ul, CMV 2.47 x 10¹² v.g./ul) into *Ctsd* ko mice at P5 and analysis of retinas at P22 revealed GFP in GFAP-positive retinal glial cells and in RPE cells (Figure 3c, 3d).

To investigate the time course of CTSD transgene expression in *Ctsd* ko retinas, we intravitreally injected scAAVshH10-GFP (1ul, CMV 2.47 x 10¹² v.g./ul) into the left eye and scAAVshH10-CTSD (1ul, CMV 2.46 x 10¹² v.g./ul) into the right eye at P5, and analyzed the retinas 4 days after injection. At this time point, transgene expression was detectable but not throughout the entire length of the retina. Usually, GFP or CTSD expression was more pronounced in central retina regions when compared to the retina periphery (Figure 4).

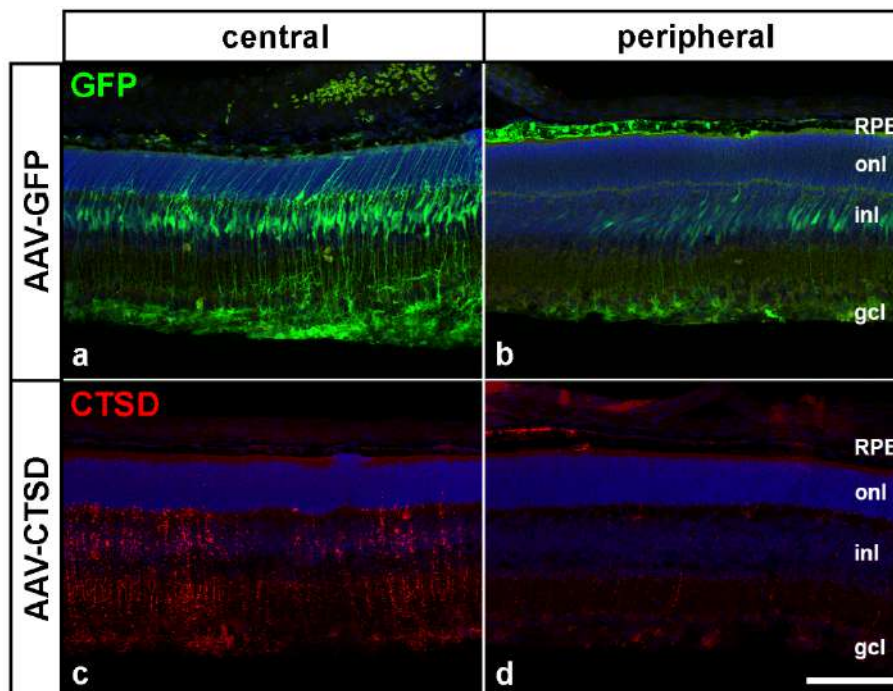


Figure 4. Rapid expression of GFP or CTSD after intravitreal injections of the scAAVshH10 serotype in *Ctsd* ko retinas. Expression of GFP (a, b) and CTSD (c, d) in central (a, c) and peripheral (b, d) regions of P9 *Ctsd* ko retinas after intravitreal injections of scAAVshH10-GFP and scAAVshH10-CTSD, respectively at P5. AAV, adeno-associated viruses; CTSD, cathepsin D; gcl, ganglion cell layer; GFP, green fluorescent protein; inl, inner nuclear layer; onl, outer nuclear layer; P, postnatal day; RPE, retinal pigment epithelium. Scale bar, 100 μ m.

3.3 Correction of the biochemical phenotype of *Ctsd ko* retinas after intravitreal injections of NSCs or AAV vectors.

Ctsd ko retinas display an early onset accumulation of storage material and a marked dysregulation of various lysosomal proteins. After intravitreal transplantations of CTSD-NSCs at P7 and analysis of retinas at P22, CTSD was detectable in all layers of the treated retinas (Figure 5b). No CTSD expression was detected in the contralateral eye with injected ko-NSCs, as expected. Uptake of CTSD after treatment with CTSD-NSCs resulted in partial correction of various pathological markers. For instance, levels of saposin D (Figure 5d) and SCMAS (Figure 5f) were reduced in mutant retinas with grafted CTSD-NSCs when compared to control retinas with grafted ko-NSCs.

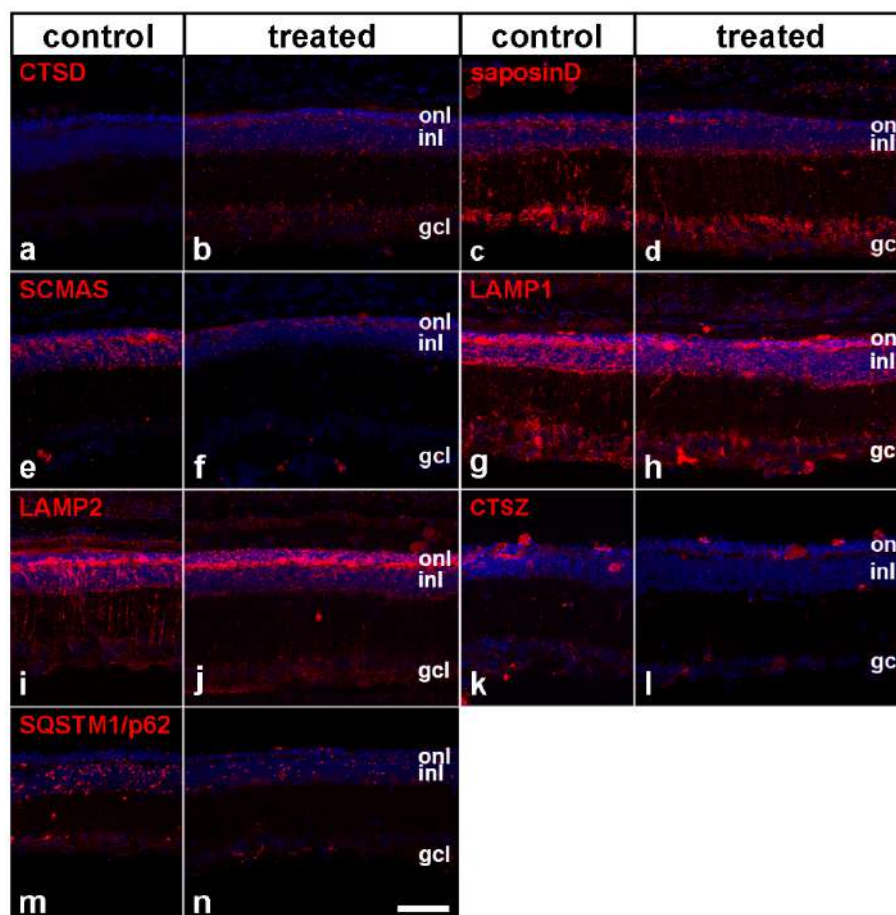


Figure 5. Storage material, lysosomal proteins and the autophagy marker SQSTM1/p62 in *Ctsd* retinas treated with CTSD overexpressing neural stem cells. Immunohistochemical analyses of retinas from P22 *Ctsd ko* eyes with grafted CTSD-NSCs (b, d, f, h, j, l, n) or contralateral control eyes with grafted ko-NSCs (a, c, e, g, i,

k, m) with antibodies to CTSD (a, b), saposin D (c, d), SCMAS (e, f), LAMP1 (g, h), LAMP2 (i, j), CTSZ (k, l) and SQSTM1/p62 (m, n). CTSD, cathepsin D; CTSZ, cathepsin X/Z/P; gcl, ganglion cell layer; inl, inner nuclear layer; LAMP1, lysosomal-associated membrane protein 1; LAMP2, lysosomal-associated membrane protein 2; onl, outer nuclear layer; SCMAS, subunit c of mitochondrial ATP synthase; SQSTM1/p62, sequestosome 1/p62. Scale bar, 50 μm .

In addition, expression levels of the lysosomal proteins LAMP1 (Figure 5h), LAMP2 (Figure 5j) and CTSZ (Figure 5l), partially decreased in CTSD-NSCs-treated *Ctsd* ko retinas when compared to control retinas, indicating attenuation of the lysosomal dysfunction. Furthermore, the number of SQSTM1/p62 (Figure 5n) positive punctae decreased after CTSD-NSCs treatment, indicating amelioration of autophagic dysfunction.

Intravitreal injections of scAAVshH10-CTSD resulted in significantly higher levels of CTSD than intravitreal transplantations of CTSD-NSCs, both in the

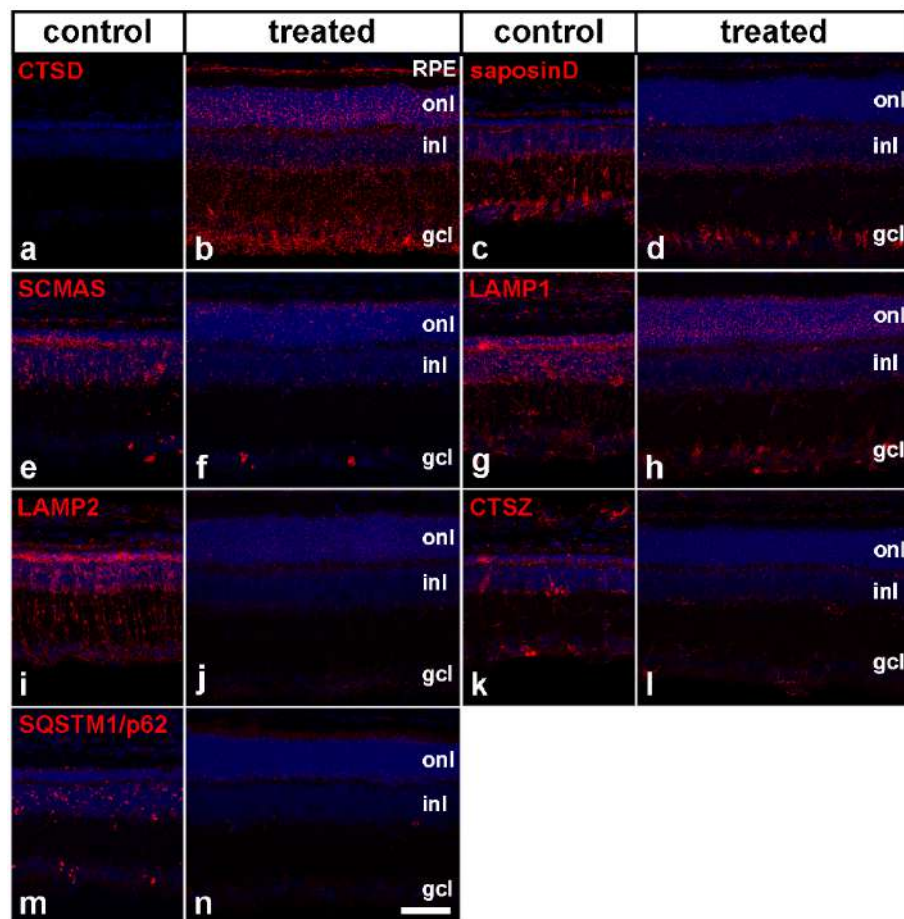


Figure 6. Storage material, lysosomal proteins and the autophagy marker SQSTM1/p62 in *Ctsd* retinas treated with scAAVshH10-CTSD. Immunohistochemical analyses of retinas from P22 *Ctsd* ko eyes injected with scAAVshH10-CTSD (b, d, f, h, j, l, n) or contralateral control eyes injected with

scAAVshH10-GFP (a, c, e, g, i, k, m) with antibodies to CTSD (a, b), saposin D (c, d), SCMAS (e, f), LAMP1 (g, h), LAMP2 (i, j), CTSZ (k, l) and SQSTM1/p62 (m, n). CTSD, cathepsin D; CTSZ, cathepsin X/Z/P; gcl, ganglion cell layer; inl, inner nuclear layer; LAMP1, lysosomal-associated membrane protein 1; LAMP2, lysosomal-associated membrane protein 2; onl, outer nuclear layer; SCMAS, subunit c of mitochondrial ATP synthase; SQSTM1/p62, sequestosome 1/p62. Scale bar, 50 μm .

neuroretina and the RPE (Figure 6b). The correction of biochemical phenotype was also more pronounced in scAAVshH10-CTSD treated retinas when compared to CTSD-NSC treated retinas. For instance, the amount of storage material in scAAVshH10-CTSD treated retinas was more reduced than in NSCs-treated retinas, as indicated by immunostainings with antibodies to saposinD (Figure 6d) and SCMAS (Figure 6f). Additionally, expression levels

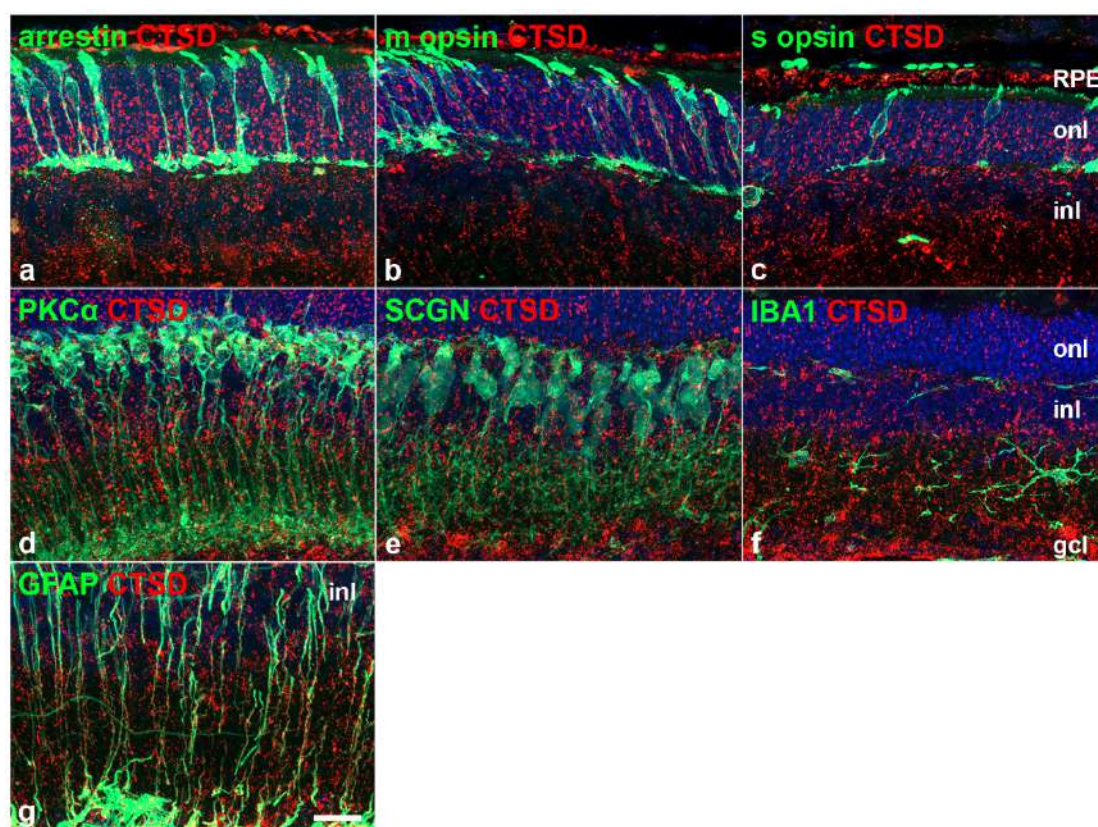


Figure 7. Localization of CTSD in the *Ctsd* ko retina after intravitreal injections of scAAVshH10-CTSD. Double-immunostainings on *Ctsd* ko retinas injected with scAAVshH10-CTSD at P5 and analyzed at P22 with antibodies to CTSD and either arrestin (a), m opsin (b), s opsin (c), PKC α (d), SCGN (e), IBA1 (f) or GFAP (g). CTSD, cathepsin D; gcl, ganglion cell layer; GFAP, glial fibrillary acidic protein; IBA1, ionized calcium-binding adapter molecule 1; inl, inner nuclear layer; onl, outer nuclear layer; PKC α , protein kinase C-alpha; RPE, retinal pigment epithelium; SCGN, secretagogin. Scale bar, 20 μm .

of LAMP1 (Figure 6h), LAMP2 (Figure 6j) and CTSZ (Figure 6l), were clearly more reduced after injections of scAAVshH10-CTSD than after transplantations of CTSD-NSCs. Furthermore and different to control retinas, scAAVshH10-CTSD treated retinas were completely devoid of SQSTM1/p62-positive punctae (compare Figure 6n and 6m). Together, immunohistochemical analyses revealed that reduction of storage material, correction of lysosomal protein dysregulation and amelioration of autophagic dysfunction was more pronounced in AAV-treated than in NSCs-treated *Ctsd* ko retinas.

Double immunostainings on scAAVshH10-CTSD injected retinas with antibodies to CTSD and various cell type-specific antigens (Figure 7) revealed the presence of the enzyme in arrestin-, m opsin-, and s opsin-positive cones, PKC α -positive rod bipolar cells, SCGN-positive cone bipolar cells, Iba1-positive microglia and GFAP-positive astrocytes/Müller cells, indicating that a fraction of CTSD expressed by Müller cells and RPE cells was released into the extracellular space and taken up by various retinal neurons.

Western blot analysis (Figure 8A) revealed pCTSD, iCTSD and mCTSD in wt retinas, with iCTSD and mCTSD being the predominant forms. Levels of pCTSD, iCTSD and mCTSD were all increased in CTSD-NSCs and scAAVshH10-CTSD treated *Ctsd* ko retinas, while untreated *Ctsd* ko retinas, ko-NSCs treated retinas and scAAVshH10-GFP treated mutant retinas were CTSD negative, as expected. Quantitative analysis (Figure 8B) of blots confirmed elevated levels of CTSD in CTSD-NSCs and scAAVshH10-CTSD treated *Ctsd* ko retinas. Compared to wt retinas, around 31% of iCTSD and 40% of mCTSD were detected in the retina with CTSD-NSCs. However, the amount of CTSD in the CTSD-NSCs-treated retinas was not significantly above the background of the ko retinas with grafted ko-NSCs. Different to CTSD-NSCs treated retinas, levels of iCTSD and mCTSD were significantly elevated in scAAVshH10-CTSD treated retinas by a factor of 5.22 ± 1.10 (mean \pm SEM) and 7.27 ± 1.13 when compared to wt retinas ($p < 0.001$ for both comparisons, one-way analysis of variance (ANOVA), Figure 8B). Furthermore, saposinD (Figure 8A, 8B) was significantly decreased in eyes with grafted CTSD-NSCs when compared to control eyes with grafted ko-NSCs ($p < 0.01$, one-way ANOVA, Figure 8B), but was still markedly elevated compared to wt retina ($p < 0.001$, one-way ANOVA, Figure 8B). However, saposinD was more significantly

decreased in ko retinas with scAAVshH10-CTSD injection compared to that with scAAVshH10-GFP injection ($p < 0.001$, one-way ANOVA, Figure 8B). Furthermore, the decrease of saposinD level was more pronounced in

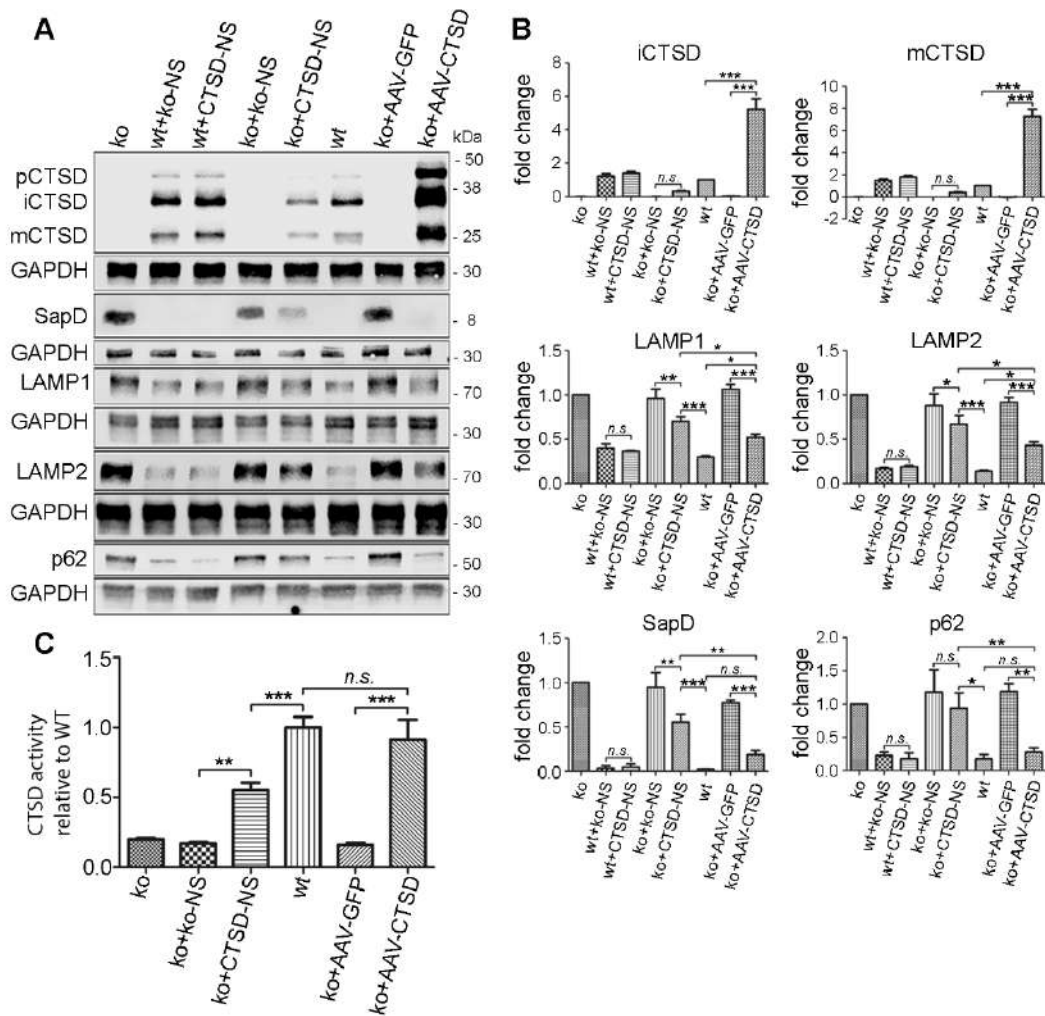


Figure 8. Immunoblot analysis and CTSD activity assay of *CtSD* ko retinas treated with neural stem cells or AAV vectors. (A) Western blot analysis of CTSD, saposin D, LAMP1, LAMP2, and SQSTM1/p62 in P22 *CtSD* ko retinas, *CtSD* wt retinas, *CtSD* wt and ko retinas treated with NSCs, and *CtSD* ko retinas treated with AAV vectors. GAPDH was loaded as an internal control. (B) Quantitative analysis of western blots. Bars represent the mean (\pm SEM) of 3 independent experiments. Statistical analysis was performed with the one-way ANOVA. *, $p < 0.05$, **, $p < 0.01$, and ***, $p < 0.001$; n.s., not significant. (C) CTSD activity assay of untreated P22 *CtSD* ko and *CtSD* wt retinas, and *CtSD* ko retinas treated with neural stem cells or AAV vectors. Each bar represents the mean value (\pm SEM) of 6 retinas. Statistical analysis was performed using the one-way ANOVA. **, $p < 0.01$, ***, $p < 0.001$; n.s., not significant. AAV, adeno-associated virus; CTSD, cathepsin D; GAPDH, glyceraldehyde-3-phosphate dehydrogenase; GFP, green fluorescent protein; iCTSD, intermediate-CTSD; ko, knockout; ko+ko-NS, *CtSD* ko retinas treated with *CtSD* ko neural stem cells; ko+CTSD-NS, *CtSD* ko retinas treated with CTSD overexpressing neural stem cells; ko+AAV-GFP, *CtSD* ko retinas treated with scAAVshH10-GFP; ko+AAV-CTSD, *CtSD* ko retinas treated with

scAAVshH10-CTSD; LAMP1, lysosomal-associated membrane protein 1; LAMP2, lysosomal-associated membrane protein 2; mCTSD, mature-CTSD; NS, neural stem cells; pCTSD, pro-CTSD; SapD, saposin D; wt, wild-type; wt+ko-NS, *Ctsd* wt retinas treated with *Ctsd* ko neural stem cells; wt+CTSD-NS, *Ctsd* wt retinas treated with CTSD overexpressing neural stem cells.

scAAVshH10-CTSD treated retinas than in CTSD-NSC treated retinas ($p < 0.01$, one-way ANOVA, Figure 8B). Of note, the amount of saposinD in scAAVshH10-CTSD injected retinas was not significantly different from that found in untreated wt retinas ($p > 0.05$, one-way ANOVA, Figure 8B). Furthermore, levels of the lysosomal transmembrane proteins LAMP1 and LAMP2 were significantly decreased in the retinas with grafted CTSD-NSCs when compared to control retinas with grafted ko-NSCs ($p < 0.01$ and $p < 0.05$, respectively, one-way ANOVA, Figure 8B), but still markedly increased compared to untreated wt retinas ($p < 0.001$ for both comparisons, one-way ANOVA, Figure 8B). After scAAVshH10-CTSD treatment, *Ctsd* ko retinas showed significantly lower level of LAMP1 and LAMP2 compared to scAAVshH10-GFP injected retinas ($p < 0.001$ for both comparisons, one-way ANOVA, Figure 8B). However, also in scAAVshH10-CTSD treated animals, levels of LAMP1 and LAMP2 were still significantly higher than in wt retinas ($p < 0.05$ for both comparisons, one-way ANOVA, Figure 8B). The autophagic dysfunction indicated by SQSTM1/p62 was not significantly attenuated in CTSD-NSCs treated retinas when compared to ko-NSCs injected retinas. However, in the retinas treated with scAAVshH10-CTSD, SQSTM1/p62 levels were markedly decreased when compared to the retinas injected with the control vector ($p < 0.01$, one-way ANOVA, Figure 8B). Similar to saposinD, there was no significant difference in the amount of SQSTM1/p62 between untreated wt retinas and scAAVshH10-CTSD treated *Ctsd* ko retinas ($p > 0.05$, one-way ANOVA, Figure 8B). Of note, levels of saposinD, LAMP1, LAMP2 and SQSTM1/p62 in wt retinas treated with CTSD-NSCs were not significantly different from those in wt retinas with grafted ko-NSCs ($p > 0.05$, one-way ANOVA, Figure 8A, 8B), demonstrating that continuous administration of CTSD didn't affect the expression level of saposinD, LAMP1, LAMP2 and SQSTM1/p62 in healthy retinas.

CTSD enzymatic activity in *Ctsd* ko retinas treated with CTSD-NSCs accounted for 55.2% of the enzymatic activity measured in untreated wt retinas, and was significantly lower than in healthy retinas ($p < 0.001$, one-way ANOVA,

Figure 8C). However, the level of CTSD activity in scAAVshH10-CTSD injected *Ctsd* ko retinas accounted for 91.4% of that found in untreated wt retinas, and was not significantly different from healthy retinas ($p > 0.05$, one-way ANOVA, Figure 8C).

3.4 Attenuation of neuroinflammation in treated *Ctsd* ko retinas

Immunohistochemical analyses of retinas injected with CTSD-NSCs or scAAVshH10-CTSD showed significant attenuation of reactive microgliosis and

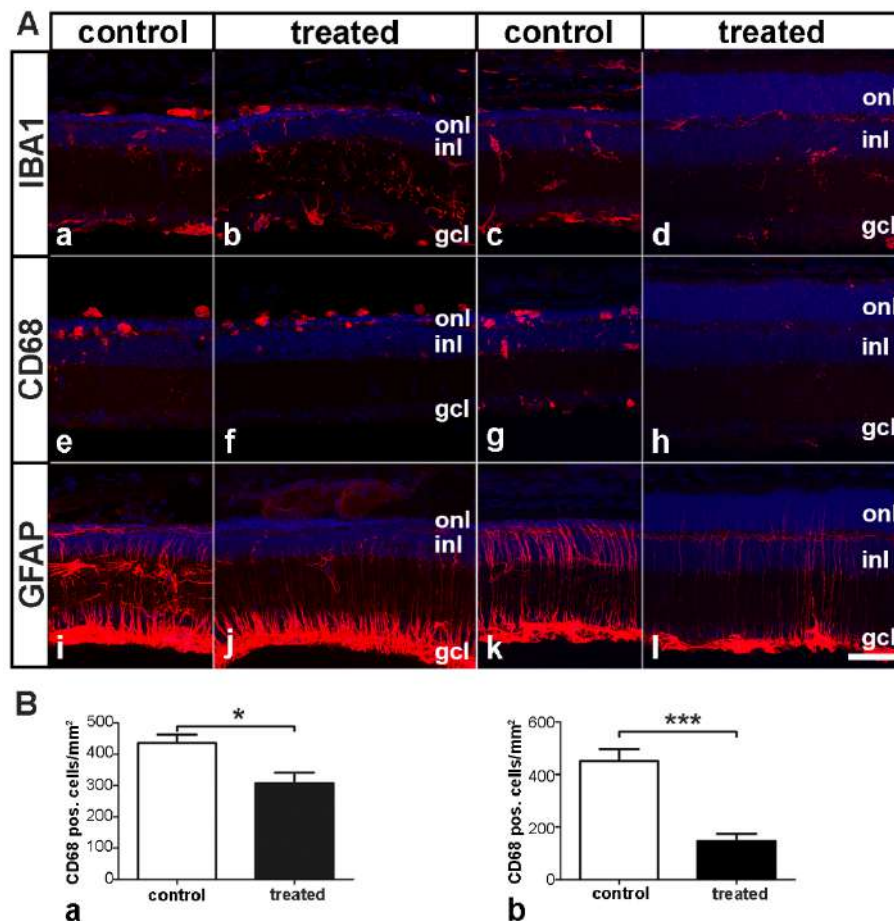


Figure 9. Attenuation of reactive microgliosis and astrogliosis in *Ctsd* ko retinas treated with neural stem cells or AAV vectors. (A) Immunostainings of IBA1-positive microglia cells (a-d), CD68-positive microglia/macrophages (e-h), GFAP-positive Müller cells and astrocytes (i-l) in NSC-treated (a, b, e, f, i, j) and AAV-treated (c, d, g, h, k, l) *Ctsd* ko retinas. (B) The density of CD68-positive cells in P22 *Ctsd* ko retinas treated with either NSCs (a) or AAV vectors (b). Each bar represents the mean (\pm SEM) of 6 animals. Statistical analysis was performed with the paired t-test. *, $p < 0.05$, ***, $p < 0.001$. CD68, cluster of differentiation 68; gcl, ganglion cell layer; GFAP,

glial fibrillary acidic protein; IBA1, ionized calcium-binding adapter molecule 1; inl, inner nuclear layer; onl, outer nuclear layer. Scale bar, 50 μm .

astrogliosis when compared to the corresponding control eyes. Qualitative analyses of sections revealed a decreased density of IBA1-positive microglia in mutant retinas with transplanted CTSD-NSCs (Figure 9Ab) when compared to retinas with transplanted ko-NSCs. However, attenuation of reactive microgliosis was more pronounced in retinas treated with scAAVshH10-CTSD (Figure 9Ad). IBA1-positive microglia cells in scAAVshH10-CTSD treated retinas had a more ramified morphology, and were almost absent from the subretinal space and outer nuclear layer, different to the contralateral control retinas (Figure 9Ac). Similarly, CD68-positive microglia/macrophages decreased markedly in number and size in CTSD-NSCs-treated retinas (Figure 9Af), but the effect was significantly more pronounced in scAAVshH10-CTSD injected retinas (Figure 9Ah). Quantitative analyses revealed that the number of CD68-positive cells was reduced by 25.6% in CTSD-NSCs treated retinas (Figure 9Ba), and by 67.4% in scAAVshH10-CTSD injected retinas (Figure 9Bb) when compared to retinas treated with ko-NSCs and scAAVshH10-GFP, respectively ($p < 0.05$ and $p < 0.001$, respectively, paired t-test).

In addition, the high expression levels of GFAP in astrocytes and Müller cells observed in control retinas were significantly reduced in eyes with injected CTSD-NSCs (Figure 9j) or scAAVshH10-CTSD (Figure 9l).

3.5 CTSD supplementation via CTSD-NSCs did not rescue retinal neurons in *Ctsd* ko mice.

Immunostainings (Figure 5b) and Western blot analyses (Figure 8A) demonstrated the presence of CTSD in CTSD-NSCs treated mutant retinas. However, the treatment did not prevent the rapidly progressing atrophy of the outer nuclear layer (Figure 10Ab, 10Ad, 10Af, 10Ah). Quantitative analysis revealed that the number of rows of photoreceptor nuclei in CTSD-NSCs treated retinas (1.75 ± 0.39 ; mean \pm SEM) was not statistically different from that found in the contralateral eyes treated with ko-NSCs (1.77 ± 0.23 ; $p > 0.05$, paired t-test) (Figure 10Ba). Furthermore, immunohistochemical analyses revealed

the presence of only a few m+s opsin- (1.71 ± 0.72 ; Figure 10Ab, 10Bb) or arrestin- (0.10 ± 0.07 ; Figure 10Ad, 10Bc) positive cones in CTSD-NSCs treated

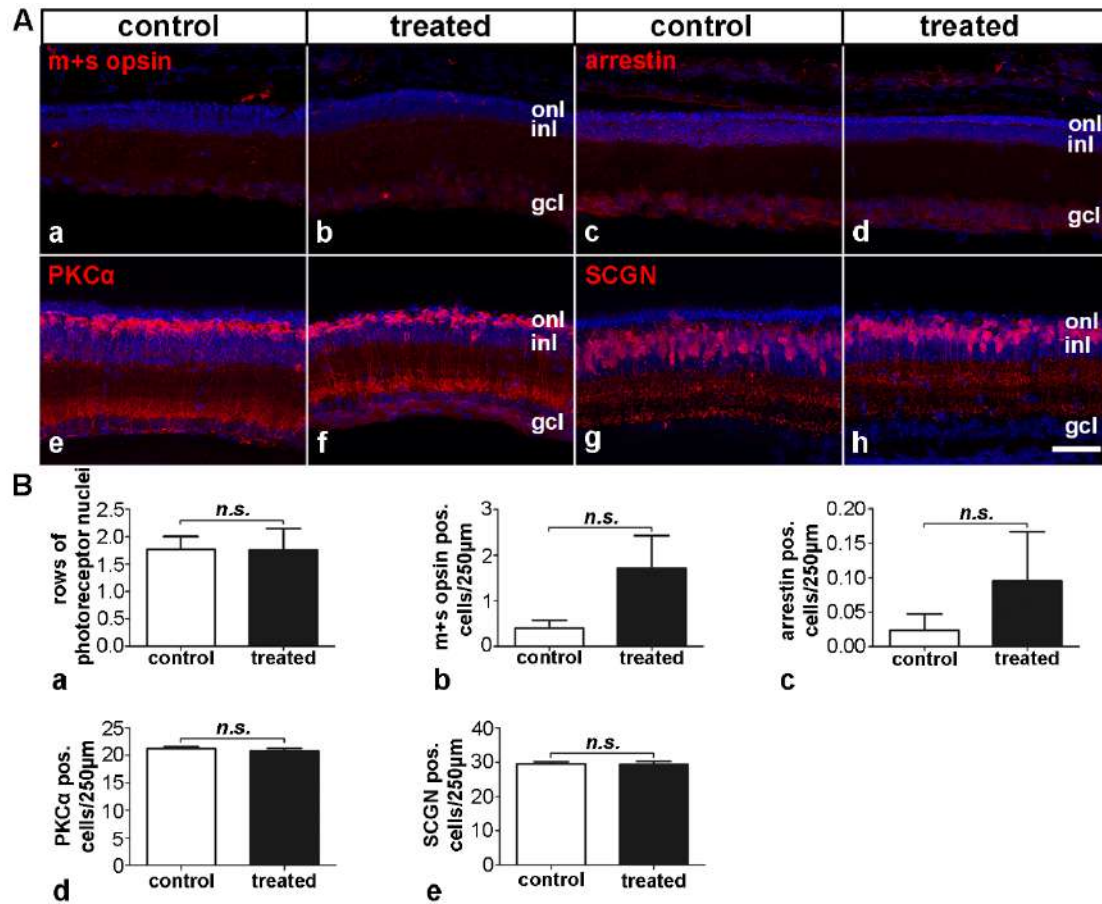


Figure 10. The impact of intravitreally grafted CTSD overexpressing neural stem cells on the survival of photoreceptors and bipolar cells in *CtSD ko* mice. (A) Immunostainings of P22 *CtSD ko* retinas treated with CTSD overexpressing NSCs (b, d, f, h) and contralateral control retinas treated with *CtSD ko* NSCs (a, c, e, g) using antibodies to m+s opsin (a, b), arrestin (c, d), PKCα (e, f) and SCGN (g, h). **(B)** The number of rows of photoreceptor nuclei (a), m+s opsin-positive cells (b), arrestin-positive cells (c), PKCα-positive cells (d), and SCGN-positive cells (e) in P22 *CtSD ko* retinas treated with *CtSD ko* NSCs (control) or CTSD overexpressing NSCs (treated). Each bar represents the mean (\pm SEM) of 7 animals. Statistical analysis was performed with the paired t-test, n.s., not significant. gcl, ganglion cell layer; inl, inner nuclear layer; onl, outer nuclear layer; PKCα, protein kinase C-alpha; SCGN, secretagogen. Scale bar, 50 μ m.

retinas, not statistically different from the number of m+s opsin- (0.40 ± 0.17 ; Figure 10Aa, 10Bb) or arrestin- (0.02 ± 0.02 ; Figure 10Ac, 10Bc) positive cones found in the contralateral control eyes ($p > 0.05$ for all comparisons, paired t-test). Similarly, we found no significant difference in the number of PKCα-positive rod bipolar cells or SCGN-positive cone bipolar cells between CTSD-

NSCs treated retinas (20.79 ± 0.48 and 29.36 ± 0.91 , respectively; Figure 10Af, 10Ah, 10Bd, 10Be) and ko-NSCs treated retinas (21.21 ± 0.37 and 29.5 ± 0.68 , respectively; Figure 10Ae, 10Ag, 10Bd, 10Be; $p > 0.05$ for all comparisons, paired t-test). These experiments demonstrated that NSCs-mediated supplementation of CTSD did not result in attenuation of the rapidly progressing retinal degeneration in *Ctsd* ko mice.

3.6 CTSD supplementation via scAAVshH10-CTSD rescued retinal neurons in *Ctsd* ko mice.

CTSD supplementation through a cell based enzyme replacement strategy resulted in small amount of CTSD in the mutant retinas, which failed to attenuate retinal degeneration in *Ctsd* ko mice. To investigate whether attenuation of retinal degeneration may be achieved through an AAV vector-mediated gene transfer of CTSD, we explored the impact of various titers of scAAVshH10-CTSD on the morphology of *Ctsd* ko retinas. Injections of scAAVshH10-CTSD with a titer of 4.75×10^{11} v.g./ μ l had no significant effects on photoreceptor survival (data not shown). However, injections of the vector with a titer of 1.23×10^{13} v.g./ μ l preserved the retina morphology in P22 *Ctsd* ko mice as indicated by an almost normal thickness of the outer nuclear layer and the presence of numerous cone photoreceptors. However, in a fraction of animals the size of the treated eyes was significantly smaller than that of the contralateral control eyes (data not shown). When scAAVshH10-CTSD was injected with a lower titer of 2.46×10^{12} v.g./ μ l, we observed significant attenuation of retinal degeneration, and normal-sized eyes. DAPI staining revealed that the outer nuclear layer of these retinas was significantly thicker (Figure 11Ab, 11Ad, 11Af, 11Ah) when compared to the contralateral control retinas (Figure 11Aa, 11Ac, 11Ae, 11Ag). Quantitative data showed that the number of rows of photoreceptor nuclei was significantly higher in scAAVshH10-CTSD treated eyes (5.60 ± 0.47 rows of nuclei) compared to that found in the control eyes (1.30 ± 0.15 rows of nuclei; $p < 0.001$, paired t-test; Figure 11Ba). Rod photoreceptors comprise about 97% of all photoreceptors in

the mouse retina. Data thus demonstrate that the gene therapy approach effectively promoted rod photoreceptor survival in *Ctsd ko* mice.

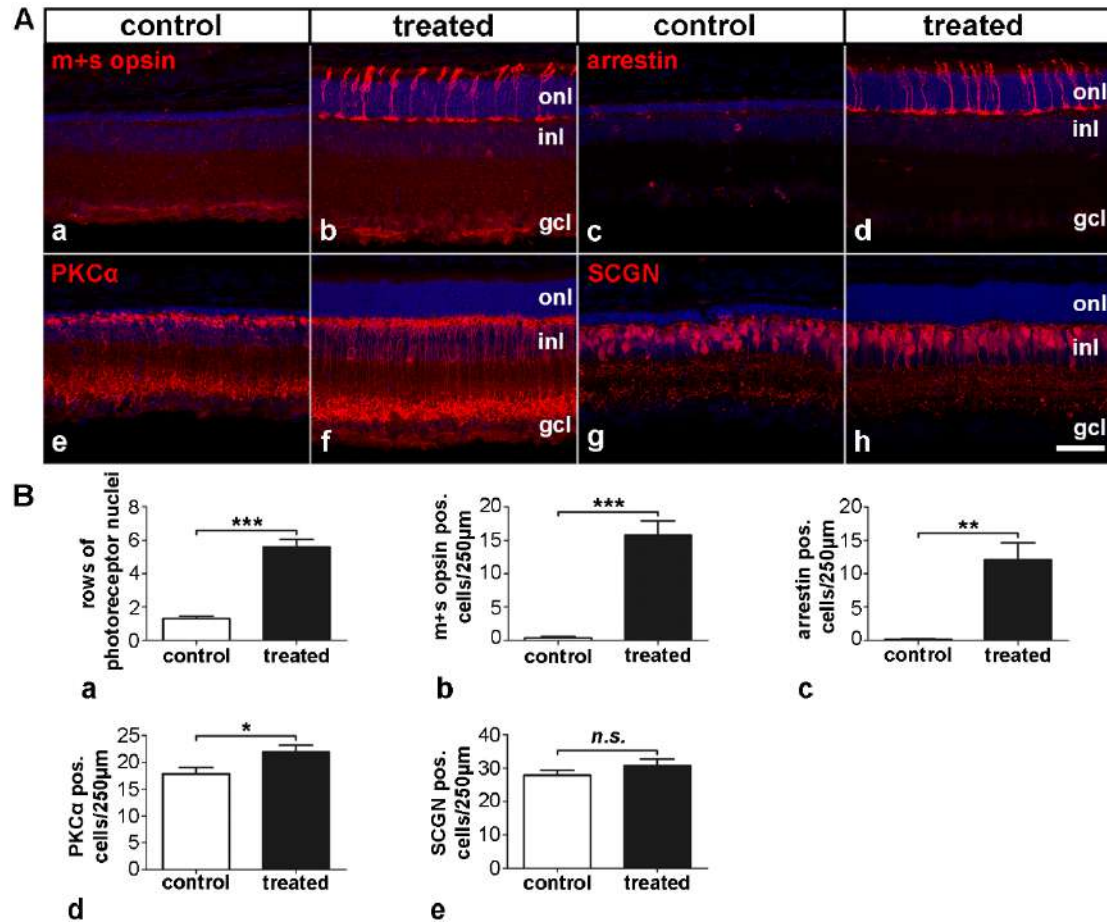


Figure 11. The impact of intravitreally injected scAAVshH10-CTSD on the survival of photoreceptors and bipolar cells in *Ctsd ko* mice. (A) Immunostainings of P22 *Ctsd ko* retinas treated with scAAVshH10-CTSD (b, d, f, h) and contralateral control retinas treated with scAAVshH10-GFP (a, c, e, g) using antibodies to m+s opsin (a, b), arrestin (c, d), PKC α (e, f) and SCGN (g, h). (B) The number of rows of photoreceptor nuclei (a), m+s opsin-positive cells (b), arrestin-positive cells (c), PKC α -positive cells (d), and SCGN-positive cells (e) in P22 retinas treated with scAAVshH10-GFP (control) or scAAVshH10-CTSD (treated). Each bar represents the mean (\pm S.E.M.) from 7 animals. Statistical analysis was performed with the paired t-test. *, $p < 0.05$, **, $p < 0.01$, ***, $p < 0.001$; n.s., not significant. gcl, ganglion cell layer; inl, inner nuclear layer; onl, outer nuclear layer; PKC α , protein kinase C-alpha; SCGN, secretagogin. Scale bar, 50 μ m.

Further analyses of the retinal histology showed the presence of numerous m+s opsin-positive (Figure 11Ab) or arrestin-positive (Figure 11Ad) cone photoreceptors in scAAVshH10-CTSD treated eyes, while cones were essentially absent from control retinas (Figure 11Aa, 11Ac). Surviving cones

showed an apparently normal overall morphology, with well-developed inner and outer segments and presynaptic terminals in the inner nuclear layer (Figure 11Ab, 11Ad, Figure 12b). Quantitative analysis confirmed a significant protection of cones with 15.74 ± 2.20 (mean \pm SEM) m+s opsin-positive cones/250 μ m retina length (Figure 11Bb) and 12.10 ± 2.55 arrestin-positive cones/250 μ m retina length (Figure 11Bc) in scAAVshH10-CTSD treated animals as opposed to 0.38 ± 0.21 m+s opsin-positive cones/250 μ m retina length and 0.17 ± 0.08 arrestin-positive cones/250 μ m in animals that received injections of scAAVshH10-GFP ($p < 0.001$, $p < 0.01$, respectively; paired t-test).

Immunostaining of scAAVshH10-CTSD treated *Ctsd* ko retinas at P22 revealed a more organized morphology of PKC α -positive rod bipolar cells (Figure 11Af) when compared to control retinas (Figure 11Ae). In addition, we found a significantly higher number of PKC α -positive rod bipolar cells in scAAVshH10-CTSD injected retinas (21.98 ± 1.27 (mean \pm SEM) cells/250 μ m retina length) than in control retinas (17.83 ± 1.21 cells/250 μ m retina length; $p < 0.05$, paired t-test; Figure 11Bd). The overall morphology of SCGN-positive cone bipolar cells also appeared more organized in scAAVshH10-CTSD treated retinas (Figure 11Ah) than in control retinas (Figure 11Ag). However, the number of cone bipolar cells in scAAVshH10-CTSD treated retinas at P22 (30.75 ± 1.99 (mean \pm SEM) cone bipolar cells/250 μ m) was not significantly different from that found in control retinas (27.92 ± 1.45 cone bipolar cells/250 μ m; $p > 0.05$, paired t-test; Figure 11Be).

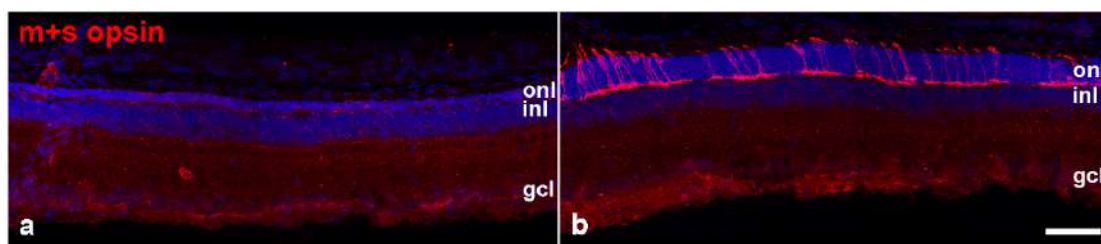


Figure 12. Intravitreal injections of scAAVshH10-CTSD attenuate the degeneration of cone photoreceptors in the *Ctsd* ko retina. Immunostainings of a *Ctsd* ko retina treated with scAAVshH10-CTSD (b) and the contralateral retina treated with scAAVshH10-GFP using antibodies to m+s opsin. gcl, ganglion cell layer; inl, inner nuclear layer; onl, outer nuclear layer. Scale bar, 50 μ m

In conclusion, intravitreal injections of scAAVshH10-CTSD resulted in a marked preservation of the retina structure in *Ctsd* ko mice.

4 Discussion

4.1 Enzyme replacement strategies

The NCLs caused by mutations in genes encoding soluble lysosomal enzymes include CLN1, CLN2, CLN5, CLN10, CLN11, and CLN13 [7]. A promising strategy to treat these NCL forms is to deliver a functional variant of the dysfunctional or deficient enzyme into the diseased tissue via injections of recombinantly produced enzymes (“classical ERT”), or via cell- or gene therapy-based administration methods.

ERT is the most common way to deliver functional lysosomal enzymes into disease models. According to the target area, the recombinant enzyme might be directly injected into the diseased tissue such as the brain, or might be applied systemically. While there are numerous preclinical studies that have demonstrated the efficacy of this treatment strategy in animal models of different NCL forms [8, 53], there is currently only one successful study on patients. Cerliponase alfa, a recombinantly produced TPP1 enzyme has been shown to delay the progression of motor impairment and language deterioration after biweekly intracerebroventricular injections into CLN2 patients [62, 63].

CLN10 is caused by dysfunction or deficiency of the lysosomal enzyme CTSD. A recent study has used rhCTSD to study the therapeutic potential of an enzyme replacement therapy in *Ctsd* ko mice. The recombinant pro-CTSD was produced in human HEK cells and appeared to be stable at 4°C to 37°C. In *Ctsd*^{-/-} mice, intracranial injection of rhCTSD at P1 and P19 resulted in significant amounts of CTSD protein and significant levels of enzymatic activity in the brain of mutant mice at P23. The treated mice showed good motor coordination and muscle strength until P33-34, whereas control *Ctsd* ko mice died around P27. Furthermore, intravenously administered rhCTSD was quickly taken up by liver, spleen, and kidney and further processed into mature CTSD, which partially corrected the pathology in these tissues [74]. However, ERTs have several limitations which narrow their therapeutic potential. First, NCLs are primarily neurodegenerative disorders. Because recombinant enzymes can hardly cross the blood-brain barrier, they cannot be applied systemically but have to be injected directly into the nervous tissue [2]. Even in case

therapeutically relevant amounts of an enzyme were delivered to the brain, this had no effect on the progression of retinal degeneration due to the blood-retina barrier, as demonstrated e.g. in a CLN2 dog model [67]. Another limitation of ERT is the short half-life of the recombinant enzymes. Intravitreal injections of rhTPP1 into CLN2 canine model, for instance, have been shown to result in a substantial amount of TPP1 in the aqueous and vitreous one day after the injection. However, in eyes analyzed at longer time intervals after the injection, TPP1 was hardly detectable in the aqueous and vitreous [73]. In our previous study, intravitreal injections of rhCTSD at P7 and P14 resulted in small amounts of CTSD in *Ctsd* ko retina. The injected enzyme was taken up by glia cells, retinal nerve cells and microglia/macrophages. Of note, several aspects of the retinal pathology became partially corrected by this treatment, such as a decrease of storage material, attenuation of reactive microgliosis or dysregulation of lysosomal proteins. However, the treatment had not impact on the progression of retinal degeneration, suggesting that the amounts of CTSD were too small to attenuate this early onset and rapidly progressing retinal dystrophy. In conclusion, preclinical studies and a clinical trial have demonstrated that ERT represents a strategy to deliver therapeutically relevant amounts of lysosomal enzymes to diseased tissues. While the amount of administered enzyme can be precisely controlled, the treatment strategy requires local and repeated injections to target nervous tissue, which subsequently increases the risk of infections and other potential complications.

A continuous administration of lysosomal enzymes to diseased tissues might be achieved through a cell-based enzyme replacement strategy. Furthermore, such a treatment strategy can be potentially translated into the clinic using e.g. the so-called encapsulated cell technology (ECT). ECT was developed to treat diseases of the CNS and the eye through a continuous administration of secreted and therapeutically relevant gene products. The technology uses living cells that are encapsulated in a semipermeable polymer membrane and supportive matrices. The encapsulated cells are genetically modified to permanently secrete a specific therapeutic gene product to target a specific disease. Once surgically implanted into the diseased organ of the patient, the semipermeable polymer membrane allows diffusion of the therapeutic substance into the diseased tissue. Furthermore, the encapsulation

prevents the modified cells from entering host tissues, and in case of complications the cell implants can be explanted.

The therapeutic potential of a cell-based administration of lysosomal enzymes has been studied in a CLN2 canine model using non-encapsulated cells. Intravitreal transplantation of mesenchymal stem cells overexpressing TPP1 into the mutant dog resulted in the presence of functional enzyme in the retina. Here, the enzyme attenuated the thinning of retinal layers and deterioration of retinal function in a dose-dependent manner [87]. In this thesis, we first analyzed whether CTSD expression, release and enzymatic activity is increased in CTSD-NSCs when compared to wt-NSCs. In vitro, *Ctsd* ko astrocytes derived from *Ctsd* ko-NSCs took up CTSD released from CTSD-astrocytes, and further processed it to iCTSD in endolysosomes. In primary retinal cell cultures, *Ctsd* ko cone- and rod-photoreceptors, rod-bipolar cells, retinal neurons, and astrocytes also took up CTSD present in the conditioned medium from CTSD-astrocytes. Together, these in vitro experiments demonstrate cellular take-up and processing of transgenic CTSD. We therefore initiated in vivo experiments to study whether intravitreal transplantations of CTSD-NSCs will result in attenuation of the retinal dystrophy in *Ctsd* ko mice. In vivo, we transplanted NSCs overexpressing CTSD into the vitreous cavity of P7 *Ctsd* ko mice. Pro-CTSD released from grafted CTSD-NSCs was taken up by retinal cells and further processed to intermediate CTSD and mature CTSD in the lysosomes of the mutant' retina. However, levels of CTSD protein and CTSD enzyme activity in these CTSD-NSCs treated retinas accounted for only 30% and 55.2% of those found in wt retinas, respectively. Together, data demonstrate that intravitreal transplantations of genetically modified cells provide a potential means to continuously deliver lysosomal enzymes to dystrophic retinas.

Gene therapy based-enzyme replacement strategy aims at genetically modifying endogenous cells of a diseased tissue to express a functional variant of the dysfunctional or missing lysosomal enzyme. Some of the transgenic enzyme released by the modified cells can be taken up by neighboring non-modified cells where it also might correct the lysosomal dysfunction, a process called cross correction. Injections of adeno-associated virus (AAV) vectors encoding CTSD in to the CNS of *Ctsd* ko mice resulted in a pronounced

prolongation of the mutant's lifespan up to 198 days [82], demonstrating the efficacy of this approach. Furthermore, after intravitreal administration of AAV2-hPPT1 into *Ppt1* ko mice, enzymatic PPT1 activity in the treated eyes was approximately five times higher than in untreated healthy wild-type eyes, also showing that a gene therapy approach allows the delivery of large amounts of enzymes to diseased tissues [26]. As outlined above, cross correction boosts the therapeutic impact of a gene therapy- enzyme replacement strategy in that non-modified endogenous cells in the neighborhood of genetically modified endogenous cells take up some enzyme that is released into the extracellular space. Co-injections of equal titers of AAV-EGFP and AAV-CTSD into the brain of *Ctsd* ko mice, for instance, resulted in large numbers of CTSD immunoreactive neurons in some distance from EGFP-positive cells, indicating secretion of CTSD from transduced cells and its uptake by remote neurons in the contralateral hemisphere and in deeper brain regions like the thalamus and the hypothalamus [82].

The efficacy of a gene therapy-based enzyme replacement strategy has been evaluated in the retina of *Ppt1* ko mice. In this study, an AAV2 serotype which shows a tropism to retinal ganglion cells has been used to express PPT1 in the mutant retina. Accordingly, intravitreal injections of AAV2-hPPT1 into the mutant mice resulted in the expression of large amounts of PPT1 in RGCs. Of note, deterioration of retinal function as assessed by ERG recordings was significantly delayed in the treated eyes. However, loss of photoreceptor cells was not significantly delayed when compared to control retinas, possibly due to the restricted location of the transgene within ganglion cells and/or diffusion of only small amounts of the transgene into the photoreceptor cell layer RGCs [26].

In the present thesis, we injected self-complimentary AAVshH10-CTSD intravitreally into P5 *Ctsd* wt and ko mice. scAAVshH10 has a tropism to retinal glial cells and retinal pigment epithelial (RPE cells). Accordingly, we observed CTSD transgene expression restricted to retinal astrocytes, Müller cells and RPE cells. Transgene expression was already detectable as early as 4 days post injection. According to biochemical analyses of treated retinas, the amount of intermediate CTSD and mature CTSD was 5 times and 7 times higher respectively than in wt retinas, and massively increased when compared to CTSD-NSCs treated retinas. In addition, CTSD activity in scAAVshH10-CTSD

treated retinas was not statistically different from untreated wt retinas. However, eyes injected with the highest titer (1.23×10^{13} v.g./ul) of scAAVshH10-CTSD were atrophied, demonstrating negative side effect of large amounts of CTSD re-expressing in *Ctsd* ko retina. In conclusion, gene therapy-based enzyme replacement strategy provides a means to continuously administer relevant amounts of lysosomal enzymes to diseased tissues. Since a gene therapy-based enzyme replacement strategy represents an irreversible therapeutic approach, the titer of the virus needs to be strictly controlled to avoid harmful side effects of the transgene.

4.2 A hallmark of NCL: accumulation of storage material

Accumulation of intracellular autofluorescent storage material is associated with aging and certain diseases, including lysosomal storage disorders [4]. The storage material in NCLs consists of proteins, lipids, metals and dolichols [142]. The major protein compounds of the storage material in NCL diseases are the subunit c of mitochondrial ATP synthase (SCMAS) and/or the sphingolipid activating proteins A and D (saposinA and saposinD) in varying compositions in different NCL forms [142-145]. At the ultrastructural level, storage bodies comprise electron dense structures that are surrounded by lysosomal membranes. Granular structures within lysosomes are supposed to be the initial stages of ceroid accumulation, while lamellated structures are more characteristic for the end stages of storage body formation. Depending on the specific NCL form, ultrastructural lipopigment structures display one or a mixture of several of the following features: granular osmiophilic deposits (GRODs), alternating dark and light short curved thin lamellar stacks (curvilinear profiles, CLP), loosely stacked membranous bodies (rectilinear complex, RLC) and similar stacks that have fingerprint like appearance (fingerprint profiles, FPP) [22, 146]. In general, storage material accumulates as a result of altered lysosomal function, autophagic disruptions, and oxidative damage of proteins [4].

4.3 Storage material and neurodegeneration

While accumulation of storage material is a hallmark of NCLs, it is a matter of discussion whether the material is a direct cause of neurodegeneration in these diseases. In fact, some studies reported that there is no strict spatio-temporal correlation between the appearance of storage material and the loss of nerve cells. For instance, in a CLN6 sheep model, storage bodies were evenly distributed throughout all regions of the brain instead of being concentrated in specific cortical areas where neuronal degeneration occurred [147]. Furthermore, massive accumulation of storage material was observed in AAV-CTSD treated brains of *Ctsd* ko mice that survived long-term after treatment but did not show significant neurological symptoms [82].

In the *Ctsd* ko retina, we also found no strict correlation between the appearance of storage material and neurodegeneration. First elevation of SCMAS and saposinD levels were observed in the inner *Ctsd* ko retina at P5. The amount of storage material increased with increasing age of the animals, and became evident in the outer retina at relatively late stages of the disease. Loss of neurons, on the contrary, was first evident in the outer nuclear layer, and only later in the inner nuclear layer and the ganglion cell layer. Furthermore, intravitreal injections of rhCTSD resulted in a decrease of storage material accumulation in the *Ctsd* ko retina, but not in a rescue of retinal cells [74]. All these data suggest that accumulation of storage material might not be causally linked to neurodegeneration.

In this thesis work, we found a significant decrease of saposinD and SCMAS after intravitreal transplantations of CTSD-NSCs. However, the amount of storage materials in treated *Ctsd* ko retinas was still high when compared to wt retinas. In addition, decreased amounts of storage material had no impact on the progression of neurodegeneration in CTSD-NSCs treated retinas. In comparison, intravitreal injections of scAAVshH10-CTSD essentially prevented accumulation of saposinD and SCMAS in *Ctsd* ko retinas, and the marked clearance of storage material coincided with a significant preservation of retinal neurons. Together, we found no strict spatio-temporal correlation between storage material accumulation and neurodegeneration in untreated *Ctsd* ko retinas, while we observed a coincidence between the amount of

storage material and the extent of neurodegeneration in treated *Ctsd* ko retinas. Clearance of storage material in scAAVshH10-CTSD treated retinas was markedly more pronounced than in rhCTSD or CTSD-NSCs treated retinas, in line with the significantly higher levels of CTSD in retinas of the former group.

4.4 Lysosomal and autophagic dysfunction

Abnormal lysosomal biogenesis is another characteristic feature in dystrophic retinas of mouse models of different NCL forms, including CLN6, CLN7 and CLN11 disease [41, 84, 148]. Upregulation of various lysosomal proteins may be regulated by the transcription factor EB (TFEB) as a result of lysosomal stress due to the accumulation of storage material [149-151]. Under physiological conditions, TFEB is phosphorylated by the lysosome-associated mammalian target of rapamycin complex 1 (mTORC1) and is retained as an inactive form in the cytosol [152]. However, under pathological conditions, TFEB become activated and is upregulated in several NCL models, resulting in elevated expression levels of various lysosomal enzymes and blockage of the autophagic flux [153, 154]. Impaired autophagy is thus a characteristic feature of many lysosomal storage disorders [74, 155, 156].

Autophagic dysfunction is indicated by elevated levels of autophagic markers such as SQSTM1/p62 and microtubule-associated protein 1 light chain 3-II (LC3-II) [40, 157-162]. Accumulation of extralysosomally located SQSTM1/p62-positive punctae have been reported in mouse models deficient in PPT1, TPP1 or arylsulfatase G [84, 163, 164]. The reason for the extralysosomal location of SQSTM1/p62 is unclear, but may be related to either an impaired fusion of autophagosomes with lysosomes, or to an increased permeability of the lysosomal membranes and leakage into the cytosol.

In this thesis, we found an elevated expression of LAMP1, LAMP2 and CTSX/Z/P in the inner retina of *Ctsd* ko mice as early as at P5. Levels of these lysosomal proteins further increased with increasing age of the animals, and abnormally high levels became also apparent in the outer retina. The spatiotemporal expression pattern of these lysosomal proteins was similar to that of storage material accumulation, indicating that it is caused by lysosomal

stress and implicating TFEB in the control of this upregulation. Different to the dysregulated expression of LAMP1, LAMP2 or CTSX/Z/P, SQSTM1/p62-positive punctae became first detectable in the outer retina of P5 *Ctsd* ko mice, from where it shifted to the inner retina in older animals. The spatio-temporal appearance of SQSTM1/p62-positive punctae was similar to that of retinal cell death, indicating that accumulation of SQSTM1/p62 might be a predictive factor of retinal degeneration in *Ctsd* ko mouse model. Interestingly, SQSTM1/p62 did not colocalize with LAMP2 in the *Ctsd* ko retina, suggesting impaired fusion of autophagosomes and lysosomes.

Intracranial administration of rhCTSD resulted in restoration of hexosaminidase B (HEXB) activity and LAMP1 levels to wt levels in the brain of P23 *Ctsd* ko mice, suggesting a significant attenuation of lysosomal hypertrophy after ERT. At the same time, SQSTM1/p62 and LC3-II were also reduced to WT levels, indicating correction of the autophagic flux after treatment with recombinant CTSD [74]. Similarly, intravitreal injections of rhCTSD also decreased the levels of LAMP1 and LAMP2 in *Ctsd* ko retina when compared to contralateral control eyes. In addition, SQSTM1/p62-positive punctae were significantly reduced in mutant retinas after treatment with rhCTSD. The combined data indicate that ERT with human recombinant CTSD resulted in partial correction of the lysosomal and autophagic dysfunction in *Ctsd* ko retinas [74].

In the present study, levels of LAMP1, LAMP2 and CTSX/Z/P were significantly reduced in retinas from eyes with transplanted CTSD-NSCs when compared to retinas from contralateral control eyes. However, levels of these proteins were still significantly higher than in wt retinas. The reduction of LAMP1, LAMP2 and CTSX/Z/P was more pronounced in scAAVshH10-CTSD treated *Ctsd* ko retinas. In fact, the amount of these proteins was similar to that found in healthy wt retinas. Similarly, there was a detectable decrease of SQSTM1/p62 in CTSD-NSCs treated retinas, although it did not reach statistical significance when compared to contralateral eyes. Intravitreal scAAVshH10-CTSD injections, in comparison, restored SQSTM1/p62 levels to those observed in healthy wt retinas. In summary, lysosomal and autophagic dysfunction in *Ctsd* ko retinas was partially corrected after ERT or the NSC-based enzyme replacement strategy. However, the AAV-mediated gene

therapy approach decreased the expression of the lysosomal proteins and the autophagy marker to a similar level as found in wt retinas, in line with the higher amounts of CTSD in *Ctsd* ko retinas after scAAVshH10-CTSD treatment when compared to the other two treatment strategies.

4.5 The role of neuroinflammation in disease progression in NCL

Neuroinflammation as assessed by reactive microgliosis and reactive astrogliosis accompanies or precedes neurodegeneration in different NCLs, and has been implicated in the progression of the neuropathological [165] [18]. Results from several studies showed that microglia and astrocytes in their activated states became evident before the onset of neuron loss, and that their initial localization more accurately predicted regions of neurodegeneration than the spatial appearance of storage material accumulation [9, 18] This spatio-temporal correlation between neuroinflammation and neurodegeneration raised the question of whether neuroinflammation is, at least in part, a cause of neuron loss in NCLs, as has been suggested for various other neurodegenerative disorders [166-169]. Pharmacological inactivation of microglia/macrophages using the CSF-1R inhibitor PLX3397 resulted in attenuation of axonal damage and neuron loss in the CNS of *Ppt1* ko mice, and ameliorated motor dysfunction and visual deterioration, and increased lifespan of the mutant mice [170]. Several other studies on animal models of CLN1, CLN3 and CLN6 disease have also demonstrated a critical role of the innate and adaptive immune system in the progression of the neuropathology in brain and retina [42, 95, 171-173].

Some studies have provided data that explain how reactive astrogliosis and microgliosis affects disease progression in NCL. For instance, studies on the brain and retina of *Ctsd* ko mice have demonstrated that reactive microgliosis is particularly pronounced in brain regions characterised by significant neurodegeneration, such as the thalamus and the inner retina. Here, reactive microglia may have an impact on neurodegeneration through the release of neurotoxic nitric oxide (NO) [49, 139, 174]. Of note, multiple

intraperitoneal injections of NO inhibitors resulted in a significant decrease of apoptotic cells in the thalamus and the inner retina of treated *Ctsd ko* mice [49, 139]. Another study showed that astrocytes and microglia from *Cln3 ko* mice showed an attenuated morphological transformation and an altered secretion of several proteins upon stimulation *in vitro*. For instance, activated astrocytes showed decreased secretion levels of several neurotrophic factors, chemokines, cytokines and mitogens, and impaired clearance of glutamate. Interestingly, via mixed culture approach, microglia and astrocytes from *Cln3 ko* mice exerted adverse effects on the morphology and survival of neurons from both *Cln3 ko* and healthy wt mice. Similar effects on *Cln3 ko* neurons were not observed when cells were co-cultured with glia cells from wt mice [175]. In addition, reactive astrocytes and microglia cells might negatively affect synaptic function [169, 176-179]

4.6 The impact of enzyme replacement strategies on neuroinflammation

In *Ctsd ko* mice, intracranial injection of rhCTSD resulted in less pronounced astrogliosis and microgliosis in the cortex and thalamus of 23 days old mutants. Furthermore, reactive microgliosis as assessed by the number of CD68-positive microglia/macrophages was also attenuated in the retina following intravitreal injections of rhCTSD [74]. An AAV-mediated gene therapy was even more efficacious in attenuating microglia cell activation than the ERT approach. Bilateral injections of AAV1/2-CTSD into the brain hemispheres resulted in complete prevention of reactive microgliosis in P27 or even P62 *Ctsd ko* mice. Furthermore, mice that received unilateral AAV-CTSD injections only showed very mild activation of microglia in the contralateral hemisphere at P27. However, some AAV-CTSD treated *Ctsd ko* mice which survived until the fourth postnatal month showed massive reactive microgliosis but no significant neurological symptoms. Contrary to the results discussed above, this observation suggests that reactive microgliosis does not play a critical role for disease progression [82].

In the *Ctsd* ko retina, evidence for reactive microgliosis as assessed by the appearance of CD68-positive cells became evident as early as at P5 in inner retinal layers. Early onset microgliosis coincided with the early degeneration of cone photoreceptor cells at P5. In older mice, reactive microglia cells were present in all retinal layers and the subretinal space. In addition, reactive retinal astrocytes and Müller cells became evident at P10 in *Ctsd* ko retinas, and expression of GFAP in these cells progressively increased until the late stage of the disease at P25. Together, these data demonstrate an early-onset reactive microgliosis and astrogliosis in the mutant retina.

A previous study showed that intravitreal administrations of 3.1mg/ml (3.1ug) rhCTSD at P7 and P14 resulted in uptake of the enzyme by several cell types of the *Ctsd* ko retina, including astrocytes, Müller cells and microglia/macrophages. Interestingly, the number of CD68-positive microglia/macrophages was significantly decreased in rhCTSD treated retinas at P23 when compared to the contralateral control eyes [74]. In this thesis, we transplanted NSCs with an overexpression of CTSD into the vitreous of P7 *Ctsd* ko mice. In these animals, we found a more pronounced attenuation of reactive microgliosis and an attenuation of astrogliosis at P22. Of note, reactive microgliosis and astrogliosis was almost prevented in *Ctsd* ko mice that received intravitreal injections of scAAVshH10-CTSD at P5. Retinal microglia, Müller cells and astrocytes colocalized with CTSD in *Ctsd* ko retinas injected with scAAVshH10-CTSD. While attenuation of reactive microgliosis and astrogliosis in CTSD-NSCs treated retinas did not coincide with attenuation of retinal degeneration, almost complete prevention of microgliosis and astrogliosis coincided with preservation of retinal neurons in AAV-CTSD treated retinas. However, these data do not solve the question whether reactive microgliosis and astrogliosis is a cause or merely a consequence of retinal degeneration in the *Ctsd* ko retina.

4.7 Loss of photoreceptors and bipolar cells

Retinal degeneration is a characteristic pathological hallmark of most NCL forms. The progression and severity of the retinal dystrophy, and the affected

retinal nerve cell types may vary between different NCL forms [180]. In the *Ctsd* ko retina, we observed a very early onset and rapidly progressing retinal dystrophy. Retinal thinning was significant as early as at P15, and progressed rapidly until the end stage of the disease at P25. The pronounced retinal thinning of the *Ctsd* ko retina was mainly the result of a severe and almost complete atrophy of the outer nuclear layer. Retinal interneurons in the inner nuclear layer and ganglion cells in the ganglion cell layer were less severely affected. Of note, cone and rod photoreceptor cells were differentially affected in the mutant. While cone numbers were already significantly reduced at postnatal day 5, rod numbers started to decrease at postnatal day 15. At the end stage of the disease at P25, both cones and rods were almost completely lost. A significant loss of cone and rod bipolar cells became evident at P20, and was pronounced at P25. A similar time course of degeneration was observed for retinal ganglion cells. At the end stage of the disease, horizontal cells were also reduced in number. CTSD deficiency thus affects all retinal nerve cell types in the mouse retina, albeit to a different extent and at different time points during disease progression.

An early-onset and rapidly progressing loss of photoreceptors has also been observed in mouse models of other NCL forms, such as CLN4 [181], CLN5 [40], CLN6 [41-43, 182], CLN7 [148] and CLN8 [45-47, 183, 184]. The frequent involvement of photoreceptor cells indicates that this retinal nerve cell type is particularly vulnerable to lysosomal dysfunctions. The identification of a few CLN3 and CLN7 patients presenting with a non-syndromic retinal dystrophy primarily characterized by a loss of photoreceptor cells is in line with this view [16, 185-194]. Photoreceptor cells are also the most severely affected cell type in the *Ctsd* ko retina, with cones degenerating at a more rapid rate than rods. As cone numbers were already reduced at P5, the earliest developmental age analyzed, it remains unclear whether the early decrease in cone number is due to a very early onset degeneration or a developmental defect or both.

While most studies on retinal degeneration in NCL are focused on photoreceptor cells, there are also several studies demonstrating that retinal degeneration initially starts in the inner retina. In CLN1 and CLN3 mouse models and a CLN2 canine model, for instance, significant neurodegeneration was first apparent in the inner nuclear layer. Furthermore, ERG recordings

revealed a reduction of the b wave, suggesting that the first abnormality of retinal function is related to a defect in bipolar cells [24, 25, 27, 34, 37, 71, 84, 195, 196]. Furthermore, as stated above, photoreceptor cells are the first cells that are affected in a CLN6 mouse model [41, 42]. However, targeting retinal photoreceptors with an AAV2/8-CLN6 vector failed to protect photoreceptors from cell death. In contrast, a *CLN6* gene transfer to bipolar cells using an AAV2/2 variant 7m8 vector resulted in preservation of the morphology and function of photoreceptors in this mouse model. Results suggest that a defect in bipolar cells is the cause of photoreceptor degeneration in the CLN6 mouse models. Of note, degeneration of bipolar cells in this animal model starts only after a significant percentage of photoreceptor cells is already lost [91].

Intravitreal administration of rhCTSD failed to attenuate retinal degeneration in the *Ctsd* ko mouse [74]. In the present thesis, we first studied the impact of intravitreally grafted CTSD-NSCs on retinal degeneration in *Ctsd* ko mice. However, analyses of mutant retinas at P22 revealed no positive therapeutic effects on retina structure, suggesting that we failed to target sufficient amounts of CTSD to the dystrophic retina using this treatment strategy. Anticipating that a gene therapy approach will enable us to administer higher amounts of CTSD to the mutant retina, we injected scAAVshH10-CTSD into *Ctsd* ko eyes. Injections of scAAVshH10-CTSD at low titer (4.75×10^{11} v.g./ul) had similar effects on the biochemical phenotype as observed with ERT and the CTSD-NSCs treatment strategy, in that pathological marker for lysosomal and autophagic dysfunction were partially corrected but retinal degeneration was not prevented. However, after injections of scAAVshH10-CTSD with a higher titer (2.46×10^{12} v.g./ul), cone photoreceptors were found colocalized with CTSD in the *Ctsd* ko retinas with scAAVshH10-CTSD injected, and thinning of the outer nuclear layer was significantly attenuated. More detailed morphological analyses of these retinas revealed the presence of significant number of cone and rod photoreceptor cells that displayed an apparently normal morphology. In the contralateral control eyes injected with a GFP encoding vector, in comparison, all photoreceptor cells lost. Immunoblot analyses revealed the presence of about 5 to 7 times more CTSD in scAAVshH10-CTSD treated retinas than in wt retinas. Furthermore, the enzymatic CTSD activity in the treated retina was in the range of the enzymatic

activity found in untreated healthy wt retinas. Studies on other lysosomal storage disorders showed that restoration of 10-15% of the enzymatic activity normally observed in healthy tissues may be sufficient to achieve meaningful therapeutic effects [197]. For instance, two intravitreal injections of rhTPP1 in a CLN2 canine model significantly rescued retinal cells in the inner and outer nuclear layer from cell death and preserved the function of photoreceptors and bipolar cells, although the amount of TPP1 was low and almost undetectable in the aqueous and vitreous after an extended time period after the injection [73]. Similarly, intravitreal transplantation of mesenchymal stem cells overexpressing TPP1 resulted in prevention of disease-related retinal detachments and attenuation of retinal thinning and ERG amplitude reduction, but the effect on retinal function in a high dose treatment group was better than that found in a low dose treatment group [87]. On the contrary, PPT1 ko mice that received intravitreal injections of AAV2-PPT1 showed improved cone and mixed rod/cone responses in ERG recordings, but no rescue of photoreceptors despite the fact that the PPT1 enzymatic activity in treated retinas was about 5 times higher than in wt retinas [26].

Targeting of CTSD specifically to RPE cells might represent a promising therapeutic strategy for the treatment of retinal degeneration in CLN10 disease. The detailed analysis of the retinal phenotype of *Ctsd* ko mice has clearly shown that neurodegeneration starts in the outer nuclear layer from where it spreads to the inner retinal layers. While CTSD is expressed in all retinal cell types, the enzyme is particularly abundant in RPE cells [198], where it plays an important role in the removal of shed photoreceptor outer segments. Thus, dysfunction of RPE cells as a result of CTSD deficiency might be the cause for the early loss of photoreceptors in mutant retina. Of note in this context, the scAAVshH10 serotype showed a tropism for RPE cells, and the gene therapy approach resulted in much higher amounts of CTSD in RPE cells than the ERT or the CTSD-NSCs treatment approach. It will be interesting to test this hypothesis in future experiments.

Intravitreal injections of rhCTSD or transplantations of CTSD-NSCs had no effect on the extent of bipolar cell degeneration. scAAVshH10-CTSD injected *Ctsd* ko retinas, in comparison, contained significantly more rod bipolar cells, but not cone bipolar cells, than the corresponding control retinas, although both

of rod bipolar cells and cone bipolar cells colocalized with CTSD in treated retinas. Data from the phenotypic analysis of the *Ctsd* ko retina provide an explanation for this apparently limited treatment effect on bipolar cells. In untreated *Ctsd* ko retinas, rod bipolar cells are significantly reduced in number at P20 while the loss of cone bipolar cells is moderate at this age. Massive loss of cone bipolar cells occurs later between postnatal day 20 and 25. However, the analysis of scAAVshH10-CTSD was performed on P22 retinas due to ethical issues in animal experimentation.

In conclusion, intravitreal injections of scAAVshH10-CTSD into *Ctsd* ko mice represent a promising strategy to treat retinal degeneration in CLN10 disease, as demonstrated by the remarkable therapy effects on the biochemical and morphological phenotype of the mutant retina. Treatment effects of the gene therapy approach were significantly more pronounced than those observed with either ERT or a cell-based enzyme replacement strategy. It would have been of interest to additionally assess the impact of the different treatment strategies on retinal function. However, such experiments were impossible to perform on the severely affected mice at the end stage of the disease. Given that a brain-directed gene therapy approach has been demonstrated to significantly prolong the lifespan of the mutant, a combination of a brain- and a retina-directed gene therapy might represent a strategy to analyze the impact of the treatment on retinal function. The limited therapy effects observed with ERT or the NSC-based enzyme replacement strategy suggest that relatively large amounts of CTSD need to be administered to attenuate the progression of the retinal dystrophy in CLN10. However, both treatment strategies might be applicable to other lysosomal storage disorders where only relatively minor levels of the normal enzyme activity have to be restored in order to achieve a positive therapy outcome.

5 Summary

Loss of vision as a result of retinal degeneration is among the characteristic symptoms of neuronal ceroid lipofuscinosis (NCL). The frequent involvement of the retina and the identification of NCL patients presenting with non-syndromic retinal dystrophies indicates a particular sensitivity of the retina to lysosomal dysfunctions. CLN10 disease, also known as congenital NCL, is the most severe NCL form and caused by mutations in the gene encoding the lysosomal enzyme cathepsin D (CTSD). To obtain insights into the retinal dystrophy associated with mutations in the *CTSD* gene at the cellular and molecular level, we performed an in-depth analysis of the retinal phenotype of a *Ctsd* knockout (*Ctsd* ko) mouse, an animal model of CLN10 disease. Retinal degeneration in this mutant mouse was characterized by an early-onset accumulation of storage material, a pronounced dysregulation of various lysosomal proteins, and an upregulation of the autophagy marker sequestosome 1 (SQSTM1)/p62. At the cellular level, we found an early loss of cone photoreceptor cells which was followed by the degeneration of rod photoreceptors, rod and cone bipolar cells, ganglion cells and amacrine cells. Rapid degeneration of multiple retinal cell types was accompanied by a massive reactive microgliosis and astrogliosis.

Data from the phenotypic analysis of the *Ctsd* ko retina served as a reference for experiments aimed at evaluating the impact of a continuous administration of an enzymatically active CTSD variant on the progression of the retinal dystrophy. Functional CTSD was administered to the *Ctsd* ko retina using intravitreal transplantations of a neural stem cell line overexpressing CTSD (CTSD-NSCs) or intravitreal injections of an adeno-associated virus (AAV) vector encoding CTSD (scAAVshH10-CTSD). Injections of a *Ctsd* ko NSC line (ko-NSCs) or an AAV encoding green fluorescent protein (scAAVshH10-GFP) into the contralateral eyes served as controls. CTSD released from the grafted CTSD-NSCs was taken up by retinal cells, and partially reduced the amount of storage material, partially corrected the dysregulation of lysosomal proteins, decreased the expression of SQSTM1/p62 and attenuated reactive microgliosis and astrogliosis. However, the treatment did not rescue retinal cell types from degeneration. Compared to the cell-based approach, the gene therapy approach resulted in higher amounts of CTSD protein and a higher CTSD enzymatic activity in the mutant retinas. In line with these data, accumulation of storage material was almost completely prevented, lysosomal proteins were expressed at almost normal levels, and upregulation of SQSTM1/p62 was prevented. More importantly, we found a significant preservation of the retinal morphology. The gene therapy treatment significantly delayed the loss of cone and rod photoreceptor cells and rod bipolar cells.

Together, the present thesis provides detailed data about the retinal phenotype of a mouse model of CLN10 disease at the cellular and molecular level. The preclinical therapy experiments suggest that gene therapy represents a promising strategy to treat retinal degeneration in CLN10 disease, and possibly retinal dystrophies associated with other lysosomal storage disorders that are caused by dysfunctions of lysosomal enzymes.

6 Zusammenfassung

Eine Erblindung als Folge einer retinalen Degeneration gehört zu den charakteristischen Symptomen der Neuronalen Ceroid-Lipofuszinose (NCL). Die Häufigkeit von Erblindungen und die Identifizierung von NCL Patienten mit nicht-syndromalen retinalen Dystrophien zeigt, dass die Netzhaut besonders empfindlich auf lysosomale Dysfunktionen reagiert. Die CLN10 Erkrankung, auch als kongenitale NCL bekannt, ist die fatalste NCL Form und wird durch Mutationen in dem Gen verursacht, das für das lysosomale Enzym Cathepsin D (CTSD) kodiert. Um auf molekularer und zellulärer Ebene Einblicke in retinale Dystrophien zu erhalten, die durch Mutationen im *CTSD* Gen verursacht werden, wurde in der vorliegenden Arbeit eine detaillierte Analyse des retinalen Phänotyps einer *Ctsd* knockout (*Ctsd* ko) Maus durchgeführt, einem Tiermodell für die CLN10 Erkrankung. Die retinale Degeneration in dieser Mutante war durch eine früh beginnende Akkumulation von Speichermaterial, einer signifikanten Dysregulation verschiedener lysosomaler Proteine und einer Hochregulation des Autophagie Markers SQSTM1/p62 charakterisiert. Auf der zellulären Ebene war ein sehr früher Verlust von Zapfen-Photorezeptoren, und eine nachfolgende Degeneration von Stäbchen-Photorezeptoren, Zapfen- und Stäbchen-Bipolarzellen, Ganglienzellen und Amakrinzellen zu beobachten. Die schnell fortschreitende Degeneration der verschiedenen retinalen Zelltypen war von einer massiven reaktiven Mikroglie und Astroglie begleitet.

Die Ergebnisse der phänotypischen Analyse der *Ctsd* ko Retina wurden in der vorliegenden Arbeit als Referenzdaten für Experimente genutzt, in denen die Auswirkungen einer kontinuierlichen Administration einer enzymatisch aktiven CTSD Variante auf das Fortschreiten der retinalen Dystrophie untersucht wurde. Eine funktionale CTSD Variante wurde mittels intravitrealer Transplantationen einer CTSD überexprimierenden neuronalen Stammzelllinie (CTSD-NSCs) oder intravitrealen Injektionen eines für CTSD kodierenden Adeno-assoziierten Virus (AAV) Vektors (scAAVshH10-CTSD) in die *Ctsd* ko Netzhaut eingeschleust. Injektionen einer *Ctsd* ko NSC Linie (ko-NSCs) oder eines für "green fluorescent protein" kodierenden AAVs (scAAVshH10-GFP) in die kontralateralen Augen dienten als Kontrolle. Das von den transplantierten CTSD-NSCs abgegebene CTSD wurde von retinalen Zelltypen aufgenommen, und bewirkte eine partielle Abnahme des Speichermaterials, eine partiell korrigierte Expression von lysosomalen Proteinen, eine verminderte Expression von SQSTM1/p62 und eine Abschwächung der reaktiven Mikroglie und Astroglie. Allerdings konnte die Behandlung die Degeneration retinaler Zellen nicht verhindern. Verglichen zu diesem Zell-basierten Ansatz konnten mit der Genterapie in der Retina der Mutante größere Mengen an CTSD Protein und eine höhere enzymatische Aktivität von CTSD nachgewiesen werden. In Einklang mit diesen Daten war die Akkumulation von Speichermaterial fast vollständig inhibiert, die Expressionsstärken der lysosomalen Proteine fast vollständig normalisiert und die Hochregulation von SQSTM1/p62 nicht mehr nachweisbar. Interessanterweise war die retinale Morphologie in einem signifikanten Umfang erhalten. Durch die genterapeutische Behandlung konnte eine signifikante Verzögerung der Degeneration von Zapfen- und Stäbchen-Photorezeptoren und Stäbchen-Bipolarzellen erreicht werden.

Insgesamt wurden in der vorliegenden Arbeit detaillierte Daten zum retinalen Phänotyp eines Mausmodells für die CLN10 Erkrankung auf zellulärer und molekularer Ebene erhoben. Die präklinischen Therapieexperimente deuten an, dass eine Gentherapie eine vielversprechende Strategie darstellt, um eine retinale Degeneration bei der CLN10 Erkrankung - und möglicherweise bei anderen lysosomalen Speichererkrankungen, die durch Dysfunktionen lysosomaler Enzyme verursacht werden - zu behandeln.

7 List of abbreviations

AAV	adeno-associated virus
AD	astrocyte differentiation
ANOVA	analysis of variance
AS	astrocytes
ATP13A2	ATPase Type 13A2
BSA	bovine serum albumin
BSD	blasticidin
CAG	chicken β -actin promoter
CD68	cluster of differentiation 68
CLP	curvilinear profiles
CMV	cytomegalovirus
CNS	central nervous systems
CNTF	ciliary neurotrophic factor
CSF	cerebrospinal fluid
CTG	cardiotopography
CTSD	cathepsin D
CTSF	cathepsin F
CTSZ	cathepsin X/ZP
DAPI	4',6-diamidino-2-phenylindole
DMEM	Dulbecco's modified Eagle's medium
ECT	encapsulated cell technology
EDTA	ethylenediaminetetraacetic acid
EEG	electroencephalogram
EF1 α	elongation factor1 α
EGFP	enhanced green fluorescent protein
ERT	enzyme replacement therapy
ERG	electroretinogram
FACS	fluorescence activated cell sorting
FPP	fingerprint profiles
GAPDH	Glyceraldehyde 3-phosphate dehydrogenase

GC	Golgi complex
gcl	ganglion cell layer
GFAP	glial fibrillary acidic protein
GFP	green fluorescent protein
GRN	progranulin
GRODs	granular osmiophilic deposits
GS	glutamine-synthetase
HEK	human embryonic kidney
HEPES	hydroxyethyl piperazineethanesulfonic acid
HEXB	hexosaminidase B
IBA1	ionized calcium-binding adapter molecule 1
ICC	immunocytochemistry
iCTSD	intermediate cathepsin D
IHC	immunohistochemistry
inl	inner nuclear layer
IRES	internal ribosome entry site
KCTD7	potassium channel tetramerization domain-containing protein 7
ko	knockout
LAMP1	lysosomal-associated membrane protein 1
LAMP2	lysosomal-associated membrane protein 2
LC3-II	microtubule-associated protein 1 light chain 3-II
LSDs	lysosomal storage disorders
M6P	mannose-6-phosphate
MAP2	microtubule-associated protein 2
mCTSD	mature cathepsin D
MeCP2	methyl-CpG-binding protein 2
mdn	motor neuron degeneration
MRI	magnetic resonance imaging
MSCs	mesenchymal stem cells
mTORC1	mammalian target of rapamycin complex 1
NCLs	neuronal ceroid lipofuscinoses

NEAA	non-Essential Amino Acids
NO	neurotoxic nitric oxide
NS	neural stem cells
NSCs	neural stem cells
onl	outer nuclear layer
P	postnatal day
PA	paraformaldehyde
PCR	polymerase chain reaction
pCTSD	pro-cathepsinD
PKC α	protein kinase C-alpha
PMSF	phenylmethylsulfonyl fluoride
PPT1	palmitoyl-protein thioesterase
RER	rough endoplasmic reticulum
RGCs	retinal ganglion cells
RIPA	radioimmunoprecipitation assay
RLC	rectilinear complex
RPE	retinal pigment epithelium
saposin A	sphingolipid activator protein A
saposin D	sphingolipid activator protein D
sc	self-complementary
SCGN	secretagogoin
SDS	sodium dodecyl sulfate
SCMAS	subunit c of mitochondrial ATP synthase
SQSTM1	sequestosome 1
TFEB	transcription factor EB
TPP1	tripeptidyl peptidase 1
WB	western blot
wt	wild-type

8 References

1. Haltia, M. and H.H. Goebel, *The neuronal ceroid-lipofuscinoses: a historical introduction*. Biochim Biophys Acta, 2013. **1832**(11): p. 1795-800.
2. Mukherjee, A.B., et al., *Emerging new roles of the lysosome and neuronal ceroid lipofuscinoses*. Mol Neurodegener, 2019. **14**(1): p. 4.
3. Santavuori, P., *Neuronal ceroid-lipofuscinoses in childhood*. Brain Dev, 1988. **10**(2): p. 80-3.
4. Seehafer, S.S. and D.A. Pearce, *You say lipofuscin, we say ceroid: defining autofluorescent storage material*. Neurobiol Aging, 2006. **27**(4): p. 576-88.
5. Mole, S.E., R.E. Williams, and H.H. Goebel, *THE NEURONAL CEROID LIPOFUSCINOSES (BATTEN DISEASE)*. 2nd ed. 2011, United States: Oxford University Press.
6. Mink, J.W., et al., *Classification and natural history of the neuronal ceroid lipofuscinoses*. J Child Neurol, 2013. **28**(9): p. 1101-5.
7. Kollmann, K., et al., *Cell biology and function of neuronal ceroid lipofuscinosis-related proteins*. Biochim Biophys Acta, 2013. **1832**(11): p. 1866-81.
8. Mole, S.E. and S.L. Cotman, *Genetics of the neuronal ceroid lipofuscinoses (Batten disease)*. Biochim Biophys Acta, 2015. **1852**(10 Pt B): p. 2237-41.
9. Mole, S.E., et al., *Clinical challenges and future therapeutic approaches for neuronal ceroid lipofuscinosis*. Lancet Neurol, 2019. **18**(1): p. 107-116.
10. Jalanko, A. and T. Braulke, *Neuronal ceroid lipofuscinoses*. Biochim Biophys Acta, 2009. **1793**(4): p. 697-709.
11. Staropoli, J.F., et al., *Large-scale phenotyping of an accurate genetic mouse model of JNCL identifies novel early pathology outside the central nervous system*. PLoS One, 2012. **7**(6): p. e38310.
12. Schulz, A., et al., *NCL diseases - clinical perspectives*. Biochim Biophys Acta, 2013. **1832**(11): p. 1801-6.
13. Craiu, D., et al., *Rett-like onset in late-infantile neuronal ceroid lipofuscinosis (CLN7) caused by compound heterozygous mutation in the MFSD8 gene and review of the literature data on clinical onset signs*. Eur J Paediatr Neurol, 2015. **19**(1): p. 78-86.

14. Radke, J., W. Stenzel, and H.H. Goebel, *Human NCL Neuropathology*. Biochim Biophys Acta, 2015. **1852**(10 Pt B): p. 2262-6.
15. Anderson, G.W., H.H. Goebel, and A. Simonati, *Human pathology in NCL*. Biochim Biophys Acta, 2013. **1832**(11): p. 1807-26.
16. Chen, F.K., et al., *Clinical and molecular characterization of non-syndromic retinal dystrophy due to c.175G>A mutation in ceroid lipofuscinosis neuronal 3 (CLN3)*. Doc Ophthalmol, 2019. **138**(1): p. 55-70.
17. Khan, K.N., et al., *Specific Alleles of CLN7/MFSD8, a Protein That Localizes to Photoreceptor Synaptic Terminals, Cause a Spectrum of Nonsyndromic Retinal Dystrophy*. Invest Ophthalmol Vis Sci, 2017. **58**(7): p. 2906-2914.
18. Palmer, D.N., et al., *NCL disease mechanisms*. Biochim Biophys Acta, 2013. **1832**(11): p. 1882-93.
19. Preising, M.N., et al., *Ocular morphology and function in juvenile neuronal ceroid lipofuscinosis (CLN3) in the first decade of life*. Ophthalmic Genet, 2017. **38**(3): p. 252-259.
20. Dulz, S., et al., *Novel morphological macular findings in juvenile CLN3 disease*. Br J Ophthalmol, 2016. **100**(6): p. 824-8.
21. Williams, R.E. and S.E. Mole, *New nomenclature and classification scheme for the neuronal ceroid lipofuscinoses*. Neurology, 2012. **79**(2): p. 183-91.
22. Nita, D.A., S.E. Mole, and B.A. Minassian, *Neuronal ceroid lipofuscinoses*. Epileptic Disord, 2016. **18**(S2): p. 73-88.
23. Faller, K.M., et al., *The neuronal ceroid lipofuscinoses: Opportunities from model systems*. Biochim Biophys Acta, 2015. **1852**(10 Pt B): p. 2267-78.
24. Groh, J., et al., *Non-invasive assessment of retinal alterations in mouse models of infantile and juvenile neuronal ceroid lipofuscinosis by spectral domain optical coherence tomography*. Acta Neuropathol Commun, 2014. **2**: p. 54.
25. Lei, B., et al., *Ocular phenotype in a mouse gene knockout model for infantile neuronal ceroid lipofuscinosis*. J Neurosci Res, 2006. **84**(5): p. 1139-49.
26. Griffey, M., et al., *AAV2-mediated ocular gene therapy for infantile neuronal ceroid lipofuscinosis*. Mol Ther, 2005. **12**(3): p. 413-21.
27. Bouchelion, A., et al., *Mice homozygous for c.451C>T mutation in Cln1 gene recapitulate INCL phenotype*. Ann Clin Transl Neurol, 2014. **1**(12): p. 1006-23.

28. Jalanko, A., et al., *Mice with Ppt1Deltaex4 mutation replicate the INCL phenotype and show an inflammation-associated loss of interneurons.* Neurobiol Dis, 2005. **18**(1): p. 226-41.
29. Thada, V., et al., *Tissue-specific variation in nonsense mutant transcript level and drug-induced read-through efficiency in the Cln1(R151X) mouse model of INCL.* J Cell Mol Med, 2016. **20**(2): p. 381-5.
30. Sleat, D.E., et al., *A mouse model of classical late-infantile neuronal ceroid lipofuscinosis based on targeted disruption of the CLN2 gene results in a loss of tripeptidyl-peptidase I activity and progressive neurodegeneration.* J Neurosci, 2004. **24**(41): p. 9117-26.
31. Geraets, R.D., et al., *A tailored mouse model of CLN2 disease: A nonsense mutant for testing personalized therapies.* PLoS One, 2017. **12**(5): p. e0176526.
32. Sappington, R.M., D.A. Pearce, and D.J. Calkins, *Optic nerve degeneration in a murine model of juvenile ceroid lipofuscinosis.* Invest Ophthalmol Vis Sci, 2003. **44**(9): p. 3725-31.
33. Wavre-Shapton, S.T., et al., *Photoreceptor phagosome processing defects and disturbed autophagy in retinal pigment epithelium of Cln3Deltaex1-6 mice modelling juvenile neuronal ceroid lipofuscinosis (Batten disease).* Hum Mol Genet, 2015. **24**(24): p. 7060-74.
34. Katz, M.L., et al., *Phenotypic characterization of a mouse model of juvenile neuronal ceroid lipofuscinosis.* Neurobiol Dis, 2008. **29**(2): p. 242-53.
35. Wendt, K.D., et al., *Behavioral assessment in mouse models of neuronal ceroid lipofuscinosis using a light-cued T-maze.* Behav Brain Res, 2005. **161**(2): p. 175-82.
36. Cotman, S.L., et al., *Cln3(Deltaex7/8) knock-in mice with the common JNCL mutation exhibit progressive neurologic disease that begins before birth.* Hum Mol Genet, 2002. **11**(22): p. 2709-21.
37. Volz, C., et al., *Retinal function in aging homozygous Cln3 (Deltaex7/8) knock-in mice.* Adv Exp Med Biol, 2014. **801**: p. 495-501.
38. Eliason, S.L., et al., *A knock-in reporter model of Batten disease.* J Neurosci, 2007. **27**(37): p. 9826-34.
39. Kopra, O., et al., *A mouse model for Finnish variant late infantile neuronal ceroid lipofuscinosis, CLN5, reveals neuropathology associated with early aging.* Hum Mol Genet, 2004. **13**(23): p. 2893-906.

40. Leinonen, H., et al., *Retinal Degeneration In A Mouse Model Of CLN5 Disease Is Associated With Compromised Autophagy*. *Sci Rep*, 2017. **7**(1): p. 1597.
41. Bartsch, U., et al., *Apoptotic photoreceptor loss and altered expression of lysosomal proteins in the nclf mouse model of neuronal ceroid lipofuscinosis*. *Invest Ophthalmol Vis Sci*, 2013. **54**(10): p. 6952-9.
42. Mirza, M., et al., *Progressive retinal degeneration and glial activation in the CLN6 (nclf) mouse model of neuronal ceroid lipofuscinosis: a beneficial effect of DHA and curcumin supplementation*. *PLoS One*, 2013. **8**(10): p. e75963.
43. Morgan, J.P., et al., *A murine model of variant late infantile ceroid lipofuscinosis recapitulates behavioral and pathological phenotypes of human disease*. *PLoS One*, 2013. **8**(11): p. e78694.
44. Damme, M., et al., *Gene disruption of Mfsd8 in mice provides the first animal model for CLN7 disease*. *Neurobiol Dis*, 2014. **65**: p. 12-24.
45. Guarneri, R., et al., *Retinal oxidation, apoptosis and age- and sex-differences in the mnd mutant mouse, a model of neuronal ceroid lipofuscinosis*. *Brain Res*, 2004. **1014**(1-2): p. 209-20.
46. Chang, B., et al., *Retinal degeneration in motor neuron degeneration: a mouse model of ceroid lipofuscinosis*. *Invest Ophthalmol Vis Sci*, 1994. **35**(3): p. 1071-6.
47. Bronson, R.T., et al., *Motor neuron degeneration of mice is a model of neuronal ceroid lipofuscinosis (Batten's disease)*. *Ann Neurol*, 1993. **33**(4): p. 381-5.
48. Koike, M., et al., *Cathepsin D deficiency induces lysosomal storage with ceroid lipofuscin in mouse CNS neurons*. *J Neurosci*, 2000. **20**(18): p. 6898-906.
49. Koike, M., et al., *Involvement of two different cell death pathways in retinal atrophy of cathepsin D-deficient mice*. *Mol Cell Neurosci*, 2003. **22**(2): p. 146-61.
50. Hafler, B.P., et al., *Progressive retinal degeneration and accumulation of autofluorescent lipopigments in Progranulin deficient mice*. *Brain Res*, 2014. **1588**: p. 168-74.
51. Ward, M.E., et al., *Early retinal neurodegeneration and impaired Ran-mediated nuclear import of TDP-43 in progranulin-deficient FTL D*. *J Exp Med*, 2014. **211**(10): p. 1937-45.
52. Bond, M., et al., *Use of model organisms for the study of neuronal ceroid lipofuscinosis*. *Biochim Biophys Acta*, 2013. **1832**(11): p. 1842-65.

53. Neverman, N.J., et al., *Experimental therapies in the neuronal ceroid lipofuscinoses*. *Biochim Biophys Acta*, 2015. **1852**(10 Pt B): p. 2292-300.
54. Donsante, A. and N.M. Boulis, *Progress in gene and cell therapies for the neuronal ceroid lipofuscinoses*. *Expert Opin Biol Ther*, 2018. **18**(7): p. 755-764.
55. Geraets, R.D., et al., *Moving towards effective therapeutic strategies for Neuronal Ceroid Lipofuscinosis*. *Orphanet J Rare Dis*, 2016. **11**: p. 40.
56. Kohan, R., et al., *Therapeutic approaches to the challenge of neuronal ceroid lipofuscinoses*. *Curr Pharm Biotechnol*, 2011. **12**(6): p. 867-83.
57. Beck, M., *New therapeutic options for lysosomal storage disorders: enzyme replacement, small molecules and gene therapy*. *Hum Genet*, 2007. **121**(1): p. 1-22.
58. Wong, A.M., et al., *Current therapies for the soluble lysosomal forms of neuronal ceroid lipofuscinosis*. *Biochem Soc Trans*, 2010. **38**(6): p. 1484-8.
59. Pierret, C., J.A. Morrison, and M.D. Kirk, *Treatment of lysosomal storage disorders: focus on the neuronal ceroid-lipofuscinoses*. *Acta Neurobiol Exp (Wars)*, 2008. **68**(3): p. 429-42.
60. Kleine Holthaus, S.M., et al., *Gene Therapy Approaches to Treat the Neurodegeneration and Visual Failure in Neuronal Ceroid Lipofuscinoses*. *Adv Exp Med Biol*, 2018. **1074**: p. 91-99.
61. Johnson, T.B., et al., *Therapeutic landscape for Batten disease: current treatments and future prospects*. *Nat Rev Neurol*, 2019. **15**(3): p. 161-178.
62. Markham, A., *Cerliponase Alfa: First Global Approval*. *Drugs*, 2017. **77**(11): p. 1247-1249.
63. Schulz, A., et al., *Study of Intraventricular Cerliponase Alfa for CLN2 Disease*. *N Engl J Med*, 2018. **378**(20): p. 1898-1907.
64. Sands, M.S. and B.L. Davidson, *Gene therapy for lysosomal storage diseases*. *Mol Ther*, 2006. **13**(5): p. 839-49.
65. Lu, J.Y., et al., *Intrathecal enzyme replacement therapy improves motor function and survival in a preclinical mouse model of infantile neuronal ceroid lipofuscinosis*. *Mol Genet Metab*, 2015. **116**(1-2): p. 98-105.
66. Hu, J., et al., *Intravenous high-dose enzyme replacement therapy with recombinant palmitoyl-protein thioesterase reduces visceral lysosomal storage and modestly prolongs survival in a preclinical mouse model of infantile neuronal ceroid lipofuscinosis*. *Mol Genet Metab*, 2012. **107**(1-2): p. 213-21.

67. Katz, M.L., et al., *Enzyme replacement therapy attenuates disease progression in a canine model of late-infantile neuronal ceroid lipofuscinosis (CLN2 disease)*. J Neurosci Res, 2014. **92**(11): p. 1591-8.
68. Vuillemenot, B.R., et al., *Nonclinical evaluation of CNS-administered TPP1 enzyme replacement in canine CLN2 neuronal ceroid lipofuscinosis*. Mol Genet Metab, 2015. **114**(2): p. 281-93.
69. Chang, M., et al., *Intraventricular enzyme replacement improves disease phenotypes in a mouse model of late infantile neuronal ceroid lipofuscinosis*. Mol Ther, 2008. **16**(4): p. 649-56.
70. Whiting, R.E., et al., *Enzyme replacement therapy delays pupillary light reflex deficits in a canine model of late infantile neuronal ceroid lipofuscinosis*. Exp Eye Res, 2014. **125**: p. 164-72.
71. Whiting, R.E., et al., *Multifocal retinopathy in Dachshunds with CLN2 neuronal ceroid lipofuscinosis*. Exp Eye Res, 2015. **134**: p. 123-32.
72. Whiting, R.E.H., et al., *Intravitreal enzyme replacement preserves retinal structure and function in canine CLN2 neuronal ceroid lipofuscinosis*. Exp Eye Res, 2020. **197**: p. 108130.
73. Whiting, R.E.H., et al., *Intravitreal enzyme replacement inhibits progression of retinal degeneration in canine CLN2 neuronal ceroid lipofuscinosis*. Exp Eye Res, 2020. **198**: p. 108135.
74. Marques, A.R.A., et al., *Enzyme replacement therapy with recombinant pro-CTSD (cathepsin D) corrects defective proteolysis and autophagy in neuronal ceroid lipofuscinosis*. Autophagy, 2019.
75. Griffey, M., et al., *Adeno-associated virus 2-mediated gene therapy decreases autofluorescent storage material and increases brain mass in a murine model of infantile neuronal ceroid lipofuscinosis*. Neurobiol Dis, 2004. **16**(2): p. 360-9.
76. Griffey, M.A., et al., *CNS-directed AAV2-mediated gene therapy ameliorates functional deficits in a murine model of infantile neuronal ceroid lipofuscinosis*. Mol Ther, 2006. **13**(3): p. 538-47.
77. Macauley, S.L., et al., *Synergistic effects of central nervous system-directed gene therapy and bone marrow transplantation in the murine model of infantile neuronal ceroid lipofuscinosis*. Ann Neurol, 2012. **71**(6): p. 797-804.

78. Shyng, C., et al., *Synergistic effects of treating the spinal cord and brain in CLN1 disease*. Proc Natl Acad Sci U S A, 2017. **114**(29): p. E5920-E5929.
79. Cabrera-Salazar, M.A., et al., *Timing of therapeutic intervention determines functional and survival outcomes in a mouse model of late infantile batten disease*. Mol Ther, 2007. **15**(10): p. 1782-8.
80. Katz, M.L., et al., *AAV gene transfer delays disease onset in a TPP1-deficient canine model of the late infantile form of Batten disease*. Sci Transl Med, 2015. **7**(313): p. 313ra180.
81. Mitchell, N.L., et al., *Longitudinal In Vivo Monitoring of the CNS Demonstrates the Efficacy of Gene Therapy in a Sheep Model of CLN5 Batten Disease*. Mol Ther, 2018. **26**(10): p. 2366-2378.
82. Shevtsova, Z., et al., *CNS-expressed cathepsin D prevents lymphopenia in a murine model of congenital neuronal ceroid lipofuscinosis*. Am J Pathol, 2010. **177**(1): p. 271-9.
83. Arrant, A.E., et al., *Progranulin Gene Therapy Improves Lysosomal Dysfunction and Microglial Pathology Associated with Frontotemporal Dementia and Neuronal Ceroid Lipofuscinosis*. J Neurosci, 2018. **38**(9): p. 2341-2358.
84. Atiskova, Y., et al., *Mice deficient in the lysosomal enzyme palmitoyl-protein thioesterase 1 (PPT1) display a complex retinal phenotype*. Sci Rep, 2019. **9**(1): p. 14185.
85. Tamaki, S.J., et al., *Neuroprotection of host cells by human central nervous system stem cells in a mouse model of infantile neuronal ceroid lipofuscinosis*. Cell Stem Cell, 2009. **5**(3): p. 310-9.
86. Tracy, C.J., et al., *Intravitreal Implantation of Genetically Modified Autologous Bone Marrow-Derived Stem Cells for Treating Retinal Disorders*. Adv Exp Med Biol, 2016. **854**: p. 571-7.
87. Tracy, C.J., et al., *Intravitreal implantation of TPP1-transduced stem cells delays retinal degeneration in canine CLN2 neuronal ceroid lipofuscinosis*. Exp Eye Res, 2016. **152**: p. 77-87.
88. Jankowiak, W., et al., *Sustained Neural Stem Cell-Based Intraocular Delivery of CNTF Attenuates Photoreceptor Loss in the nclf Mouse Model of Neuronal Ceroid Lipofuscinosis*. PLoS One, 2015. **10**(5): p. e0127204.

89. Meyer, J.S., et al., *Embryonic stem cell-derived neural progenitors incorporate into degenerating retina and enhance survival of host photoreceptors*. Stem Cells, 2006. **24**(2): p. 274-83.
90. Bosch, M.E., et al., *Self-Complementary AAV9 Gene Delivery Partially Corrects Pathology Associated with Juvenile Neuronal Ceroid Lipofuscinosis (CLN3)*. J Neurosci, 2016. **36**(37): p. 9669-82.
91. Kleine Holthaus, S.M., et al., *Prevention of Photoreceptor Cell Loss in a Cln6(nc1f) Mouse Model of Batten Disease Requires CLN6 Gene Transfer to Bipolar Cells*. Mol Ther, 2018. **26**(5): p. 1343-1353.
92. Kay, G.W. and D.N. Palmer, *Chronic oral administration of minocycline to sheep with ovine CLN6 neuronal ceroid lipofuscinosis maintains pharmacological concentrations in the brain but does not suppress neuroinflammation or disease progression*. J Neuroinflammation, 2013. **10**: p. 97.
93. Macauley, S.L., et al., *An anti-neuroinflammatory that targets dysregulated glia enhances the efficacy of CNS-directed gene therapy in murine infantile neuronal ceroid lipofuscinosis*. J Neurosci, 2014. **34**(39): p. 13077-82.
94. Seehafer, S.S., et al., *Immunosuppression alters disease severity in juvenile Batten disease mice*. J Neuroimmunol, 2011. **230**(1-2): p. 169-72.
95. Groh, J., K. Berve, and R. Martini, *Fingolimod and Teriflunomide Attenuate Neurodegeneration in Mouse Models of Neuronal Ceroid Lipofuscinosis*. Mol Ther, 2017. **25**(8): p. 1889-1899.
96. Patel, S., et al., *Cathepsins: Proteases that are vital for survival but can also be fatal*. Biomed Pharmacother, 2018. **105**: p. 526-532.
97. Vasiljeva, O., et al., *Emerging roles of cysteine cathepsins in disease and their potential as drug targets*. Curr Pharm Des, 2007. **13**(4): p. 387-403.
98. Stoka, V., V. Turk, and B. Turk, *Lysosomal cathepsins and their regulation in aging and neurodegeneration*. Ageing Res Rev, 2016. **32**: p. 22-37.
99. Brix, K., et al., *Cysteine cathepsins: cellular roadmap to different functions*. Biochimie, 2008. **90**(2): p. 194-207.
100. Turk, V., et al., *Cysteine cathepsins: from structure, function and regulation to new frontiers*. Biochim Biophys Acta, 2012. **1824**(1): p. 68-88.
101. Lowry, J.R. and A. Klegeris, *Emerging roles of microglial cathepsins in neurodegenerative disease*. Brain Res Bull, 2018. **139**: p. 144-156.

102. Carcel-Trullols, J., A.D. Kovacs, and D.A. Pearce, *Cell biology of the NCL proteins: What they do and don't do*. Biochim Biophys Acta, 2015. **1852**(10 Pt B): p. 2242-55.
103. Masson, O., et al., *Pathophysiological functions of cathepsin D: Targeting its catalytic activity versus its protein binding activity?* Biochimie, 2010. **92**(11): p. 1635-43.
104. Metcalf, P. and M. Fusek, *Two crystal structures for cathepsin D: the lysosomal targeting signal and active site*. Embo j, 1993. **12**(4): p. 1293-302.
105. Whitaker, J.N. and R.H. Rhodes, *The distribution of cathepsin D in rat tissues determined by immunocytochemistry*. Am J Anat, 1983. **166**(4): p. 417-28.
106. Rakoczy, P.E., et al., *Distribution of cathepsin D in human eyes with or without age-related maculopathy*. Exp Eye Res, 1999. **69**(4): p. 367-74.
107. Bańkowska, A., et al., *Biological and diagnostic role of cathepsin D*. Roczn Akad Med Białymst, 1997. **42 Suppl 1**: p. 79-85.
108. Morikawa, W., et al., *Angiostatin generation by cathepsin D secreted by human prostate carcinoma cells*. J Biol Chem, 2000. **275**(49): p. 38912-20.
109. Piwnica, D., et al., *Cathepsin D processes human prolactin into multiple 16K-like N-terminal fragments: study of their antiangiogenic properties and physiological relevance*. Mol Endocrinol, 2004. **18**(10): p. 2522-42.
110. Lkhider, M., et al., *Cathepsin D released by lactating rat mammary epithelial cells is involved in prolactin cleavage under physiological conditions*. J Cell Sci, 2004. **117**(Pt 21): p. 5155-64.
111. Ferreras, M., et al., *Generation and degradation of human endostatin proteins by various proteinases*. FEBS Lett, 2000. **486**(3): p. 247-51.
112. Wolf, M., et al., *Cathepsin D specifically cleaves the chemokines macrophage inflammatory protein-1 alpha, macrophage inflammatory protein-1 beta, and SLC that are expressed in human breast cancer*. Am J Pathol, 2003. **162**(4): p. 1183-90.
113. Nishimura, Y., T. Kawabata, and K. Kato, *Identification of latent procathepsins B and L in microsomal lumen: characterization of enzymatic activation and proteolytic processing in vitro*. Arch Biochem Biophys, 1988. **261**(1): p. 64-71.
114. van der Stappen, J.W., et al., *Activation of cathepsin B, secreted by a colorectal cancer cell line requires low pH and is mediated by cathepsin D*. Int J Cancer, 1996. **67**(4): p. 547-54.

115. Nishimura, Y., et al., *Evidence that aspartic proteinase is involved in the proteolytic processing event of procathepsin L in lysosomes*. Arch Biochem Biophys, 1989. **271**(2): p. 400-6.
116. Egberts, F., et al., *Cathepsin D is involved in the regulation of transglutaminase 1 and epidermal differentiation*. J Cell Sci, 2004. **117**(Pt 11): p. 2295-307.
117. Kim, Y.J., et al., *Lysosomal proteases are involved in generation of N-terminal huntingtin fragments*. Neurobiol Dis, 2006. **22**(2): p. 346-56.
118. Zhou, W., et al., *Cathepsin D-mediated proteolysis of apolipoprotein E: possible role in Alzheimer's disease*. Neuroscience, 2006. **143**(3): p. 689-701.
119. Takahashi, M., et al., *Oxidative stress-induced phosphorylation, degradation and aggregation of alpha-synuclein are linked to upregulated CK2 and cathepsin D*. Eur J Neurosci, 2007. **26**(4): p. 863-74.
120. Banay-Schwartz, M., et al., *The breakdown of the individual neurofilament proteins by cathepsin D*. Neurochem Res, 1987. **12**(4): p. 361-7.
121. Jones, T.L., et al., *Susceptibilities of cardiac myofibrillar proteins to cathepsin D-catalyzed degradation*. Am J Physiol, 1983. **245**(2): p. H294-9.
122. Okitani, A., et al., *Purification of cathepsin D from rabbit skeletal muscle and its action towards myofibrils*. Biochim Biophys Acta, 1981. **662**(2): p. 202-9.
123. Simon, D.I., A.M. Ezratty, and J. Loscalzo, *The fibrin(ogen)olytic properties of cathepsin D*. Biochemistry, 1994. **33**(21): p. 6555-63.
124. Loscalzo, J., *The macrophage and fibrinolysis*. Semin Thromb Hemost, 1996. **22**(6): p. 503-6.
125. Heinrich, M., et al., *Cathepsin D links TNF-induced acid sphingomyelinase to Bid-mediated caspase-9 and -3 activation*. Cell Death Differ, 2004. **11**(5): p. 550-63.
126. Pimenta, D.C., et al., *Alpha1-antichymotrypsin and kallistatin hydrolysis by human cathepsin D*. J Protein Chem, 2000. **19**(5): p. 411-8.
127. el-Hifnawi, E., *Localization of cathepsin D in rat ocular tissues. An immunohistochemical study*. Ann Anat, 1995. **177**(1): p. 11-7.
128. Bosch, E., J. Horwitz, and D. Bok, *Phagocytosis of outer segments by retinal pigment epithelium: phagosome-lysosome interaction*. J Histochem Cytochem, 1993. **41**(2): p. 253-63.

129. Deguchi, J., et al., *Acidification of phagosomes and degradation of rod outer segments in rat retinal pigment epithelium*. Invest Ophthalmol Vis Sci, 1994. **35**(2): p. 568-79.
130. Steinfeld, R., et al., *Cathepsin D deficiency is associated with a human neurodegenerative disorder*. Am J Hum Genet, 2006. **78**(6): p. 988-98.
131. Hersheson, J., et al., *Cathepsin D deficiency causes juvenile-onset ataxia and distinctive muscle pathology*. Neurology, 2014. **83**(20): p. 1873-5.
132. Fritchie, K., et al., *Novel mutation and the first prenatal screening of cathepsin D deficiency (CLN10)*. Acta Neuropathol, 2009. **117**(2): p. 201-8.
133. Siintola, E., et al., *Cathepsin D deficiency underlies congenital human neuronal ceroid-lipofuscinosis*. Brain, 2006. **129**(Pt 6): p. 1438-45.
134. Kousi, M., A.E. Lehesjoki, and S.E. Mole, *Update of the mutation spectrum and clinical correlations of over 360 mutations in eight genes that underlie the neuronal ceroid lipofuscinoses*. Hum Mutat, 2012. **33**(1): p. 42-63.
135. Doccini, S., et al., *Early infantile neuronal ceroid lipofuscinosis (CLN10 disease) associated with a novel mutation in CTSD*. J Neurol, 2016. **263**(5): p. 1029-1032.
136. Meyer, S., et al., *Congenital CLN disease in two siblings*. Wien Med Wochenschr, 2015. **165**(9-10): p. 210-3.
137. Saftig, P., et al., *Mice deficient for the lysosomal proteinase cathepsin D exhibit progressive atrophy of the intestinal mucosa and profound destruction of lymphoid cells*. EMBO J, 1995. **14**(15): p. 3599-608.
138. Haapanen, A., et al., *In vivo MRI reveals the dynamics of pathological changes in the brains of cathepsin D-deficient mice and correlates changes in manganese-enhanced MRI with microglial activation*. Magn Reson Imaging, 2007. **25**(7): p. 1024-31.
139. Nakanishi, H., et al., *Involvement of nitric oxide released from microglia-macrophages in pathological changes of cathepsin D-deficient mice*. J Neurosci, 2001. **21**(19): p. 7526-33.
140. Klimczak, R.R., et al., *A novel adeno-associated viral variant for efficient and selective intravitreal transduction of rat Müller cells*. PLoS One, 2009. **4**(10): p. e7467.

141. Fukumoto, Y., et al., *Cost-effective gene transfection by DNA compaction at pH 4.0 using acidified, long shelf-life polyethylenimine*. Cytotechnology, 2010. **62**(1): p. 73-82.
142. Palmer, D.N., et al., *Ovine ceroid-lipofuscinosis. I: Lipopigment composition is indicative of a lysosomal proteinosis*. Am J Med Genet Suppl, 1988. **5**: p. 141-58.
143. Palmer, D.N., et al., *Ceroid lipofuscinosis in sheep. II. The major component of the lipopigment in liver, kidney, pancreas, and brain is low molecular weight protein*. J Biol Chem, 1986. **261**(4): p. 1773-7.
144. Palmer, D.N., et al., *Ovine ceroid lipofuscinosis. The major lipopigment protein and the lipid-binding subunit of mitochondrial ATP synthase have the same NH2-terminal sequence*. J Biol Chem, 1989. **264**(10): p. 5736-40.
145. Tynnela, J., et al., *Storage of saposins A and D in infantile neuronal ceroid-lipofuscinosis*. FEBS Lett, 1993. **330**(1): p. 8-12.
146. Elleder, M., *Primary extracellular ceroid type lipopigment. A histochemical and ultrastructural study*. Histochem J, 1991. **23**(6): p. 247-58.
147. Oswald, M.J., et al., *Glial activation spreads from specific cerebral foci and precedes neurodegeneration in presymptomatic ovine neuronal ceroid lipofuscinosis (CLN6)*. Neurobiol Dis, 2005. **20**(1): p. 49-63.
148. Jankowiak, W., et al., *Retinal Degeneration in Mice Deficient in the Lysosomal Membrane Protein CLN7*. Invest Ophthalmol Vis Sci, 2016. **57**(11): p. 4989-4998.
149. Sardiello, M., et al., *A gene network regulating lysosomal biogenesis and function*. Science, 2009. **325**(5939): p. 473-7.
150. Settembre, C. and A. Ballabio, *Lysosomal adaptation: how the lysosome responds to external cues*. Cold Spring Harb Perspect Biol, 2014. **6**(6).
151. Ballabio, A., *The awesome lysosome*. EMBO Mol Med, 2016. **8**(2): p. 73-6.
152. Settembre, C., et al., *A lysosome-to-nucleus signalling mechanism senses and regulates the lysosome via mTOR and TFEB*. EMBO J, 2012. **31**(5): p. 1095-108.
153. Chandra, G., et al., *Cln1 gene disruption in mice reveals a common pathogenic link between two of the most lethal childhood neurodegenerative lysosomal storage disorders*. Hum Mol Genet, 2015. **24**(19): p. 5416-32.

154. Nicastrì, M.C., et al., *Dimeric quinacrines as chemical tools to identify PPT1, a new regulator of autophagy in cancer cells*. Mol Cell Oncol, 2018. **5**(1): p. e1395504.
155. Seranova, E., et al., *Dysregulation of autophagy as a common mechanism in lysosomal storage diseases*. Essays Biochem, 2017. **61**(6): p. 733-749.
156. Parenti, G., D.L. Medina, and A. Ballabio, *The rapidly evolving view of lysosomal storage diseases*. EMBO Mol Med, 2021. **13**(2): p. e12836.
157. Settembre, C., et al., *A block of autophagy in lysosomal storage disorders*. Hum Mol Genet, 2008. **17**(1): p. 119-29.
158. Brandenstein, L., et al., *Lysosomal dysfunction and impaired autophagy in a novel mouse model deficient for the lysosomal membrane protein Cln7*. Hum Mol Genet, 2016. **25**(4): p. 777-91.
159. Thelen, M., et al., *Disruption of the autophagy-lysosome pathway is involved in neuropathology of the nclf mouse model of neuronal ceroid lipofuscinosis*. PLoS One, 2012. **7**(4): p. e35493.
160. Koike, M., et al., *Participation of autophagy in storage of lysosomes in neurons from mouse models of neuronal ceroid-lipofuscinoses (Batten disease)*. Am J Pathol, 2005. **167**(6): p. 1713-28.
161. Tanaka, Y., et al., *Possible involvement of lysosomal dysfunction in pathological changes of the brain in aged progranulin-deficient mice*. Acta Neuropathol Commun, 2014. **2**: p. 78.
162. von Eisenhart-Rothe, P., et al., *Failure of Autophagy-Lysosomal Pathways in Rod Photoreceptors Causes the Early Retinal Degeneration Phenotype Observed in Cln6nclf Mice*. Invest Ophthalmol Vis Sci, 2018. **59**(12): p. 5082-5097.
163. Micsenyi, M.C., et al., *Lysosomal membrane permeability stimulates protein aggregate formation in neurons of a lysosomal disease*. J Neurosci, 2013. **33**(26): p. 10815-27.
164. Kowalewski, B., et al., *Ataxia is the major neuropathological finding in arylsulfatase G-deficient mice: similarities and dissimilarities to Sanfilippo disease (mucopolysaccharidosis type III)*. Hum Mol Genet, 2015. **24**(7): p. 1856-68.
165. Bosch, M.E. and T. Kielian, *Neuroinflammatory paradigms in lysosomal storage diseases*. Front Neurosci, 2015. **9**: p. 417.

166. Garwood, C.J., et al., *Review: Astrocytes in Alzheimer's disease and other age-associated dementias: a supporting player with a central role*. *Neuropathol Appl Neurobiol*, 2017. **43**(4): p. 281-298.
167. Leyns, C.E.G. and D.M. Holtzman, *Glial contributions to neurodegeneration in tauopathies*. *Mol Neurodegener*, 2017. **12**(1): p. 50.
168. Wolf, S.A., H.W. Boddeke, and H. Kettenmann, *Microglia in Physiology and Disease*. *Annu Rev Physiol*, 2017. **79**: p. 619-643.
169. Nelvagal, H.R., et al., *Pathomechanisms in the neuronal ceroid lipofuscinoses*. *Biochim Biophys Acta Mol Basis Dis*, 2019: p. 165570.
170. Berve, K., et al., *Sex- and region-biased depletion of microglia/macrophages attenuates CLN1 disease in mice*. *J Neuroinflammation*, 2020. **17**(1): p. 323.
171. Groh, J., et al., *Immune cells perturb axons and impair neuronal survival in a mouse model of infantile neuronal ceroid lipofuscinosis*. *Brain*, 2013. **136**(Pt 4): p. 1083-101.
172. Groh, J., et al., *Sialoadhesin promotes neuroinflammation-related disease progression in two mouse models of CLN disease*. *Glia*, 2016. **64**(5): p. 792-809.
173. Dannhausen, K., C. Mohle, and T. Langmann, *Immunomodulation with minocycline rescues retinal degeneration in juvenile neuronal ceroid lipofuscinosis mice highly susceptible to light damage*. *Dis Model Mech*, 2018. **11**(9).
174. Yamasaki, R., et al., *Involvement of lysosomal storage-induced p38 MAP kinase activation in the overproduction of nitric oxide by microglia in cathepsin D-deficient mice*. *Mol Cell Neurosci*, 2007. **35**(4): p. 573-84.
175. Parviainen, L., et al., *Glial cells are functionally impaired in juvenile neuronal ceroid lipofuscinosis and detrimental to neurons*. *Acta Neuropathol Commun*, 2017. **5**(1): p. 74.
176. Shyng, C. and M.S. Sands, *Astrocytosis in infantile neuronal ceroid lipofuscinosis: friend or foe?* *Biochem Soc Trans*, 2014. **42**(5): p. 1282-5.
177. Blanco-Suárez, E., A.L. Caldwell, and N.J. Allen, *Role of astrocyte-synapse interactions in CNS disorders*. *J Physiol*, 2017. **595**(6): p. 1903-1916.
178. Colonna, M. and O. Butovsky, *Microglia Function in the Central Nervous System During Health and Neurodegeneration*. *Annu Rev Immunol*, 2017. **35**: p. 441-468.

179. Singh, A. and W.C. Abraham, *Astrocytes and synaptic plasticity in health and disease*. Exp Brain Res, 2017. **235**(6): p. 1645-1655.
180. Kohlschutter, A., et al., *Current and Emerging Treatment Strategies for Neuronal Ceroid Lipofuscinoses*. CNS Drugs, 2019. **33**(4): p. 315-325.
181. Schmitz, F., et al., *CSPalpha-deficiency causes massive and rapid photoreceptor degeneration*. Proc Natl Acad Sci U S A, 2006. **103**(8): p. 2926-31.
182. Bronson, R.T., et al., *Neuronal ceroid lipofuscinosis (nclf), a new disorder of the mouse linked to chromosome 9*. Am J Med Genet, 1998. **77**(4): p. 289-97.
183. Messer, A., et al., *Retinal degeneration in motor neuron degeneration (mnd) mutant mice*. Exp Eye Res, 1993. **57**(5): p. 637-41.
184. Seigel, G.M., et al., *Progression of early postnatal retinal pathology in a mouse model of neuronal ceroid lipofuscinosis*. Eye (Lond), 2005. **19**(12): p. 1306-12.
185. Wang, F., et al., *Next generation sequencing-based molecular diagnosis of retinitis pigmentosa: identification of a novel genotype-phenotype correlation and clinical refinements*. Hum Genet, 2014. **133**(3): p. 331-45.
186. Ku, C.A., et al., *Detailed Clinical Phenotype and Molecular Genetic Findings in CLN3-Associated Isolated Retinal Degeneration*. JAMA Ophthalmol, 2017. **135**(7): p. 749-760.
187. Wang, X., et al., *Comprehensive molecular diagnosis of 179 Leber congenital amaurosis and juvenile retinitis pigmentosa patients by targeted next generation sequencing*. J Med Genet, 2013. **50**(10): p. 674-88.
188. Roosing, S., et al., *Mutations in MFSD8, encoding a lysosomal membrane protein, are associated with nonsyndromic autosomal recessive macular dystrophy*. Ophthalmology, 2015. **122**(1): p. 170-9.
189. Jarvela, I., et al., *Clinical and magnetic resonance imaging findings in Batten disease: analysis of the major mutation (1.02-kb deletion)*. Ann Neurol, 1997. **42**(5): p. 799-802.
190. Lauronen, L., et al., *Delayed classic and protracted phenotypes of compound heterozygous juvenile neuronal ceroid lipofuscinosis*. Neurology, 1999. **52**(2): p. 360-5.
191. Wisniewski, K.E., et al., *Compound heterozygous genotype is associated with protracted juvenile neuronal ceroid lipofuscinosis*. Ann Neurol, 1998. **43**(1): p. 106-10.

192. Aberg, L., et al., *A 30-year follow-up of a neuronal ceroid lipofuscinosis patient with mutations in CLN3 and protracted disease course*. *Pediatr Neurol*, 2009. **40**(2): p. 134-7.
193. Munroe, P.B., et al., *Spectrum of mutations in the Batten disease gene, CLN3*. *Am J Hum Genet*, 1997. **61**(2): p. 310-6.
194. Kousi, M., et al., *Mutations in CLN7/MFSD8 are a common cause of variant late-infantile neuronal ceroid lipofuscinosis*. *Brain*, 2009. **132**(Pt 3): p. 810-9.
195. Katz, M.L., et al., *Retinal pathology in a canine model of late infantile neuronal ceroid lipofuscinosis*. *Invest Ophthalmol Vis Sci*, 2008. **49**(6): p. 2686-95.
196. Whiting, R.E., et al., *Pupillary light reflex deficits in a canine model of late infantile neuronal ceroid lipofuscinosis*. *Exp Eye Res*, 2013. **116**: p. 402-10.
197. Edelmann, M.J. and G.H.B. Maegawa, *CNS-Targeting Therapies for Lysosomal Storage Diseases: Current Advances and Challenges*. *Front Mol Biosci*, 2020. **7**: p. 559804.
198. Im, E. and A. Kazlauskas, *The role of cathepsins in ocular physiology and pathology*. *Exp Eye Res*, 2007. **84**(3): p. 383-8.

9 Publication 1



Article

Rapid and Progressive Loss of Multiple Retinal Cell Types in Cathepsin D-Deficient Mice—An Animal Model of CLN10 Disease [†]

Mahmoud Bassal ^{1,‡}, Junling Liu ^{1,‡}, Wanda Jankowiak ¹, Paul Saftig ² and Udo Bartsch ^{1,*}

¹ Department of Ophthalmology, Experimental Ophthalmology, University Medical Center Hamburg-Eppendorf, 20246 Hamburg, Germany; mahmoubassal@outlook.com (M.B.); junling.liu@stud.uke.uni-hamburg.de (J.L.); wandajankowiak@gmx.de (W.J.)

² Institute of Biochemistry, Christian-Albrechts-University Kiel, 24118 Kiel, Germany; psaftig@biochem.uni-kiel.de

* Correspondence: ubartsch@uke.de; Tel.: +49-40-7410-55945

[†] A first draft of this manuscript is part of the unpublished doctoral thesis of Mahmoud Bassal.

[‡] These authors contributed equally to this work.



Citation: Bassal, M.; Liu, J.; Jankowiak, W.; Saftig, P.; Bartsch, U. Rapid and Progressive Loss of Multiple Retinal Cell Types in Cathepsin D-Deficient Mice—An Animal Model of CLN10 Disease [†]. *Cells* **2021**, *10*, 696. <https://doi.org/10.3390/cells10030696>

Academic Editor: Steven J. Pittler

Received: 19 February 2021

Accepted: 19 March 2021

Published: 21 March 2021

Publisher's Note: MDPI stays neutral with regard to jurisdictional claims in published maps and institutional affiliations.



Copyright: © 2021 by the authors. Licensee MDPI, Basel, Switzerland. This article is an open access article distributed under the terms and conditions of the Creative Commons Attribution (CC BY) license (<https://creativecommons.org/licenses/by/4.0/>).

Abstract: Vision loss is among the characteristic symptoms of neuronal ceroid lipofuscinosis (NCL), a fatal neurodegenerative lysosomal storage disorder. Here, we performed an in-depth analysis of retinal degeneration at the molecular and cellular levels in mice lacking the lysosomal aspartyl protease cathepsin D, an animal model of congenital CLN10 disease. We observed an early-onset accumulation of storage material as indicated by elevated levels of saposin D and subunit C of the mitochondrial ATP synthase. The accumulation of storage material was accompanied by reactive astrogliosis and microgliosis, elevated expression of the autophagy marker sequestosome 1/p62 and a dysregulated expression of several lysosomal proteins. The number of cone photoreceptor cells was reduced as early as at postnatal day 5. At the end stage of the disease, the outer nuclear layer was almost atrophied, and all cones were lost. A significant loss of rod and cone bipolar cells, amacrine cells and ganglion cells was found at advanced stages of the disease. Results demonstrate that cathepsin D deficiency results in an early-onset and rapidly progressing retinal dystrophy that involves all retinal cell types. Data of the present study will serve as a reference for studies aimed at developing treatments for retinal degeneration in CLN10 disease.

Keywords: bipolar cells; ganglion cells; lysosomal storage disorder; neuronal ceroid lipofuscinosis; photoreceptor cells; retinal degeneration; storage material

1. Introduction

Neuronal ceroid lipofuscinosis (NCL) comprises a group of mainly recessively inherited neurodegenerative lysosomal storage diseases usually starting in childhood [1–3]. While NCLs represent a genetically heterogeneous group of disorders, they are all characterized by the intracellular accumulation of autofluorescent storage material as a result of lysosomal dysfunction. The storage material, also termed ceroid, is composed of proteins, lipids, dolichols and metals [4]. Depending on the specific NCL form, the subunit c of mitochondrial ATP synthase (SCMAS) or sphingolipid activator proteins saposin A and D are major protein components of the storage material [4,5].

Originally classified mainly by the age at disease onset and ultrastructural characteristics of the storage material, NCLs are now grouped according to the affected gene [2,6,7]. To date, about 500 mutations (<https://www.ucl.ac.uk/ncl-disease/mutation-and-patient-database/mutation-and-patient-datasheets-human-ncl-genes>; accessed on 21 March 2021) in 13 different genes have been shown to cause different NCL forms (CLN1–8 and CLN10–CLN14) [7,8]. The identification of patients presenting with a NCL-like pathology but harboring no mutation in any of the currently known NCL-related genes suggests the

presence of additional genetically distinct forms [9]. The majority of patients affected by lysosomal storage disorders (LSDs), including NCLs, present with clinical symptoms that are neuronal in origin, such as brain atrophy, seizures, cognitive deterioration and retinopathy [10,11].

CLN10 disease is caused by mutations in the gene encoding the lysosomal enzyme cathepsin D (CTSD), a ubiquitously expressed aspartyl protease [12,13]. To date, at least 12 different pathogenic mutations have been identified in the *CTSD* gene [14]. In addition to the critical role of the enzyme in the degradation of autophagic material in lysosomes, CTSD has been implicated in diverse other functions, including the activation and degradation of hormones and growth factors, activation of enzyme precursors, processing of brain antigens and regulation of apoptosis [15,16]. Loss-of-function mutations in the *CTSD* gene cause congenital NCL, the most severe NCL variant with prenatal disease onset and death within days or weeks after birth. Affected patients present with a severe phenotype, including skull and brain deformation, microcephaly, seizures and respiratory insufficiency [14,17–19]. Patients harbouring mutations in the *CTSD* gene resulting in decreased CTSD enzymatic activity, in comparison, present with an infantile or juvenile disease onset and a milder and more slowly progressing phenotype [20–22]. At the cellular level, pronounced neurodegeneration in CLN10 patients is accompanied by reactive astrogliosis, reactive microgliosis and demyelination. The inspection of brain biopsies and extraneural tissues, such as skin or muscle, revealed the presence of storage material displaying the ultrastructure of granular osmiophilic deposits (GRODs) [17,18,20,21].

Naturally occurring and transgenic animal models carrying mutations in the *Ctsd* gene display many phenotypic similarities to affected patients [23,24]. Similar to CLN10 patients, the severity of the phenotype correlates with the level of residual enzyme activity [25–28]. Cathepsin D knockout (*Ctsd* ko) mice are born viable and initially develop normally [25]. However, mutant mice start to accumulate SCMAS- and saposin D-containing storage material in different tissues early during development [29,30]. At 2 weeks of age, *Ctsd* ko mice display a progressive regression of visceral organs. In the brain, pronounced neurodegeneration becomes apparent during the third postnatal week and is accompanied by seizures, ataxia and bradykinesia. Reactive astrogliosis and microgliosis and progressive neuronal loss in different brain regions are accompanied by an accumulation of storage material with the ultrastructure of GRODs and fingerprint profiles [25,31–33]. The rapidly progressing phenotype of mutant mice ultimately results in premature death in the fourth postnatal week [25]. Together, findings demonstrate that the *Ctsd* ko mouse recapitulates many of the characteristic pathological features of congenital CLN10 disease.

Progressive visual impairment as a result of retinal degeneration is among the characteristic clinical symptoms of most NCLs [13,34]. Ophthalmic examinations of CLN10 patients with an infantile or juvenile disease onset revealed the deterioration of the retinal function and retinal structure with similarities to retinitis pigmentosa, as assessed by electroretinogram recordings and fundus examinations, respectively [20–22,35]. A follow-up examination of one of these patients revealed retinal atrophy at advanced stages of the disease, demonstrating the progressive nature of retinal degeneration in CLN10 [20]. Retinal degeneration is also among the pathological features of *Ctsd* ko mice [29,36]. Retinal degeneration in the mutant starts around postnatal day (P) 12, resulting in almost complete loss of photoreceptor cells at P25, shortly before the animal's death [36]. Data on the progression of the retinal dystrophy, the different retinal cell types affected by the cathepsin D deficiency, and the molecular changes associated with the severe retinal pathology in this animal model are, however, limited. We, therefore, performed an in-depth analysis of the retinal phenotype of *Ctsd* ko mice, and quantified the thinning of different retinal layers, the progressive loss of various retinal cell types and the dysregulation of various lysosomal proteins. Results will serve as a reference for preclinical studies aimed at evaluating the efficacy of therapeutic strategies for the treatment of retinal degeneration in CLN10 disease.

2. Materials and Methods

2.1. Animals

Cathepsin D knockout (*Ctsd* ko) mice [25] on a C57BL/6J genetic background were obtained from heterozygous breeding pairs. Heterozygous mice displayed no pathological phenotype, in line with other studies [25,29]. We, therefore, used wild-type and heterozygous littermates as controls. Mice were genotyped using polymerase chain reaction and housed under standard conditions with ad libitum access to water and food in the animal facility at the University Medical Center Hamburg-Eppendorf (Hamburg, Germany).

2.2. Immunohistochemistry

Ctsd ko mice have a life expectancy of only around 26 days [25]. In the present study, we analysed retinas from 5-, 10-, 15-, 20-, 25-day-old *Ctsd* ko and age-matched wild-type or heterozygous mice of both sexes. Eyes were enucleated and fixed overnight in 4% paraformaldehyde (PA; Carl Roth GmbH, Karlsruhe, Germany) in phosphate buffered saline (PBS; pH 7.4). After cryoprotection with an ascending series of sucrose, eyes were frozen in Tissue-Tek (Sakura Finetek, Zouterwoude, The Netherlands) and serially sectioned with a cryostat (LEICA CM 1950, Leica Biosystems Nussloch GmbH, Nussloch, Germany) at a thickness of 25 μm , blocked in PBS (pH 7.4) containing 0.1% bovine serum albumin (BSA) and 0.3% Triton X-100 (both from Sigma-Aldrich Corp., St. Louis, MO, USA), incubated with primary antibodies (see Table 1) overnight, washed and incubated with appropriate Cy3-conjugated secondary antibodies (all diluted 1:200; all from Jackson ImmunoResearch Laboratories, West Grove, PA, USA; research resource identifiers (RRIDs): donkey anti-rat Cy3: AB_2340666; donkey anti-rabbit Cy3: AB_2307443; donkey anti-goat Cy3: AB_2307351; donkey anti-sheep Cy3: AB_2315778; donkey anti-mouse Cy3: AB_2340813). Cone photoreceptor cells were labelled with biotinylated peanut agglutinin (PNA; 1:5000; Vector Laboratories, Burlingame, CA, USA) and Cy3-conjugated streptavidin (1:500; Jackson ImmunoResearch Laboratories; RRID: AB_2337244). Preparations of retina flatmounts and immunostainings of retinal ganglion cells with antibodies to brain-specific homeobox/POU domain protein-3A (BRN-3A) were performed as described in [37,38]. Sections and flatmounts were stained with 4', 6-diamidino-2-phenylindole (DAPI; Sigma-Aldrich) before mounting. Specificity of primary antibodies was controlled in immunoblot analyses of retina extracts and/or the localization and morphology of labelled cells. To control the specificity of secondary antibodies, incubation of some retina sections with primary antibodies was omitted in each experiment.

2.3. Retina Thickness Measurements and Cell Counting

Optical sections with a thickness of 0.24 μm were taken from entire central retina sections using an AxioObserverZ.1 microscope equipped with an ApoTome.2 (Zeiss, Oberkochen, Germany) and ZEN2.3 software. The thickness of the entire retina, the outer retina (i.e., from the outer plexiform layer to the retinal pigment epithelium (RPE)) and the inner nuclear layer was measured at 18 equidistant positions between the nasal and temporal retina periphery using Fiji Image J 1.51 s software (Rasband, W.S., U.S. National Institutes of Health, Bethesda, MD, USA).

Table 1. Primary antibodies.

Antigen	Dilution	Company/Reference	Catalog Number	RRID
brain-specific homeobox/POU domain protein 3A (BRN-3A)	1:200	Santa Cruz Biotechnology Inc., Santa Cruz, CA, USA	Sc-31984	AB_2167511
calbindin	1:2000	Sigma-Aldrich, St. Louis, MO, USA	C 9848	AB_476894
cathepsin D (CTSD)	1:2000	Santa Cruz Biotechnology, Inc.	Sc-6486	AB_637896
cathepsin X/Z/P (CTS _Z)	1:100	R&D Systems GmbH	AF1033	AB_2088116
cluster of differentiation 68 (CD68)	1:1000	Bio Rad Laboratories, Kidlington, UK	MCA1957	AB_322219
arrestin	1:5000	Millipore, Temecula, CA, USA	AB15282	AB_1163387
glial fibrillary acidic protein (GFAP)	1:500	Dako Cytomation GmbH, Hamburg, Germany	Z0334	AB_10013382
ionized calcium-binding adapter molecule 1 (IBA1)	1:500	Wako Chemicals GmbH, Neuss, Germany	019-19741	AB_839504
lysosomal-associated membrane protein 1 (LAMP1)	1:2000	Santa Cruz Biotechnology, Inc.	Sc-19992	AB_2134495
lysosomal-associated membrane protein 2 (LAMP2)	1:200	Developmental Studies Hybridoma Bank, Iowa City, IA, USA	ABL93	AB_2134767
protein kinase C alpha (PKC α)	1:500	Santa Cruz Biotechnology, Inc.	Sc-208	AB_2168668
recoverin	1:3000	Millipore, Temecula, CA, USA	AB5585	AB_2253622
saposin D	1:4000	Konrad Sandhoff, Bonn, Germany [39]	N/A	N/A
secretagogin (SCGN)	1:2000	BioVendor Research and Diagnostic Products	RD184120100	AB_2034062
sequestosome 1/p62 (SQSTM1/p62)	1:1000	Enzo Life Sciences GmbH, Lörrach, Germany	BML-PW9860	AB_2196009
subunit c of mitochondrial ATP synthase (SCMAS)	1:1000	Abcam, Cambridge, UK	Ab181243	N/A

N/A, not available; RRID, research resource identifier.

Rows of photoreceptor cell nuclei were counted in both the temporal and nasal retina close to the optic disc in sections stained with DAPI and antibodies to recoverin. BRN-3A-positive ganglion cells and calbindin-positive horizontal cells with a clearly visible nucleus were counted in entire retina sections, and their numbers per 1000 μm retina length were calculated. The density of ganglion cells in retinal flatmounts was determined as described in [37,38]. Numbers of arrestin-positive cone photoreceptor cells, protein kinase C alpha (PKC α)-positive rod bipolar cells and secretagogin (SCGN)-positive cone bipolar cells with a clearly visible nucleus were determined in three equidistant areas between the retina periphery and the optic disc in both the temporal and nasal retina, each with a width of 250 μm . PNA-labelled cone inner segments in P10 and older retinas were counted in the same areas, provided they were in direct contact with the outer nuclear layer to exclude obliquely oriented inner and outer segments from neighbouring optical sections from the analysis. In P5 retinas, all of the developing and very short PNA-positive inner and outer segments were considered. The density of ionized calcium-binding adapter molecule 1 (IBA1)-positive microglia cells was determined in the inner retina (i.e., from the inner nuclear layer to the vitreal margin) and the outer retina. All thickness measurements and cell counting were performed in a blinded manner on at least six animals of each genotype and age (i.e., 10-, 15-, 20- and 25-day-old animals) unless stated otherwise. Statistical analyses of cell numbers determined in retina sections were performed using the two-way ANOVA with “age” and “genotype” as between-group factors followed by a Bonferroni post hoc test using Prism 5.02 software (GraphPad Software, San Diego, CA, USA). Statistical analyses

of ganglion cell numbers in retinal flatmounts and numbers of PNA-labelled cones in P5 retina sections were performed with an unpaired Student's *t*-test. Retinal thickness measurements were analysed using a mixed three-way ANOVA with "genotype" and "age" as between-group factors and "distance from the optic nerve head" as within-group factor followed by a Bonferroni post hoc test for the interaction between "genotype" and "age" using Statistica 7 software (StatSoft, Inc., Tulsa, OK, USA).

3. Results

Ctsd ko mice display an early-onset and rapidly progressing phenotype characterized by lymphopenia, intestinal necrosis, loss of body weight, brain atrophy, motor impairment and retinal degeneration, and die around P26 [25,29,36]. To obtain detailed information on the progression of the retinal pathology, we analysed the retinal phenotype of this mouse model of CLN10 disease at the molecular and cellular levels.

3.1. Progressive Thinning of *Ctsd* ko Retinas

The inspection of central retina sections stained with DAPI revealed an apparently normal histology of the *Ctsd* ko retina at P5 and P10 (Figure 1Ab,Ac). A significant thinning of the *Ctsd* ko retina became evident at P15 (Figure 1Ad), and was pronounced at P20 and P25 (Figure 1Ae,Af, respectively). At the latter ages, the outer nuclear layer was almost completely atrophied when compared with age-matched control retinas (for a P25 control retina, see Figure 1Ag). We next determined the thickness of the entire retina, the outer retina (i.e., from the outer plexiform layer to the RPE) and the inner nuclear layer to quantify the progression of the retinal dystrophy in *Ctsd* ko mice, and to obtain hints whether retinal cell types other than photoreceptor cells are affected in the mutant retina (Figure 1B). There was a significant effect of the interaction among the "distance from optic nerve head", "genotype" and "age" for the thickness measurements of the entire retina ($F_{51,680} = 2.04, p < 0.001$) and the outer nuclear layer ($F_{51,680} = 3.65, p < 0.001$), but not the inner nuclear layer ($F_{51,680} = 0.94, p > 0.05$). Interactions between "genotype and age" were significant for all thickness measurements (entire retina: ($F_{3,40} = 58.02, p < 0.001$); outer nuclear layer: ($F_{3,40} = 94.17, p < 0.001$); inner nuclear layer: ($F_{3,40} = 10.41, p < 0.001$). The Bonferroni post hoc test revealed no significant differences in the thickness of the entire retina (Figure 1Ba), the outer nuclear layer (Figure 1Bb) or the inner nuclear layer (Figure 1Bc) between 10-day-old mutant and age-matched wild-type mice. However, the thickness of the entire retina, outer nuclear layer and inner nuclear layer was significantly decreased when compared to age-matched wild-type mice at P15 ($p < 0.001$), P20 ($p < 0.001$) and P25 ($p < 0.001$), as indicated by the Bonferroni post hoc test (Figure 1Ba–Bc).

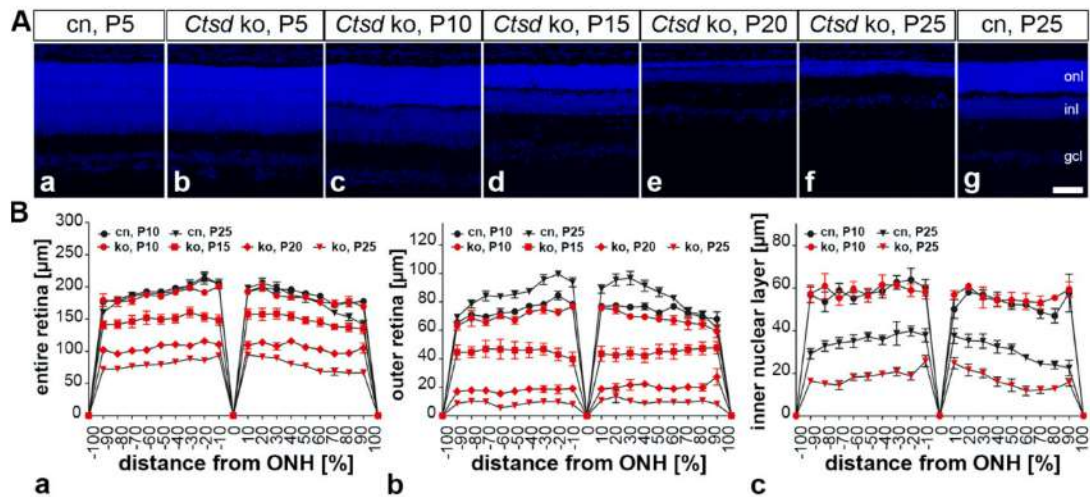


Figure 1. Progressive thinning of the *Ctsd* ko retina. (A) Retina sections from *Ctsd* ko mice at different ages (b–f) demonstrate a rapidly progressing retinal dystrophy in the mutant. Retinas from 5- (a) and 25-day-old control mice (g) are shown for comparison. (B) Quantitative analyses revealed no significant thinning of the entire retina (Ba), outer retina (Bb) or inner nuclear layer (Bc) in 10-day-old *Ctsd* ko mice when compared with age-matched control mice. Significant thinning of the entire retina (Ba), outer retina (Bb) and inner nuclear layer became apparent in 15-day-old *Ctsd* ko mice and further progressed with increasing age of the mutants (i.e., P20 and P25). For reasons of clarity, only data for selected ages are shown in (B). cn, control; gcl, ganglion cell layer; inl, inner nuclear layer; ko, knock-out; ONH, optic nerve head; onl, outer nuclear layer; P, postnatal day. Scale bar: 50 μm .

3.2. Reactive Microgliosis and Astrogliosis

To investigate the impact of CTSD deficiency on microglia cells/macrophages, retina sections were stained with anti-IBA1 and anti-cluster of differentiation 68 (CD68) antibodies. In the inner retina of 5-day-old control retinas (Figure 2Aa), the density of IBA1-positive cells was higher than in age-matched *Ctsd* ko retinas (Figure 2Ab). Quantitative analyses showed that the density of IBA1-positive cells in control mice was also increased in the inner retina, but not in the outer retina, at P10 (Figure 2B). At P15, we found a pronounced increase in the number of IBA1-positive cells in the mutant, with 362.7 ± 21.8 (mean \pm SEM) positive cells/ mm^2 in the outer retina and 380.6 ± 28.4 positive cells/ mm^2 in the inner retina compared to 41.8 ± 2.5 and 98.2 ± 4.6 positive cells/ mm^2 in the outer and inner retina of the control mice, respectively (Figure 2Ac,Ad,B; $p < 0.001$ for both comparisons; two-way ANOVA). Similar numbers of IBA1-positive cells were found in the retinas of older *Ctsd* ko mice with the only exception of the outer retina, where the density of IBA1-positive cells decreased significantly between P20 and P25 ($p < 0.001$; Figure 2Ae,Af,B). CD68-positive microglia/macrophages became detectable in the inner retina of 5-day-old mutants (Figure 2Ah). In older mutants, CD68-positive cells were found throughout all retinal layers, including the outer nuclear layer, and were also frequently found in the subretinal space (for P15 and P25 *Ctsd* ko retinas, see Figure 2Aj,AI, respectively). CD68-positive cells were essentially absent from control retinas at all ages analysed (Figure 2Ag,Ai,Ak).

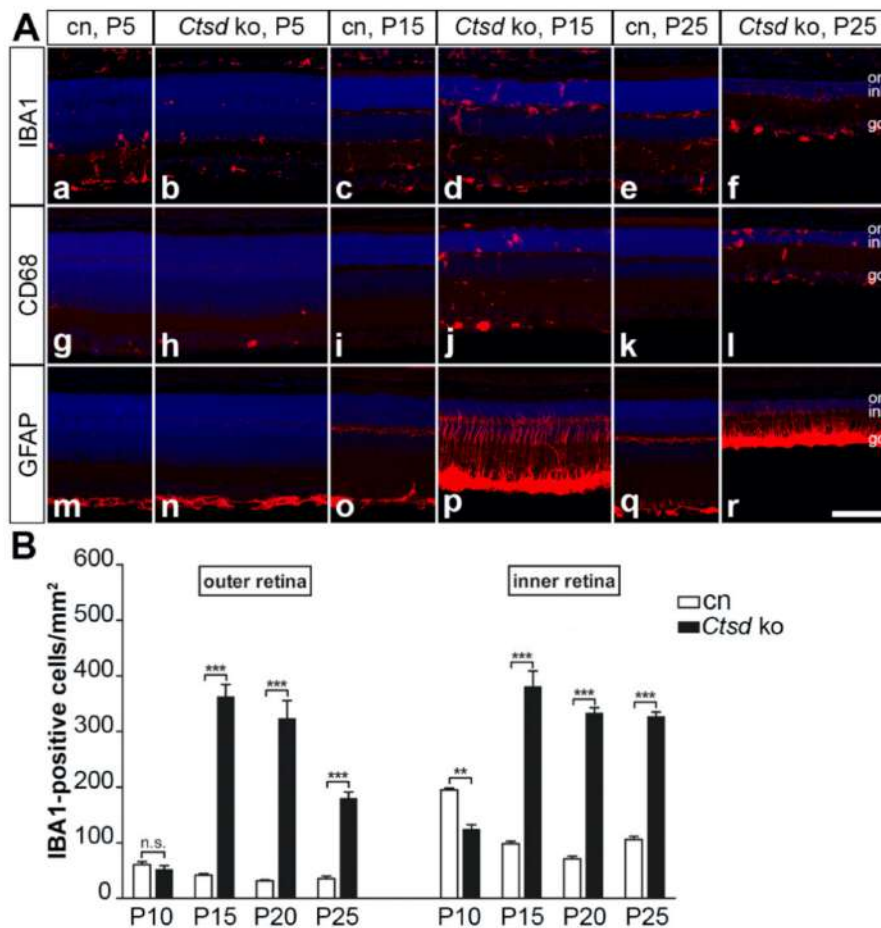


Figure 2. Reactive microgliosis and astrogliosis in *Ctsd ko* retinas. (A) At P5, IBA1-positive microglia cells were more numerous in control retinas (Aa) than in mutant retinas (Ab), while at P15 and P25, the density of IBA1-positive cells was markedly increased in mutant retinas (Ad and Af, respectively) when compared with age-matched control retinas (Ac,Ae, respectively). CD68-positive cells were confined to the inner retina of mutant mice at P5 (Ah), and increased in number and became additionally detectable in the outer nuclear layer and subretinal space of P15 (Aj) and P25 (Al). Control retinas were almost devoid of CD68-positive cells at all ages analysed (Ag,Ai,Ak). Expression of GFAP in control (Am,Ao,Aq) and P5 mutant retinas (An) was confined to retinal astrocytes. In P15 (Ap) and P25 (Ar) *Ctsd ko* retinas, expression levels of GFAP were markedly elevated in retinal astrocytes, and Müller cells were strongly GFAP-immunoreactive. (B) The density of IBA1-positive cells in the outer and inner retina of control (open bars) and *Ctsd ko* mice (filled bars) at different ages. Each bar represents the mean value (\pm SEM) of 6 animals. n.s., not significant; **, $p < 0.01$; ***, $p < 0.001$, two-way ANOVA. CD68, cluster of differentiation 68; cn, control; gcl, ganglion cell layer; GFAP, glial fibrillary acidic protein; IBA1, ionized calcium-binding adapter molecule 1; inl, inner nuclear layer; ko, knock-out; onl, outer nuclear layer; P, postnatal day. Scale bar: 100 μ m.

The expression of glial fibrillary acidic protein (GFAP) in the control retinas was confined to retinal astrocytes at all ages analysed (Figure 2Am,Ao,Aq). A similar expression pattern of GFAP was observed in 5-day-old mutant retinas (Figure 2An). In P10 *Ctsd ko* retinas, a few Müller cell processes were GFAP-positive, and GFAP expression in retinal

astrocytes was elevated compared to the control retinas (Figure S1). In older *Ctsd* ko mice, the expression levels of GFAP in retinal astrocytes were massively increased, and Müller cells were strongly GFAP-immunoreactive (for 15- and 25-day-old retinas; see Figure 2Ap,Ar, respectively).

3.3. Accumulation of Storage Material and Dysregulation of Lysosomal Proteins

To analyse the accumulation of storage material in *Ctsd* ko retinas, we performed immunostainings with antibodies to SCMAS and saposin D (Figure 3). The levels of both SCMAS (Figure 3b) and saposin D (Figure 3h) were elevated in *Ctsd* ko mice as early as at P5 when compared with the age-matched control retinas (Figure 3a,g, respectively), and further increased with the increasing age of the animals (Figure 3). SCMAS-immunoreactivity gradually shifted from inner retinal layers at P5 (Figure 3b) towards the outer retina at P15 (Figure 3d) and P25 (Figure 3f). The accumulation of saposin D also started preferentially in the inner retina and was particularly pronounced in the ganglion cell layer (Figure 3h). In older mutants, high levels of saposin D immunoreactivity were also observed in outer retinal layers (Figure 3j,l). Elevated levels of saposin D in mutant RPE cells were particularly evident at P25 (Figure S2). Compared to *Ctsd* ko retinas, levels of SCMAS- and saposin D-immunoreactivity in the control retinas were low at all ages analysed (Figure 3).

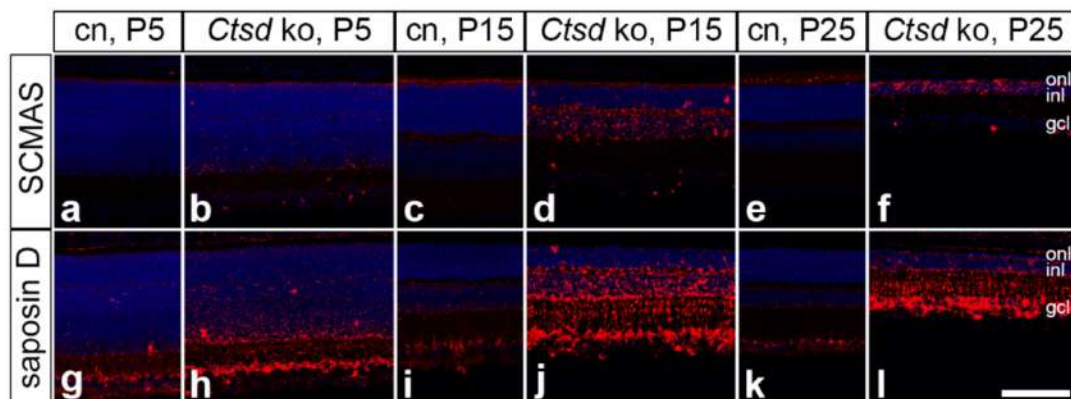


Figure 3. Accumulation of SCMAS and saposin D in *Ctsd* ko retinas. Levels of SCMAS and saposin D were moderately increased in P5 *Ctsd* ko retinas (b,h, respectively) when compared with age-matched control mice (a,g, respectively). A marked increase in SCMAS- and saposin D-immunoreactivity was observed in 15- (d,j, respectively) and 25-day-old mutant retinas (f,l, respectively) when compared to the corresponding control retinas (c,e,i,k). cn, control; gcl, ganglion cell layer; inl, inner nuclear layer; ko, knock-out; onl, outer nuclear layer; P, postnatal day; SCMAS, subunit c of mitochondrial ATP synthase. Scale bar: 100 μ m.

Next, we analysed the expression of the lysosomal proteins, lysosomal-associated membrane protein 1 (LAMP1) and lysosomal-associated membrane protein 2 (LAMP2; Figure 4). Elevated levels of LAMP1 and LAMP2 in *Ctsd* ko mice were evident as early as at P5 when compared with the control mice (compare Figure 4b with Figures 4a and 4h with Figure 4g, respectively). At this age, prominent LAMP1 and LAMP2 expression was particularly evident in the inner retina. In older *Ctsd* ko retinas, increased expression levels of both proteins were also apparent in outer retinal layers (for 15- and 25-day-old *Ctsd* ko retinas; see Figure 4d,j and Figure 4f,l, respectively). In addition, there was a pronounced increase in LAMP2 in P25 *Ctsd* ko RPE cells (Figure S2). The expression levels of the lysosomal enzyme cathepsin X/Z/P (CTSZ) were also elevated in *Ctsd* ko retinas at P5, particularly in the inner retina (compare Figure 4m,n). As the retinal pathology advanced, levels of CTSZ further increased, and also became prominent in the outer retina

(Figure 4p,r) and the RPE (Figure S2). Age-matched control retinas were almost devoid of CTSZ immunoreactivity (Figure 4o,q).

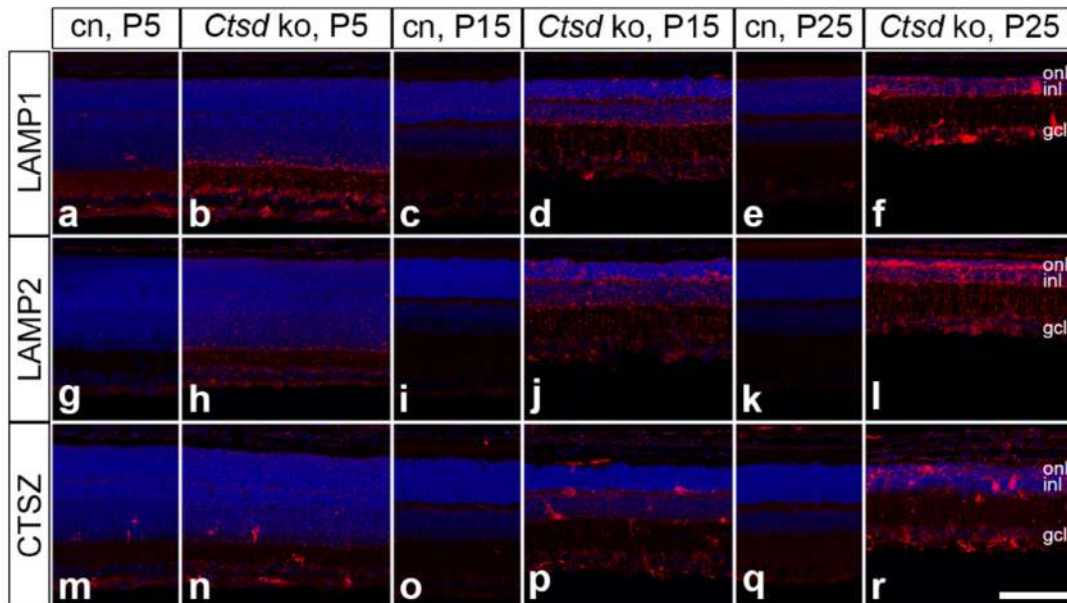


Figure 4. Dysregulation of lysosomal proteins in the *Ctsd* ko retina. LAMP1 (b), LAMP2 (h) and CTSZ (n) were moderately upregulated mainly in the ganglion cell layer and inner plexiform layer of P5 *Ctsd* ko mice when compared with age-matched control retinas (a,g,m, respectively). Expression levels of LAMP1, LAMP2 and CTSZ were further increased in P15 *Ctsd* ko retinas (d,j,p, respectively), and were prominent in all retinal layers of P25 mutant mice (f,l,r, respectively) when compared with the corresponding control retinas (c,e,i,k,o,q). Note the presence of strongly CTSZ-immunoreactive cells in mutant retinas at all ages analysed. cn, control; CTSZ, cathepsin X/Z/P; gcl, ganglion cell layer; inl, inner nuclear layer; ko, knock-out; LAMP1, lysosomal-associated membrane protein 1; LAMP2, lysosomal-associated membrane protein 2; onl, outer nuclear layer; P, postnatal day. Scale bar: 100 μ m.

3.4. Expression of the Autophagy Marker SQSTM1/p62

In 5- and 10-day-old *Ctsd* ko retinas, sequestosome 1/p62 (SQSTM1/p62)-positive punctae were mainly confined to the outer nuclear layer (Figure 5a,b). In older *Ctsd* ko mice, in comparison, the expression of SQSTM1/p62 was mainly restricted to the inner nuclear layer (Figure 5c–e), where immunoreactive punctae became progressively more prominent with the increasing age of the animals. At P25, SQSTM1/p62 became additionally detectable in the ganglion cell layer (Figure 5e). No SQSTM1/p62 expression was found in the control retinas at any age analysed (for a P25 control retina, see Figure 5f). Of note, double immunostainings with antibodies to SQSTM1/p62 and LAMP2 revealed negligible co-localization of both proteins (Figure 5g–i), suggesting the localization of SQSTM1/p62 in early autophagic vesicles which have not yet fused with lysosomes.

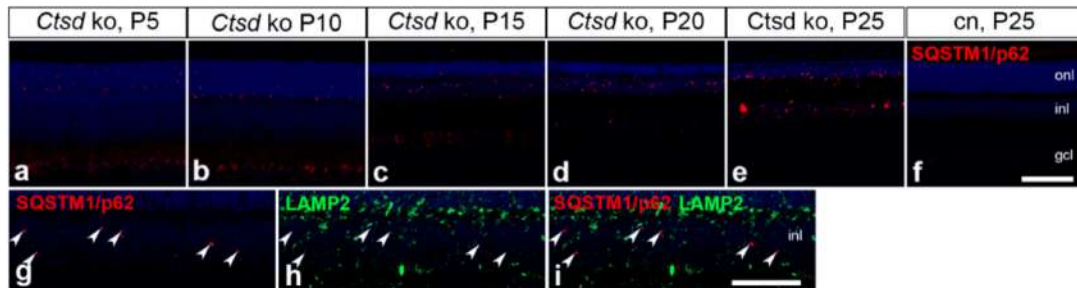


Figure 5. Expression of SQSTM1/p62 in *Ctsd* ko retinas. SQSTM1/p62-immunoreactive punctae in P5 (a) and P10 *Ctsd* ko retinas (b) were mainly restricted to the outer nuclear layer. In 15- (c), 20- (d) and 25- (e) day-old mutants, in comparison, expression of the autophagy marker was mainly confined to the inner nuclear layer. SQSTM1/p62-positive punctae were not detectable in retinas from control mice (for a P25 retina, see (f)). SQSTM1/p62 (g) and LAMP2 (h) showed hardly any co-localization (white arrowheads in g–i) in P15 *Ctsd* ko retinas. cn, control; gcl, ganglion cell layer; inl, inner nuclear layer; ko, knock-out; LAMP2, lysosomal-associated membrane protein 2; onl, outer nuclear layer; P, postnatal day; SQSTM1/p62, sequestosome 1/p62. Scale bar in (f): 100 μ m; in (i): 50 μ m.

3.5. Progressive Loss of Multiple Retinal Cell Types

Morphometric analyses of *Ctsd* ko retinas revealed a pronounced and rapidly progressing thinning of all retinal layers (Figure 1), suggesting the degeneration of multiple retinal cell types in the mutant retina. We, therefore, used a panel of cell type-specific markers to identify the retinal cell types affected by the CTSD deficiency and determined the time course of their degeneration.

3.5.1. Rod and Cone Photoreceptor Cells

In the mouse retina, cone photoreceptor cells comprise only about 3% of all photoreceptors, while the rest are rod photoreceptors [40]. To analyse whether cones and rods are differentially affected in the mutant, we stained retina sections with antibodies to cone-arrestin or with the lectin peanut agglutinin to specifically visualize cones. Remarkably, PNA staining revealed a significantly reduced number of cones in *Ctsd* ko retinas already at P5, with 29.8 ± 3.5 (mean \pm SEM) cones/250 μ m retina length in mutant retinas compared to 42.4 ± 3.4 cones/250 μ m in age-matched control retinas ($p < 0.05$, Student's *t*-test; Figure S3). The determination of cone numbers in P5 retinas with anti-cone-arrestin antibodies was impossible due to the weak expression of the antigen at this early age. However, immunostainings of 10-day-old *Ctsd* ko retinas with anti-cone-arrestin antibodies confirmed a reduced density of cones (Figure 6Ab) when compared with age-matched control retinas (Figure 6Aa). Quantitative analyses revealed that the number of cones was reduced by more than 50% in the mutant at this age, with 9.0 ± 0.8 cones/250 μ m retina length in *Ctsd* ko retinas as compared to 19.1 ± 0.6 cones/250 μ m in control retinas ($p < 0.001$; two-way ANOVA; Figure 6Ba). Of note, *Ctsd* ko retinas were completely devoid of arrestin-positive cones at P25 (Figure 6Ad,Ba). Analyses of PNA-labelled retinas at P10 and P15 (Figure S4A) confirmed the data obtained with anti-arrestin antibodies. At P10 and P15, mutant retinas contained 8.4 ± 0.9 and 1.6 ± 0.4 PNA-labelled cones/250 μ m retina length, respectively, while control retinas contained 17.8 ± 0.6 and 16.1 ± 0.5 PNA-labelled cones/250 μ m, respectively ($p < 0.001$ for both comparisons; Figure S4B). In older retinas, the lectin produced a pronounced background, which made the reliable quantification of cones impossible.

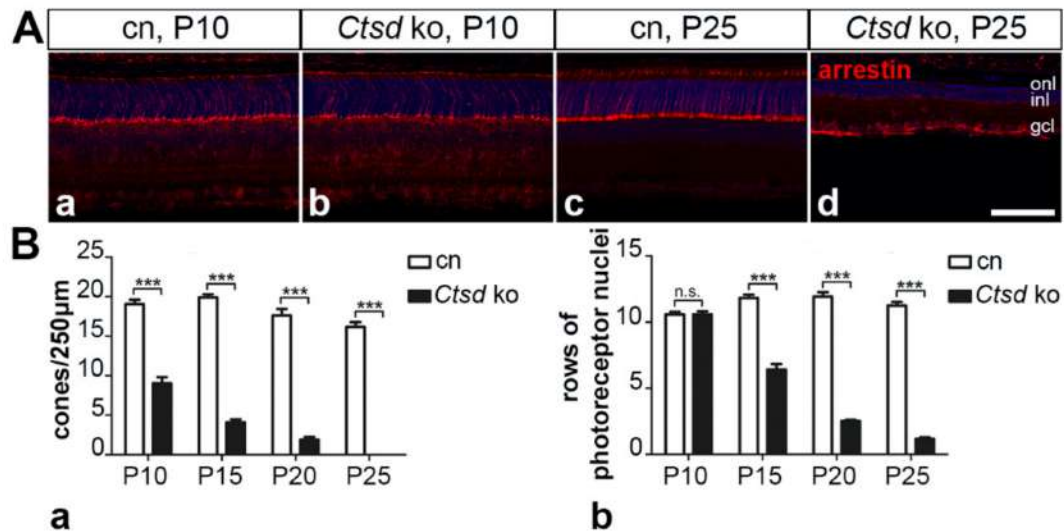


Figure 6. Degeneration of cone and rod photoreceptor cells. (A) The density of arrestin-positive cone photoreceptor cells was markedly reduced in *Ctsd* ko retinas at P10 (Ab) when compared with age-matched control retinas (Aa). At P25, mutant retinas were devoid of arrestin-positive cones (Ad; for a control retina, see Ac). (B) Quantitative analyses of mutant (filled bars) and control retinas (open bars) confirmed a significantly reduced density of cones in 10-day-old *Ctsd* ko mouse retinas, and a progressive loss of cones until P25 (Ba). The number of rows of photoreceptor nuclei was similar in *Ctsd* ko (filled bars) and control retinas (open bars) at P10, but then decreased rapidly in the mutant retinas with increasing age of the animals (Bb). Each bar represents the mean value (\pm SEM) of at least 6 animals. n.s., not significant; ***, $p < 0.001$, two-way ANOVA. cn, control; gcl, ganglion cell layer; inl, inner nuclear layer; ko, knock-out; n.s., not significant; onl, outer nuclear layer; P, postnatal day. Scale bar: 100 μ m.

Pronounced thinning of the outer nuclear layer (Figure 1A) additionally indicated a rapidly progressing loss of rod photoreceptors in the mutant. As rods comprise the vast majority of photoreceptor cells in the mouse retina, we determined the number of rows of photoreceptor nuclei at different ages to estimate the time course of rod degeneration. No significant difference in the number of photoreceptor nuclei was apparent between P10 mutant (10.6 ± 0.2 (mean \pm SEM) rows) and control retinas (10.6 ± 0.2 rows; Figure 6Bb). However, in older mutants, the number of rows of photoreceptor nuclei decreased rapidly, with only 1.2 ± 0.1 rows remaining in mutants at P25 compared to 11.3 ± 0.3 rows in the age-matched control ($p < 0.001$, two-way ANOVA; Figure 6Bb). The morphological organization of the RPE as assessed by light microscopy was indistinguishable between the mutant and control mice until the terminal stage of the disease (Figure S2).

3.5.2. Rod and Cone Bipolar Cells

Significant thinning of the inner nuclear layer of mutant mice (Figure 1Bc) additionally suggested the degeneration of retinal interneurons. We, therefore, determined the number of PKC α -positive rod bipolar cells and SCGN-positive cone bipolar cells (Figure 7), and calbindin-positive horizontal cells (Figure S5) in the mutant and control retinas at different ages. At P10 and P15, we found similar numbers of rod and cone bipolar cells in the mutant and control retinas (Figure 7). However, the density of both cell types was significantly decreased in 20-day-old mutants, with 21.2 ± 0.6 (mean \pm SEM) rod bipolar cells/250 μ m retina length and 29.4 ± 1.6 cone bipolar cells/250 μ m in *Ctsd* ko retinas compared to 26.8 ± 0.8 rod bipolar cells/250 μ m and 34.5 ± 0.4 cone bipolar cells/250 μ m in control retinas ($p < 0.001$ and $p < 0.05$, respectively, two-way ANOVA; Figure 7B). At P25, rod

and cone bipolar cell numbers in mutant retinas accounted for only 33.5% and 14.1%, respectively, of the rod and cone bipolar cell numbers observed in the age-matched control retinas (Figure 7B). Different to bipolar cells, the number of calbindin-positive horizontal cells was not significantly altered in mutant retinas at P20 (Figure S5). At this age, *Ctsd* ko retinas contained 11.0 ± 0.8 (mean \pm SEM) horizontal cells/mm retina length compared to 12.0 ± 0.5 horizontal cells/mm in control retinas. However, at P25, the density of horizontal cells was significantly reduced in the mutant (9.2 ± 0.4 horizontal cells/mm) when compared with the control mice (12.8 ± 0.6 horizontal cells/mm; $p < 0.001$, two-way ANOVA).

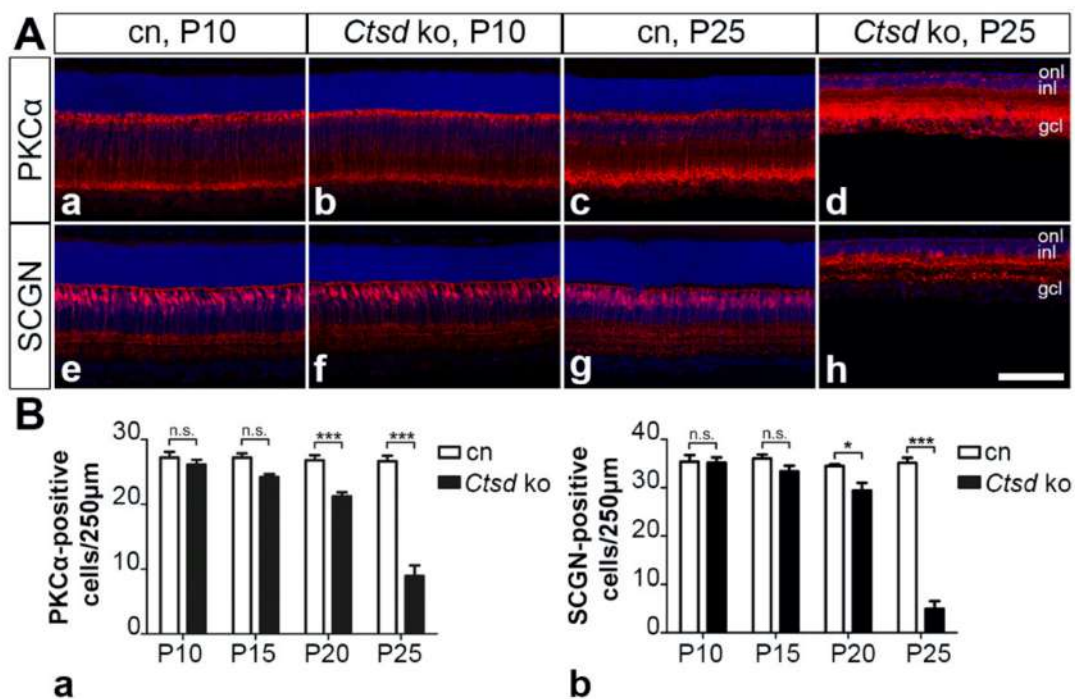


Figure 7. Degeneration of rod and cone bipolar cells. (A) The density of PKC α -positive rod bipolar cells and SCGN-positive cone bipolar cells in P10 *Ctsd* ko mice (Ab,Af, respectively) was similar to that in age-matched control mice (Aa,Ae, respectively). A pronounced loss of rod and cone bipolar cells was evident in 25-day-old mutant retinas (Ad,Ah, respectively) when compared with control retinas (Ac,Ag, respectively). (B) Quantitative analyses of mutant (filled bars) and control retinas (open bars) revealed a significant loss of rod (Ba) and cone bipolar cells (Bb) starting from P20. Each bar represents the mean value (\pm SEM) of 6 animals. n.s., not significant; *, $p < 0.05$; ***, $p < 0.001$, two-way ANOVA. cn, control; gcl, ganglion cell layer; inl, inner nuclear layer; ko, knock-out; onl, outer nuclear layer; P, postnatal day; PKC α , protein kinase C alpha; SCGN, secretogogin. Scale bar: 100 μ m.

3.5.3. Retinal Ganglion Cells

Finally, we analysed the impact of CTSD deficiency on retinal ganglion cell (RGC) survival using anti-BRN-3A antibodies. At P10 (Figure 8Aa,Ab) and P15, the control and mutant retinas contained similar numbers of ganglion cells (Figure 8Ae). However, starting from P20, there was a significant loss of ganglion cells of ~12% in *Ctsd* ko retinas (37.6 ± 1.1 (mean \pm SEM) RGCs/mm retina length) when compared with the control retinas (42.8 ± 1.8 RGCs/mm; $p < 0.05$, two-way ANOVA; Figure 8Ae). At P25, the density of ganglion cells in the mutant was decreased by ~20% (35.0 ± 1.1 RGCs/mm) when compared

with the control (43.7 ± 2.2 RGCs/mm; $p < 0.001$; compare Figure 8Ac–e). These findings were in line with results obtained from analyses of BRN-3A-stained retinal flatmounts from 25-day-old animals, where we found 3165.1 ± 84.9 (mean \pm SEM) RGCs/mm² in *Ctsd* ko retinas as compared to 4032.3 ± 88.6 RGCs/mm² in control retinas, corresponding to a loss of 21.5% ganglion cells in *Ctsd* ko mice ($p < 0.001$; Student's *t*-test; Figure 8B).

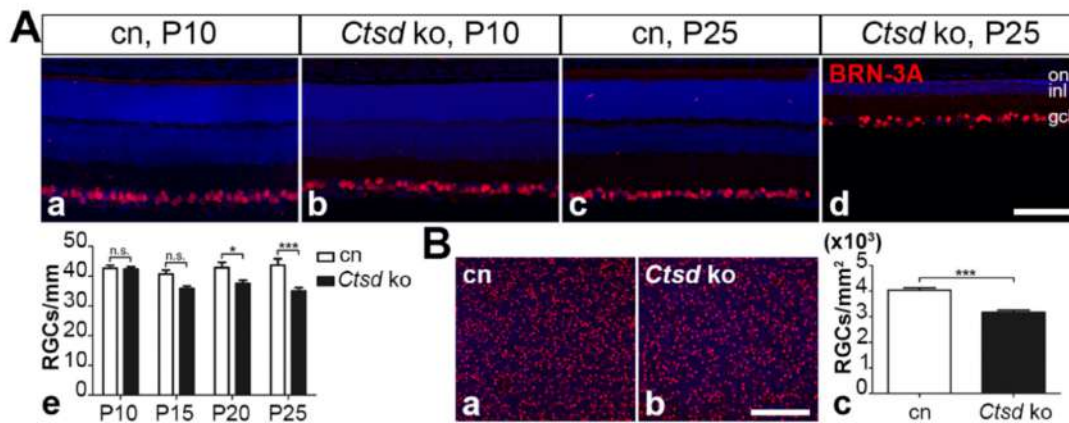


Figure 8. Degeneration of retinal ganglion cells. (A) Retina sections from *Ctsd* ko mice contained normal numbers of BRN-3A-positive ganglion cells at P10 (Ab) but reduced ganglion cell numbers at P25 (Ad) when compared with age-matched control retinas (Aa,Ac, respectively). Quantitative analyses of retina sections confirmed a significantly decreased RGC density in *Ctsd* ko retinas (filled bars in Ae) starting from P20 when compared with age-matched control retinas (open bars in Ae). n.s., not significant; *, $p < 0.05$; ***, $p < 0.001$, two-way ANOVA. (B) Analyses of retinal flatmounts from P25 *Ctsd* ko (Bb) and control mice (Ba) confirmed a significant loss of ganglion cells in the mutant at this age (Bc). ***, $p < 0.001$, Student's *t*-test. Each bar in (A,B) represents the mean value (\pm SEM) of at least 6 animals. BRN-3A, brain-specific homeobox/POU domain protein 3A; cn, control; gcl, ganglion cell layer; inl, inner nuclear layer; ko, knock-out; onl, outer nuclear layer; P, postnatal day. Scale bars: 100 μ m.

4. Discussion

CLN10 disease, the most severe NCL form, is caused by dysfunctions of the lysosomal aspartyl protease CTSD [17,20]. *Ctsd* ko mice [25] faithfully recapitulate many of the pathological features observed in CLN10 patients, including retinal degeneration [29,36]. In the present study, we performed a detailed analysis of the retinal dystrophy in *Ctsd* ko mice to obtain insights into the pathological alterations associated with CTSD deficiency. Specifically, we studied the molecular changes associated with retinal degeneration in this mutant mouse, identified the cell types affected in the *Ctsd* ko retina and quantified their degeneration during the course of the disease. A retinal pathology was already evident in young postnatal *Ctsd* ko mice, as indicated by an accumulation of storage material and a significant loss of cone photoreceptor cells. Reactive astrogliosis, reactive microgliosis and degeneration of rod photoreceptor cells became evident slightly later, while a significant loss of retinal interneurons and ganglion cells was observed at the end stage of the disease.

Neuroinflammation characterized by reactive microgliosis and reactive astrogliosis closely accompanies or even precedes neurodegeneration in different NCLs, and has been implicated in the progression of the neuropathology [41,42]. In the *Ctsd* ko retina, we found a few CD68-positive microglia/macrophages as early as at P5, and elevated levels of GFAP expression in retinal astrocytes and some Müller cells at P10. In older animals and coincident with the massive loss of photoreceptor cells, the density of microglial cells increased dramatically when compared with control mice, in line with a previous report [36]. Microglia had an amoeboid morphology indicative of an activated state. Of note, previous

studies on the brain and retina of *Ctsd* ko mice have implicated activated microglia in the progression of neurodegeneration through the production of neurotoxic levels of nitric oxide. In support of this view, multiple intraperitoneal injections of nitric oxide inhibitors were shown to result in the significant attenuation of neuron loss in the thalamus and the inner retina of the mutant mouse [33,36,43]. A critical role of inflammatory immune responses in the progression of retinal dystrophies in NCL has also been demonstrated in mouse models of CLN1, CLN3 and CLN6 disease. Attenuation of the retinal pathology in these animal models was observed upon treatment with various immunomodulatory compounds, such as fingolimod, teriflunomide, minocyclin, curcumin or docosahexaenoic acid, and in genetic models with a compromised immune system [44–48].

The accumulation of storage material is a hallmark of all NCL forms, and was among the earliest pathological alterations observed in the developing *Ctsd* ko retina. The prevalence of two of the major components of lysosomal storage material, SCMAS and the sphingolipid activator proteins saposin A and D, differs between different NCL forms [5,13,34,49]. In the *Ctsd* ko retina, we detected elevated levels of SCMAS and saposin D as early as at P5. At this age, the accumulation of both proteins was mainly confined to the inner retina, from which they spread to the outer retina later during disease progression. The loss of retinal neurons, in comparison, was first apparent in the outer nuclear layer, subsequently in the inner nuclear layer and finally in the ganglion cell layer (see below). Thus, we observed no strict spatio-temporal correlation between the accumulation of storage material and neurodegeneration, similar to findings in the brain of a CLN6 sheep model [50,51]. Results from preclinical therapy experiments also suggest that the accumulation of storage material and neurodegeneration may not be causally linked. For instance, an AAV vector-mediated gene transfer of CTSD to the brain of *Ctsd* ko mice resulted in an attenuation of the neurological deficits and a pronounced extension of the mutant's lifespan, despite the presence of high amounts of storage material in the brain [52]. Moreover, we recently showed that intravitreally injected human recombinant pro-CTSD significantly reduced the amount of storage material in the *Ctsd* ko retina without, however, attenuating retinal degeneration in the treated animals [53].

Similar to our observations in the dystrophic retinas of CLN1, CLN6 and CLN7 mouse models [54–56], we found an early and pronounced upregulation of lysosomal biogenesis in *Ctsd* ko retinas, as indicated by the increased expression levels of LAMP1, LAMP2 and the lysosomal cysteine protease CTSX/P/Z. The elevated expression of lysosomal proteins followed a spatiotemporal pattern closely resembling that of storage material accumulation, suggesting a link to lysosomal stress and activation of the transcription factor EB (TFEB) [57–59]. Impaired autophagy is a pathological hallmark of many lysosomal storage disorders [60–62], including CLN10 disease [53,63]. Accordingly, we found a striking accumulation of SQSTM1/p62, a receptor for autophagic cargo involved in the degradation of ubiquitinated proteins via the autophagosome-lysosome pathway [64,65]. SQSTM1/p62-positive aggregates were already apparent at P5, indicating early autophagic dysfunction in the mutant retina. In older animals, aggregates became detectable in a pattern that was similar to, but slightly preceded, that of retinal cell death. The lack of colocalization with LAMP2 suggested the impaired fusion of autophagosomes and lysosomes [66].

Morphometric analyses revealed a progressive thinning of the *Ctsd* ko retina starting at P15. Retina thinning was mainly the result of a rapidly progressing atrophy of the outer nuclear layer, in agreement with another report [36]. However, the thinning of other retinal layers was also observed. To identify the different cell types that are affected in the mutant retina and to quantify the progression of their degeneration, we analysed the retinal dystrophy at cellular level.

Of note, we found a significantly reduced density of cone photoreceptors in *Ctsd* ko retinas as early as at P5, slightly before a pronounced reactive microgliosis or astrogliosis became evident. In the mouse retina, cones are generated prenatally [67,68], suggesting that cones in the *Ctsd* ko retina start to degenerate shortly after they are born. However,

it is also possible that the reduced number of cones is the result of a developmental defect. In older mutants, the loss of cones progressed rapidly, with no cones remaining at P25. Cones constitute only 3% of the total photoreceptor population [40]. The majority of photoreceptors are rods, which started to degenerate at P15. Similar to cones, the degeneration of rods progressed rapidly resulting in the loss of 90% of rods at P25. Together, the results demonstrate that the *Ctsd* ko mouse suffers from a cone-rod dystrophy. Early-onset photoreceptor degeneration has also been observed in mouse models of other NCLs, such as CLN4 [69], CLN5 [70], CLN6 [47,54,71], CLN7 [55] and CLN8 [72–74], indicating that photoreceptors are particularly sensitive to lysosomal dysfunctions. The identification of a few CLN3 and CLN7 patients presenting with visual impairment due to the loss of photoreceptors but without other neurological symptoms characteristic for these disorders is in line with this view [75–81]. Retinal pigment epithelial cells are essential for photoreceptor survival and function [82]. Disruption of the autophagy-lysosomal pathway and dysfunction of these phagocytically active cells may thus provide an explanation for the frequent involvement of photoreceptor cells in lysosomal storage disorders. While several studies have demonstrated the morphological, molecular and/or functional defects of RPE cells in different NCL forms, the precise impact of these pathological alterations on photoreceptor cell survival in these conditions is unknown [70,83–87]. The most prominent pathological alterations of *Ctsd* ko RPE cells found in the present study were significantly elevated levels of LAMP2 and saposin D, while the morphological organization of the retinal pigment epithelium, as assessed by light microscopy, was indistinguishable between the mutant and control mice until the terminal stages of the disease.

Another prominent feature of the retinal pathology of *Ctsd* ko mice was a significant thinning of the inner nuclear layer, although it was not as pronounced as that observed for the outer nuclear layer. At the cellular level, the thinning of this layer was mainly the result of a progressive degeneration of rod and cone bipolar cells. The loss of rod and bipolar cells was moderate at P20 (~21% and ~15%, respectively), but pronounced at P25 (~66% and ~86%, respectively). At the end stage of the disease, we additionally observed a significantly reduced number of horizontal cells. The degeneration of retinal interneurons has also been observed in animal models of other NCL forms. In fact, in some NCL forms, the retinal pathology has been reported to start mainly in the inner retina with the outer retina being only mildly affected. In a canine CLN2 model and in murine CLN1 and CLN3 models, for example, the retinal phenotype is characterized by a thinning of the inner nuclear layer and a relative preservation of the outer nuclear layer, a significant neurodegeneration in the inner nuclear layer and/or reduced b/a wave ratios in electroretinogram recordings [56,84,88–91]. Furthermore, results from a recent study suggest that the loss of photoreceptor cells in the *Cln6^{ndf}* mouse is caused by defects in bipolar cells, which, however, start to degenerate only after a significant number of photoreceptors is lost [92]. Finally, we found a moderate loss of about 12% RGCs in the *Ctsd* ko retina at P20, which increased to ~20% at P25. The accumulation of high amounts of storage material in these large projection neurons already at initial stages of the disease, but the onset of RGC degeneration at relatively late stages of the retinal pathology, has also been observed in animal models of other NCL forms [55,56,93,94]. The loss of RGCs might be a direct consequence of lysosomal dysfunction in these neurons, or might occur secondary to pathological alterations in visual target centres in the brain or the myelinated optic nerve and tract [44,95,96]. Of interest in this context is that the lack of CTSD resulted in reduced levels of proteolipid protein and myelin basic protein, impaired lipid homeostasis, delayed the maturation of oligodendrocytes and disrupted central nervous system myelination [97,98]. Together, data demonstrate a striking variability of the retinal pathologies at the structural and functional levels between different NCL forms and highlight the need for precise knowledge of the retinal pathology of each NCL form in order to develop effective treatments.

Results from preclinical studies suggest that enzyme replacement strategies represent promising treatment options for NCLs caused by the dysfunction of soluble lysosomal

enzymes, such as palmitoyl-protein thioesterase 1 (PPT1) in CLN1 disease, tripeptidyl peptidase 1 (TPP1) in CLN2 disease or CTSD in CLN10 disease [8,99–102]. Of note, the significant attenuation of disease progression has also been observed in a recent clinical trial on CLN2 patients treated biweekly with intracerebroventricular injections of recombinant TPP1 [103]. Remarkable therapeutic outcomes have also been achieved in the *Ctsd* ko mouse, despite the rapid disease progression using an adeno-associated virus (AAV) vector-mediated gene transfer to the brain and/or the viscera [52,104]. Furthermore, we recently showed that injections of recombinant human pro-CTSD (rhCTSD) resulted in the partial correction of various pathological markers in the brain, the attenuation of the visceral pathology and a prolonged life span of treated mice [53]. In addition, we also showed that intravitreal injections of rhCTSD resulted in a partial correction of several pathological markers and the attenuation of reactive microgliosis in the retina. However, the treatment had no significant impact on the progression of retinal degeneration [53]. Results from the present study will serve as a reference for ongoing work aimed at establishing treatments for retinal degeneration in CLN10 disease using AAV- and cell-based enzyme replacement strategies. Of interest in this context is that CLN10 patients carrying mutations in the *CTSD* gene that impair, but not completely abolish, the enzymatic activity of CTSD present with an infantile or juvenile disease onset and progressive retinal degeneration [20,21,35].

Supplementary Materials: The following are available online at <https://www.mdpi.com/2073-4409/10/3/696/s1>, Figure S1: Expression of GFAP in 10-day-old *Ctsd* ko retinas; Figure S2: The retinal pigment epithelium of the degenerated *Ctsd* ko retina; Figure S3: Reduced number of cone photoreceptor cells in 5 days old *Ctsd* ko mice; Figure S4: Degeneration of PNA-labelled cones; Figure S5: Degeneration of horizontal cells.

Author Contributions: Conceptualization, U.B.; methodology, M.B., J.L., W.J. and U.B.; validation, M.B., J.L., W.J. and U.B.; investigation, M.B., J.L. and W.J.; resources, P.S. and U.B.; writing—original draft preparation, M.B., J.L., W.J. and U.B.; writing—review and editing, M.B., J.L., W.J., P.S. and U.B.; supervision, U.B.; funding acquisition, P.S. and J.L. All authors have read and agreed to the published version of the manuscript.

Funding: This research was funded by the German Research Foundation (SFB 877 A3 and Z2 to P.S.) and the China Scholarship Council (201708310088 to J.L.). The APC was not funded by external institutions.

Institutional Review Board Statement: The study was conducted according to the guidelines of the Declaration of Helsinki, and approved by the Ethics Committee of the “Freie und Hansestadt Hamburg, Behörde für Gesundheit und Verbraucherschutz” (protocol code ORG842; date of approval 3 March 2017).

Informed Consent Statement: Not applicable.

Data Availability Statement: The data presented in this study are available on request from the corresponding author.

Acknowledgments: The authors are grateful to Stefanie Schlichting and Elke Becker for excellent technical assistance, to Ali Derin and Susanne Conrad for animal care, to Susanne Bartsch for helpful discussions and critically reading the manuscript, and to Fabio Morellini for help with statistical analyses.

Conflicts of Interest: The authors declare no conflict of interest. The funders had no role in the design of the study; in the collection, analyses, or interpretation of data; in the writing of the manuscript, or in the decision to publish the results.

References

1. Cárcel-Trullols, J.; Kovács, A.D.; Pearce, D.A. Cell biology of the NCL proteins: What they do and don't do. *Biochim. Biophys. Acta (BBA) Mol. Basis Dis.* **2015**, *1852*, 2242–2255. [[CrossRef](#)] [[PubMed](#)]
2. Mole, S.E.; Cotman, S.L. Genetics of the neuronal ceroid lipofuscinoses (Batten disease). *Biochim. Biophys. Acta (BBA) Mol. Basis Dis.* **2015**, *1852*, 2237–2241. [[CrossRef](#)] [[PubMed](#)]
3. Mukherjee, A.B.; Appu, A.P.; Sadhukhan, T.; Casey, S.; Mondal, A.; Zhang, Z.; Bagh, M.B. Emerging new roles of the lysosome and neuronal ceroid lipofuscinoses. *Mol. Neurodegener.* **2019**, *14*, 1–23. [[CrossRef](#)] [[PubMed](#)]
4. Seehafer, S.S.; Pearce, D.A. You say lipofuscin, we say ceroid: Defining autofluorescent storage material. *Neurobiol. Aging* **2006**, *27*, 576–588. [[CrossRef](#)] [[PubMed](#)]
5. Palmer, D.N. The relevance of the storage of subunit c of ATP synthase in different forms and models of Batten disease (NCLs). *Biochim. Biophys. Acta (BBA) Mol. Basis Dis.* **2015**, *1852*, 2287–2291. [[CrossRef](#)] [[PubMed](#)]
6. Haltia, M.; Goebel, H.H. The neuronal ceroid-lipofuscinoses: A historical introduction. *Biochim. Biophys. Acta (BBA) Mol. Basis Dis.* **2013**, *1832*, 1795–1800. [[CrossRef](#)]
7. Kousi, M.; Lehesjoki, A.-E.; Mole, S.E. Update of the mutation spectrum and clinical correlations of over 360 mutations in eight genes that underlie the neuronal ceroid lipofuscinoses. *Hum. Mutat.* **2011**, *33*, 42–63. [[CrossRef](#)] [[PubMed](#)]
8. Kohlschütter, A.; Schulz, A.; Bartsch, U.; Storch, S. Current and Emerging Treatment Strategies for Neuronal Ceroid Lipofuscinoses. *CNS Drugs* **2019**, *33*, 315–325. [[CrossRef](#)]
9. Di Fruscio, G.; Schulz, A.; De Cegli, R.; Savarese, M.; Mutarelli, M.; Parenti, G.; Banfi, S.; Bralke, T.; Nigro, V.; Ballabio, A. Lysoplex: An efficient toolkit to detect DNA sequence variations in the autophagy-lysosomal pathway. *Autophagy* **2015**, *11*, 928–938. [[CrossRef](#)]
10. Boustany, R.-M.N. Lysosomal storage diseases—The horizon expands. *Nat. Rev. Neurol.* **2013**, *9*, 583–598. [[CrossRef](#)] [[PubMed](#)]
11. Onyenwoke, R.U.; Brenman, J.E. Lysosomal Storage Diseases—Regulating Neurodegeneration. *J. Exp. Neurosci.* **2015**, *9*, JEN-S25475. [[CrossRef](#)] [[PubMed](#)]
12. Getty, A.L.; Rothberg, P.G.; Pearce, D.A. Diagnosis of neuronal ceroid lipofuscinosis: Mutation detection strategies. *Expert Opin. Med. Diagn.* **2007**, *1*, 351–362. [[CrossRef](#)] [[PubMed](#)]
13. Anderson, G.W.; Goebel, H.H.; Simonati, A. Human pathology in NCL. *Biochim. Biophys. Acta (BBA) Mol. Basis Dis.* **2013**, *1832*, 1807–1826. [[CrossRef](#)] [[PubMed](#)]
14. Varvagiannis, K.; Hanquinet, S.; Billieux, M.H.; De Luca, R.; Rimensberger, P.; Lidgren, M.; Guipponi, M.; Makrythanasis, P.; Blouin, J.L.; Antonarakis, S.E.; et al. Congenital Neuronal Ceroid Lipofuscinosis with a Novel CTSD Gene Mutation: A Rare Cause of Neonatal-Onset Neurodegenerative Disorder. *Neuropediatrics* **2017**, *49*, 150–153. [[CrossRef](#)] [[PubMed](#)]
15. Benes, P.; Vetvicka, V.; Fusek, M. Cathepsin D—Many functions of one aspartic protease. *Crit. Rev. Oncol.* **2008**, *68*, 12–28. [[CrossRef](#)]
16. Pereira, H.; Oliveira, C.; Castro, L.; Preto, A.; Chaves, S.R.; Côrte-Real, M. Yeast as a tool to explore cathepsin D function. *Microb. Cell* **2015**, *2*, 225–234. [[CrossRef](#)] [[PubMed](#)]
17. Siintola, E.; Partanen, S.; Strömme, P.; Haapanen, A.; Haltia, M.; Maehlen, J.; Lehesjoki, A.-E.; Tyynelä, J. Cathepsin D deficiency underlies congenital human neuronal ceroid-lipofuscinosis. *Brain* **2006**, *129*, 1438–1445. [[CrossRef](#)] [[PubMed](#)]
18. Fritchie, K.; Siintola, E.; Armao, D.; Lehesjoki, A.-E.; Marino, T.; Powell, C.; Tennison, M.; Booker, J.M.; Koch, S.; Partanen, S.; et al. Novel mutation and the first prenatal screening of cathepsin D deficiency (CLN10). *Acta Neuropathol.* **2008**, *117*, 201–208. [[CrossRef](#)]
19. Meyer, S.; Yilmaz, U.; Kim, Y.-J.; Steinfeld, R.; Meyberg-Solomayer, G.; Oehl-Jaschkowitz, B.; Tzschach, A.; Gortner, L.; Igel, J.; Schofer, O. Congenital CLN disease in two siblings. *Wien. Med. Wochenschr.* **2015**, *165*, 210–213. [[CrossRef](#)] [[PubMed](#)]
20. Steinfeld, R.; Reinhardt, K.; Schreiber, K.; Hillebrand, M.; Kraetzner, R.; Brück, W.; Saftig, P.; Gärtner, J. Cathepsin D Deficiency Is Associated with a Human Neurodegenerative Disorder. *Am. J. Hum. Genet.* **2006**, *78*, 988–998. [[CrossRef](#)]
21. Hersheson, J.; Burke, D.; Clayton, R.; Anderson, G.; Jacques, T.S.; Mills, P.; Wood, N.W.; Gissen, P.; Clayton, P.; Fearnley, J.; et al. Cathepsin D deficiency causes juvenile-onset ataxia and distinctive muscle pathology. *Neurology* **2014**, *83*, 1873–1875. [[CrossRef](#)]
22. Doccini, S.; Sartori, S.; Maeser, S.; Pezzini, F.; Rossato, S.; Moro, F.; Toldo, I.; Przybylski, M.; Santorelli, F.M.; Simonati, A. Early infantile neuronal ceroid lipofuscinosis (CLN10 disease) associated with a novel mutation in CTSD. *J. Neurol.* **2016**, *263*, 1029–1032. [[CrossRef](#)]
23. Bond, M.; Holthaus, S.-M.K.; Tammen, I.; Tear, G.; Russell, C. Use of model organisms for the study of neuronal ceroid lipofuscinosis. *Biochim. Biophys. Acta (BBA) Mol. Basis Dis.* **2013**, *1832*, 1842–1865. [[CrossRef](#)] [[PubMed](#)]
24. Faller, K.M.; Gutierrez-Quintana, R.; Mohammed, A.; Rahim, A.A.; Tuxworth, R.L.; Wager, K.; Bond, M. The neuronal ceroid lipofuscinoses: Opportunities from model systems. *Biochim. Biophys. Acta (BBA) Mol. Basis Dis.* **2015**, *1852*, 2267–2278. [[CrossRef](#)] [[PubMed](#)]
25. Saftig, P.; Hetman, M.; Schmahl, W.; Weber, K.; Heine, L.; Mossmann, H.; Köster, A.; Hess, B.; Evers, M.; Von Figura, K. Mice deficient for the lysosomal proteinase cathepsin D exhibit progressive atrophy of the intestinal mucosa and profound destruction of lymphoid cells. *EMBO J.* **1995**, *14*, 3599–3608. [[CrossRef](#)] [[PubMed](#)]
26. Tyynelä, J.; Sohar, I.; Sleat, D.E.; Gin, R.M.; Nelly, R.J.D.; Baumann, M.; Haltia, M.; Lobel, P. Congenital ovine neuronal ceroid lipofuscinosis—Acathepsin D deficiency with increased levels of the inactive enzyme. *Eur. J. Paediatr. Neurol.* **2001**, *5*, 43–45. [[CrossRef](#)] [[PubMed](#)]

27. Rakoczy, P.E.; Zhang, D.; Robertson, T.; Barnett, N.L.; Papadimitriou, J.; Constable, I.J.; Lai, C.-M. Progressive Age-Related Changes Similar to Age-Related Macular Degeneration in a Transgenic Mouse Model. *Am. J. Pathol.* **2002**, *161*, 1515–1524. [\[CrossRef\]](#)
28. Awano, T.; Katz, M.L.; O'Brien, D.P.; Taylor, J.F.; Evans, J.; Khan, S.; Sohar, I.; Lobel, P.; Johnson, G.S. A mutation in the cathepsin D gene (CTSD) in American Bulldogs with neuronal ceroid lipofuscinosis. *Mol. Genet. Metab.* **2006**, *87*, 341–348. [\[CrossRef\]](#) [\[PubMed\]](#)
29. Koike, M.; Nakanishi, H.; Säftig, P.; Ezaki, J.; Isahara, K.; Ohsawa, Y.; Schulz-Schaeffer, W.; Watanabe, T.; Waguri, S.; Kametaka, S.; et al. Cathepsin D Deficiency Induces Lysosomal Storage with Ceroid Lipofuscin in Mouse CNS Neurons. *J. Neurosci.* **2000**, *20*, 6898–6906. [\[CrossRef\]](#) [\[PubMed\]](#)
30. Götzl, J.K.; Mori, K.; Damme, M.; Fellerer, K.; Tahirovic, S.; Kleinberger, G.; Janssens, J.; Van Der Zee, J.; Lang, C.M.; Kremmer, E.; et al. Common pathobiochemical hallmarks of progranulin-associated frontotemporal lobar degeneration and neuronal ceroid lipofuscinosis. *Acta Neuropathol.* **2014**, *127*, 845–860. [\[CrossRef\]](#)
31. Haapanen, A.; Ramadan, U.A.; Autti, T.; Joensuu, R.; Tyynelä, J. In vivo MRI reveals the dynamics of pathological changes in the brains of cathepsin D-deficient mice and correlates changes in manganese-enhanced MRI with microglial activation. *Magn. Reson. Imaging* **2007**, *25*, 1024–1031. [\[CrossRef\]](#)
32. Partanen, S.; Haapanen, A.; Kielar, C.; Pontikis, C.; Alexander, N.; Inkinen, T.; Saftig, P.; Gillingwater, T.H.; Cooper, J.D.; Tyynelä, J. Synaptic Changes in the Thalamocortical System of Cathepsin D-Deficient Mice. *J. Neuropathol. Exp. Neurol.* **2008**, *67*, 16–29. [\[CrossRef\]](#)
33. Nakanishi, H.; Zhang, J.; Koike, M.; Nishioku, T.; Okamoto, Y.; Kominami, E.; Von Figura, K.; Peters, C.; Yamamoto, K.; Saftig, P.; et al. Involvement of Nitric Oxide Released from Microglia-Macrophages in Pathological Changes of Cathepsin D-Deficient Mice. *J. Neurosci.* **2001**, *21*, 7526–7533. [\[CrossRef\]](#)
34. Radke, J.; Stenzel, W.; Goebel, H.H. Human NCL Neuropathology. *Biochim. Biophys. Acta (BBA) Mol. Basis Dis.* **2015**, *1852*, 2262–2266. [\[CrossRef\]](#) [\[PubMed\]](#)
35. Thottath, J.; Vellarikkal, S.K.; Jayarajan, R.; Verma, A.; Manamel, M.; Singh, A.; Rajendran, V.R.; Sivasubbu, S.; Scaria, V. A novel cathepsin D mutation in 2 siblings with late infantile neuronal ceroid lipofuscinosis. *Neurol. Genet.* **2019**, *5*, e302. [\[CrossRef\]](#)
36. Koike, M.; Shibata, M.; Ohsawa, Y.; Nakanishi, H.; Koga, T.; Kametaka, S.; Waguri, S.; Momoi, T.; Kominami, E.; Peters, C.; et al. Involvement of two different cell death pathways in retinal atrophy of cathepsin D-deficient mice. *Mol. Cell. Neurosci.* **2003**, *22*, 146–161. [\[CrossRef\]](#)
37. Flachsbarth, K.; Kruszewski, K.; Jung, G.; Jankowiak, W.; Riecken, K.; Wagenfeld, L.; Richard, G.; Fehse, B.; Bartsch, U. Neural Stem Cell-Based Intraocular Administration of Ciliary Neurotrophic Factor Attenuates the Loss of Axotomized Ganglion Cells in Adult Mice. *Investig. Ophthalmol. Vis. Sci.* **2014**, *55*, 7029–7039. [\[CrossRef\]](#)
38. Dulz, S.; Bassal, M.; Flachsbarth, K.; Riecken, K.; Fehse, B.; Schlichting, S.; Bartsch, S.; Bartsch, U. Intravitreal Co-Administration of GDNF and CNTF Confers Synergistic and Long-Lasting Protection against Injury-Induced Cell Death of Retinal Ganglion Cells in Mice. *Cells* **2020**, *9*, 2082. [\[CrossRef\]](#) [\[PubMed\]](#)
39. Klein, A.; Henseler, M.; Klein, C.; Suzuki, K.; Harzer, K.; Sandhoff, K. Sphingolipid Activator Protein D (sap-D) Stimulates the Lysosomal Degradation of Ceramide in Vivo. *Biochem. Biophys. Res. Commun.* **1994**, *200*, 1440–1448. [\[CrossRef\]](#) [\[PubMed\]](#)
40. Jeon, C.-J.; Strettoi, E.; Masland, R.H. The Major Cell Populations of the Mouse Retina. *J. Neurosci.* **1998**, *18*, 8936–8946. [\[CrossRef\]](#)
41. Palmer, D.N.; Barry, L.A.; Tyynelä, J.; Cooper, J.D. NCL disease mechanisms. *Biochim. Biophys. Acta (BBA) Mol. Basis Dis.* **2013**, *1832*, 1882–1893. [\[CrossRef\]](#) [\[PubMed\]](#)
42. Bosch, M.E.; Ekielien, T. Neuroinflammatory paradigms in lysosomal storage diseases. *Front. Neurosci.* **2015**, *9*, 417. [\[CrossRef\]](#) [\[PubMed\]](#)
43. Yamasaki, R.; Zhang, J.; Koshiishi, I.; Suniarti, D.F.S.; Wu, Z.; Peters, C.; Schwake, M.; Uchiyama, Y.; Kira, J.-I.; Saftig, P.; et al. Involvement of lysosomal storage-induced p38 MAP kinase activation in the overproduction of nitric oxide by microglia in cathepsin D-deficient mice. *Mol. Cell. Neurosci.* **2007**, *35*, 573–584. [\[CrossRef\]](#)
44. Groh, J.; Kühl, T.G.; Ip, C.W.; Nelvagal, H.R.; Sri, S.; Duckett, S.; Mirza, M.; Langmann, T.; Cooper, J.D.; Martini, R. Immune cells perturb axons and impair neuronal survival in a mouse model of infantile neuronal ceroid lipofuscinosis. *Brain* **2013**, *136*, 1083–1101. [\[CrossRef\]](#)
45. Groh, J.; Ribechini, E.; Stadler, D.; Schilling, T.; Lutz, M.B.; Martini, R. Sialoadhesin promotes neuroinflammation-related disease progression in two mouse models of CLN disease. *Glia* **2016**, *64*, 792–809. [\[CrossRef\]](#) [\[PubMed\]](#)
46. Groh, J.; Berve, K.; Martini, R. Fingolimod and Teriflunomide Attenuate Neurodegeneration in Mouse Models of Neuronal Ceroid Lipofuscinosis. *Mol. Ther.* **2017**, *25*, 1889–1899. [\[CrossRef\]](#)
47. Mirza, M.; Volz, C.; Karlstetter, M.; Langiu, M.; Somogyi, A.; Ruonala, M.O.; Tamm, E.R.; Jägle, H.; Langmann, T. Progressive Retinal Degeneration and Glial Activation in the CLN6nclf Mouse Model of Neuronal Ceroid Lipofuscinosis: A Beneficial Effect of DHA and Curcumin Supplementation. *PLoS ONE* **2013**, *8*, e75963. [\[CrossRef\]](#)
48. Dannhausen, K.; Möhle, C.; Langmann, T. Immunomodulation with minocycline rescues retinal degeneration in juvenile neuronal ceroid lipofuscinosis mice highly susceptible to light damage. *Dis. Model. Mech.* **2018**, *11*, dmm033597. [\[CrossRef\]](#)
49. Tyynelä, J.; Suopanki, J.; Baumann, M.; Haltia, M. Sphingolipid Activator Proteins (SAPs) in Neuronal Ceroid Lipofuscinoses (NCL). *Neuropediatrics* **1997**, *28*, 49–52. [\[CrossRef\]](#)

50. Oswald, M.J.; Palmer, D.N.; Kay, G.W.; Shemilt, S.; Rezaie, P.; Cooper, J.D.; Shemilt, S.J.A. Glial activation spreads from specific cerebral foci and precedes neurodegeneration in presymptomatic ovine neuronal ceroid lipofuscinosis (CLN6). *Neurobiol. Dis.* **2005**, *20*, 49–63. [[CrossRef](#)]
51. Kay, G.W.; Jay, N.P.; Palmer, D.N. The specific loss of GnRH-positive neurons from the hypothalamus of sheep with CLN6 neuronal ceroid lipofuscinosis occurs without glial activation and has only minor effects on reproduction. *Neurobiol. Dis.* **2011**, *41*, 614–623. [[CrossRef](#)] [[PubMed](#)]
52. Shevtsova, Z.; Garrido, M.; Weishaupt, J.; Saftig, P.; Bähr, M.; Lühder, F.; Kügler, S. CNS-Expressed Cathepsin D Prevents Lymphopenia in a Murine Model of Congenital Neuronal Ceroid Lipofuscinosis. *Am. J. Pathol.* **2010**, *177*, 271–279. [[CrossRef](#)] [[PubMed](#)]
53. Marques, A.R.A.; Di Spiezio, A.; Thießen, N.; Schmidt, L.; Grötzinger, J.; Lüllmann-Rauch, R.; Damme, M.; Storck, S.E.; Pietrzik, C.U.; Fogh, J.; et al. Enzyme replacement therapy with recombinant pro-CTSD (cathepsin D) corrects defective proteolysis and autophagy in neuronal ceroid lipofuscinosis. *Autophagy* **2020**, *16*, 811–825. [[CrossRef](#)] [[PubMed](#)]
54. Bartsch, U.; Galliciotti, G.; Jofre, G.F.; Jankowiak, W.; Hagel, C.; Braulke, T. Apoptotic Photoreceptor Loss and Altered Expression of Lysosomal Proteins in the nclf Mouse Model of Neuronal Ceroid Lipofuscinosis. *Investig. Ophthalmol. Vis. Sci.* **2013**, *54*, 6952–6959. [[CrossRef](#)]
55. Jankowiak, W.; Brandenstein, L.; Dulz, S.; Hagel, C.; Storch, S.; Bartsch, U. Retinal Degeneration in Mice Deficient in the Lysosomal Membrane Protein CLN7. *Investig. Ophthalmol. Vis. Sci.* **2016**, *57*, 4989. [[CrossRef](#)] [[PubMed](#)]
56. Atiskova, Y.; Bartsch, S.; Danyukova, T.; Becker, E.; Hagel, C.; Storch, S.; Bartsch, U. Mice deficient in the lysosomal enzyme palmitoyl-protein thioesterase 1 (PPT1) display a complex retinal phenotype. *Sci. Rep.* **2019**, *9*, 1–15. [[CrossRef](#)] [[PubMed](#)]
57. Sardiello, M.; Palmieri, M.; Di Ronza, A.; Medina, D.L.; Valenza, M.; Gennarino, V.A.; Di Malta, C.; Donaudo, F.; Embrione, V.; Polishchuk, R.S.; et al. A Gene Network Regulating Lysosomal Biogenesis and Function. *Science* **2009**, *325*, 473–477. [[CrossRef](#)]
58. Settembre, C.; Ballabio, A. Lysosomal Adaptation: How the Lysosome Responds to External Cues. *Cold Spring Harb. Perspect. Biol.* **2014**, *6*, a016907. [[CrossRef](#)]
59. Ballabio, A. The awesome lysosome. *EMBO Mol. Med.* **2016**, *8*, 73–76. [[CrossRef](#)]
60. Seranova, E.; Connolly, K.J.; Zatyka, M.; Rosenstock, T.R.; Barrett, T.; Tuxworth, R.L.; Sarkar, S. Dysregulation of autophagy as a common mechanism in lysosomal storage diseases. *Essays Biochem.* **2017**, *61*, 733–749. [[CrossRef](#)]
61. Marques, A.R.A.; Saftig, P. Lysosomal storage disorders—Challenges, concepts and avenues for therapy: Beyond rare diseases. *J. Cell Sci.* **2019**, *132*, jcs221739. [[CrossRef](#)] [[PubMed](#)]
62. Parenti, G.; Medina, D.L.; Ballabio, A. The rapidly evolving view of lysosomal storage diseases. *EMBO Mol. Med.* **2021**, *13*, e12836. [[CrossRef](#)] [[PubMed](#)]
63. Koike, M.; Shibata, M.; Waguri, S.; Yoshimura, K.; Tanida, I.; Kominami, E.; Gotow, T.; Peters, C.; von Figura, K.; Mizushima, N.; et al. Participation of Autophagy in Storage of Lysosomes in Neurons from Mouse Models of Neuronal Ceroid-Lipofuscinoses (Batten Disease). *Am. J. Pathol.* **2005**, *167*, 1713–1728. [[CrossRef](#)]
64. Bjørkøy, G.; Lamark, T.; Brech, A.; Outzen, H.; Perander, M.; Øvervatn, A.; Stenmark, H.; Johansen, T. p62/SQSTM1 forms protein aggregates degraded by autophagy and has a protective effect on huntingtin-induced cell death. *J. Cell Biol.* **2005**, *171*, 603–614. [[CrossRef](#)] [[PubMed](#)]
65. Pankiv, S.; Clausen, T.H.; Lamark, T.; Brech, A.; Bruun, J.-A.; Outzen, H.; Øvervatn, A.; Bjørkøy, G.; Johansen, T. p62/SQSTM1 Binds Directly to Atg8/LC3 to Facilitate Degradation of Ubiquitinated Protein Aggregates by Autophagy. *J. Biol. Chem.* **2007**, *282*, 24131–24145. [[CrossRef](#)] [[PubMed](#)]
66. Thelen, M.; Dammé, M.; Schweizer, M.; Hagel, C.; Wong, A.M.; Cooper, J.D.; Braulke, T.; Galliciotti, G. Disruption of the Autophagy-Lysosome Pathway Is Involved in Neuropathology of the nclf Mouse Model of Neuronal Ceroid Lipofuscinosis. *PLoS ONE* **2012**, *7*, e35493. [[CrossRef](#)]
67. Carter-Dawson, L.D.; Lavail, M.M. Rods and cones in the mouse retina. II. Autoradiographic analysis of cell generation using tritiated thymidine. *J. Comp. Neurol.* **1979**, *188*, 263–272. [[CrossRef](#)] [[PubMed](#)]
68. Young, R.W. Cell differentiation in the retina of the mouse. *Anat. Rec. Adv. Integr. Anat. Evol. Biol.* **1985**, *212*, 199–205. [[CrossRef](#)]
69. Schmitz, F.; Tabares, L.; Khimich, D.; Strenzke, N.; De La Villa-Polo, P.; Castellano-Muñoz, M.; Bulankina, A.; Moser, T.; Fernández-Chacón, R.; Südhof, T.C. CSP -deficiency causes massive and rapid photoreceptor degeneration. *Proc. Natl. Acad. Sci. USA* **2006**, *103*, 2926–2931. [[CrossRef](#)] [[PubMed](#)]
70. Leinonen, H.; Keksa-Goldsteine, V.; Ragauskas, S.; Kohlmann, P.; Singh, Y.; Savchenko, E.; Puranen, J.; Malm, T.; Kalesnykas, G.; Koistinaho, J.; et al. Retinal Degeneration In A Mouse Model Of CLN5 Disease Is Associated With Compromised Autophagy. *Sci. Rep.* **2017**, *7*, 1–12. [[CrossRef](#)]
71. Bronson, R.T.; Donahue, L.R.; Johnson, K.R.; Tanner, A.; Lane, P.W.; Faust, J.R. Neuronal ceroid lipofuscinosis (nclf), a new disorder of the mouse linked to chromosome 9. *Am. J. Med. Genet.* **1998**, *77*, 289–297. [[CrossRef](#)]
72. Bronson, R.T.; Lake, B.D.; Cook, S.; Taylor, S.; Davisson, M.T. Motor neuron degeneration of mice is a model of neuronal ceroid lipofuscinosis (Batten's disease). *Ann. Neurol.* **1993**, *33*, 381–385. [[CrossRef](#)]
73. Messer, A.; Plummer, J.; Wong, V.; Lavail, M. Retinal Degeneration in Motor Neuron Degeneration (mnd) Mutant Mice. *Exp. Eye Res.* **1993**, *57*, 637–641. [[CrossRef](#)]

74. Guarneri, R.; Russo, D.; Cascio, C.; D'Agostino, S.; Galizzi, G.; Bigini, P.; Mennini, T.; Guarneri, P. Retinal oxidation, apoptosis and age- and sex-differences in the mnd mutant mouse, a model of neuronal ceroid lipofuscinosis. *Brain Res.* **2004**, *1014*, 209–220. [[CrossRef](#)]
75. Wang, F.; Wang, H.; Tuan, H.-F.; Nguyen, D.H.; Sun, V.; Keser, V.; Bowne, S.J.; Sullivan, L.S.; Luo, H.; Zhao, L.; et al. Next generation sequencing-based molecular diagnosis of retinitis pigmentosa: Identification of a novel genotype-phenotype correlation and clinical refinements. *Qual. Life Res.* **2014**, *133*, 331–345. [[CrossRef](#)] [[PubMed](#)]
76. Roosing, S.; Born, L.I.V.D.; Sangermano, R.; Banfi, S.; Koenekoop, R.K.; Zonneveld-Vrieling, M.N.; Klaver, C.C.; Van Lith-Verhoeven, J.J.; Cremers, F.P.; Hollander, A.I.D.; et al. Mutations in MFSD8, Encoding a Lysosomal Membrane Protein, Are Associated with Nonsyndromic Autosomal Recessive Macular Dystrophy. *Ophthalmology* **2015**, *122*, 170–179. [[CrossRef](#)] [[PubMed](#)]
77. Khan, K.N.; El-Asrag, M.E.; Ku, C.A.; Holder, G.E.; McKibbin, M.; Arno, G.; Poulter, J.A.; Carss, K.; Bommireddy, T.; Bagheri, S.; et al. Specific Alleles of CLN7/MFSD8, a Protein That Localizes to Photoreceptor Synaptic Terminals, Cause a Spectrum of Nonsyndromic Retinal Dystrophy. *Investig. Ophthalmol. Vis. Sci.* **2017**, *58*, 2906–2914. [[CrossRef](#)]
78. Ku, C.A.; Hull, S.; Arno, G.; Vincent, A.; Carss, K.; Kayton, R.; Weeks, D.; Anderson, G.W.; Geraets, R.; Parker, C.; et al. Detailed Clinical Phenotype and Molecular Genetic Findings in CLN3-Associated Isolated Retinal Degeneration. *JAMA Ophthalmol.* **2017**, *135*, 749–760. [[CrossRef](#)]
79. Birtel, J.; Gliem, M.; Mangold, E.; Müller, P.L.; Holz, F.G.; Neuhaus, C.; Lenzner, S.; Zahnleiter, D.; Betz, C.; Eisenberger, T.; et al. Next-generation sequencing identifies unexpected genotype-phenotype correlations in patients with retinitis pigmentosa. *PLoS ONE* **2018**, *13*, e0207958. [[CrossRef](#)] [[PubMed](#)]
80. Chen, F.K.; Zhang, X.; Eintracht, J.; Zhang, D.; Arunachalam, S.; Thompson, J.A.; Chelva, E.; Mallon, D.; Chen, S.-C.; McLaren, T.; et al. Clinical and molecular characterization of non-syndromic retinal dystrophy due to c.175G>A mutation in ceroid lipofuscinosis neuronal 3 (CLN3). *Doc. Ophthalmol.* **2018**, *138*, 55–70. [[CrossRef](#)] [[PubMed](#)]
81. Smirnov, V.M.; Nassisi, M.; Hernandez, C.S.; Méjécase, C.; El Shamieh, S.; Condroyer, C.; Antonio, A.; Meunier, I.; Andrieu, C.; Defoort-Dhellemmes, S.; et al. Retinal Phenotype of Patients With Isolated Retinal Degeneration Due to CLN3 Pathogenic Variants in a French Retinitis Pigmentosa Cohort. *JAMA Ophthalmol.* **2021**. [[CrossRef](#)] [[PubMed](#)]
82. Strauss, O. The Retinal Pigment Epithelium. In *Webovision: The Organization of the Retina and Visual System*; Kolb, H., Fernandez, E., Nelson, R., Eds.; University of Utah Health Sciences Center: Salt Lake City, UT, USA, 1995.
83. Zhong, Y.; Mohan, K.; Liu, J.; Al-Attar, A.; Lin, P.; Flight, R.M.; Sun, Q.; Warmoes, M.O.; Deshpande, R.R.; Liu, H.; et al. Loss of CLN3, the gene mutated in juvenile neuronal ceroid lipofuscinosis, leads to metabolic impairment and autophagy induction in retinal pigment epithelium. *Biochim. Biophys. Acta (BBA) Mol. Basis Dis.* **2020**, *1866*, 165883. [[CrossRef](#)]
84. Katz, M.L.; Johnson, G.S.; Tullis, G.E.; Lei, B. Phenotypic characterization of a mouse model of juvenile neuronal ceroid lipofuscinosis. *Neurobiol. Dis.* **2008**, *29*, 242–253. [[CrossRef](#)]
85. Goebel, H.H.; Dopfmer, I. An ultrastructural study on retinal neural and pigment epithelial cells in ovine neuronal ceroid-lipofuscinosis. *Ophthalmic Paediatr. Genet.* **1990**, *11*, 61–69. [[CrossRef](#)] [[PubMed](#)]
86. Wavre-Shapton, S.T.; Calvi, A.A.; Turmaine, M.; Seabra, M.C.; Cutler, D.F.; Futter, C.E.; Mitchison, H.M. Photoreceptor phagosome processing defects and disturbed autophagy in retinal pigment epithelium of Cln3 Δ ex1-6 mice modelling juvenile neuronal ceroid lipofuscinosis (Batten disease). *Hum. Mol. Genet.* **2015**, *24*, 7060–7074. [[CrossRef](#)]
87. Von Eisenhart-Rothe, P.; Grubman, A.; Greferath, U.; Fothergill, L.J.; Jobling, A.I.; Phipps, J.A.; White, A.R.; Fletcher, E.L.; Vessey, K.A. Failure of Autophagy–Lysosomal Pathways in Rod Photoreceptors Causes the Early Retinal Degeneration Phenotype Observed in Cln6nclfMice. *Investig. Ophthalmol. Vis. Sci.* **2018**, *59*, 5082–5097. [[CrossRef](#)] [[PubMed](#)]
88. Lei, B.; Tullis, G.E.; Kirk, M.D.; Zhang, K.; Katz, M.L. Ocular phenotype in a mouse gene knockout model for infantile neuronal ceroid lipofuscinosis. *J. Neurosci. Res.* **2006**, *84*, 1139–1149. [[CrossRef](#)] [[PubMed](#)]
89. Katz, M.L.; Coates, J.R.; Cooper, J.J.; O'Brien, D.P.; Jeong, M.; Narfström, K. Retinal Pathology in a Canine Model of Late Infantile Neuronal Ceroid Lipofuscinosis. *Investig. Ophthalmol. Vis. Sci.* **2008**, *49*, 2686–2695. [[CrossRef](#)] [[PubMed](#)]
90. Groh, J.; Stadler, D.; Buttman, M.; Martini, R. Non-invasive assessment of retinal alterations in mouse models of infantile and juvenile neuronal ceroid lipofuscinosis by spectral domain optical coherence tomography. *Acta Neuropathol. Commun.* **2014**, *2*, 1–12. [[CrossRef](#)] [[PubMed](#)]
91. Volz, C.; Mirza, M.; Langmann, T.; Jäggle, H. Retinal Function in Aging Homozygous Cln3 Δ ex7/8 Knock-In Mice. In *Retinal Degenerative Diseases; Advances in Experimental Medicine and Biology Series*; Springer: Berlin/Heidelberg, Germany, 2014; Volume 801, pp. 495–501. [[CrossRef](#)]
92. Holthaus, S.-M.K.; Ribeiro, J.; Abelleira-Hervas, L.; Pearson, R.A.; Duran, Y.; Georgiadis, A.; Sampson, R.D.; Rizzi, M.; Hoke, J.; Maswood, R.; et al. Prevention of Photoreceptor Cell Loss in a Cln6 Mouse Model of Batten Disease Requires CLN6 Gene Transfer to Bipolar Cells. *Mol. Ther.* **2018**, *26*, 1343–1353. [[CrossRef](#)]
93. Seigel, G.M.; Wagner, J.; Wronska, A.; Campbell, L.; Ju, W.; Zhong, N. Progression of early postnatal retinal pathology in a mouse model of neuronal ceroid lipofuscinosis. *Eye* **2004**, *19*, 1306–1312. [[CrossRef](#)] [[PubMed](#)]
94. Hafler, B.P.; Klein, Z.A.; Zhou, Z.J.; Strittmatter, S.M. Progressive retinal degeneration and accumulation of autofluorescent lipopigments in Progranulin deficient mice. *Brain Res.* **2014**, *1588*, 168–174. [[CrossRef](#)]
95. Sappington, R.M.; Pearce, D.A.; Calkins, D.J. Optic Nerve Degeneration in a Murine Model of Juvenile Ceroid Lipofuscinosis. *Investig. Ophthalmol. Vis. Sci.* **2003**, *44*, 3725–3731. [[CrossRef](#)] [[PubMed](#)]

96. Weimer, J.M.; Custer, A.W.; Benedict, J.W.; Alexander, N.A.; Kingsley, E.; Federoff, H.J.; Cooper, J.D.; Pearce, D.A. Visual deficits in a mouse model of Batten disease are the result of optic nerve degeneration and loss of dorsal lateral geniculate thalamic neurons. *Neurobiol. Dis.* **2006**, *22*, 284–293. [[CrossRef](#)] [[PubMed](#)]
97. Mutka, A.-L.; Haapanen, A.; Käkälä, R.; Lindfors, M.; Wright, A.K.; Inkinen, T.; Hermansson, M.; Rokka, A.; Corthals, G.; Jauhainen, M.; et al. Murine cathepsin D deficiency is associated with dysmyelination/myelin disruption and accumulation of cholesteryl esters in the brain. *J. Neurochem.* **2009**, *112*, 193–203. [[CrossRef](#)] [[PubMed](#)]
98. Guo, D.-Z.; Xiao, L.; Liu, Y.-J.; Shen, C.; Lou, H.-F.; Lv, Y.; Pan, S.-Y. Cathepsin D deficiency delays central nervous system myelination by inhibiting proteolipid protein trafficking from late endosome/lysosome to plasma membrane. *Exp. Mol. Med.* **2018**, *50*, e457. [[CrossRef](#)] [[PubMed](#)]
99. Neverman, N.J.; Best, H.L.; Hofmann, S.L.; Hughes, S.M. Experimental therapies in the neuronal ceroid lipofuscinoses. *Biochim. Biophys. Acta (BBA) Mol. Basis Dis.* **2015**, *1852*, 2292–2300. [[CrossRef](#)] [[PubMed](#)]
100. Geraets, R.D.; Koh, S.Y.; Hastings, M.L.; Kielian, T.; Pearce, D.A.; Weimer, J.M. Moving towards effective therapeutic strategies for Neuronal Ceroid Lipofuscinosis. *Orphanet J. Rare Dis.* **2016**, *11*, 1–13. [[CrossRef](#)]
101. Johnson, T.B.; Cain, J.T.; White, K.A.; Ramirez-Montealegre, D.; Pearce, D.A.; Weimer, J.M. Therapeutic landscape for Batten disease: Current treatments and future prospects. *Nat. Rev. Neurol.* **2019**, *15*, 161–178. [[CrossRef](#)] [[PubMed](#)]
102. Mole, S.E.; Anderson, G.; Band, H.A.; Berkovic, S.F.; Cooper, J.D.; Holthaus, S.-M.K.; McKay, T.R.; Medina, D.L.; Rahim, A.A.; Schulz, A.; et al. Clinical challenges and future therapeutic approaches for neuronal ceroid lipofuscinosis. *Lancet Neurol.* **2019**, *18*, 107–116. [[CrossRef](#)]
103. Schulz, A.; Ajayi, T.; Specchio, N.; Reyes, E.D.L.; Gissen, P.; Ballon, D.; Dyke, J.P.; Cahan, H.; Slasor, P.; Jacoby, D.; et al. Study of Intraventricular Cerliponase Alfa for CLN2 Disease. *N. Engl. J. Med.* **2018**, *378*, 1898–1907. [[CrossRef](#)] [[PubMed](#)]
104. Pike, L.S.; Tannous, B.A.; Deliollanis, N.C.; Hsich, G.; Morse, D.; Tung, C.-H.; Sena-Esteves, M.; Breakefield, X.O. Imaging gene delivery in a mouse model of congenital neuronal ceroid lipofuscinosis. *Gene Ther.* **2011**, *18*, 1173–1178. [[CrossRef](#)] [[PubMed](#)]

Supplementary Materials

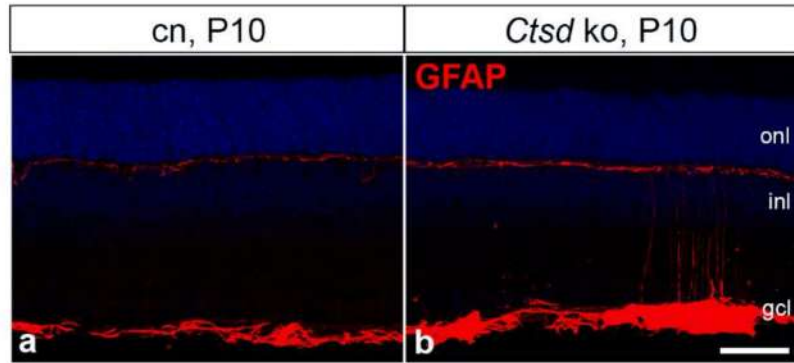


Figure S1. Expression of GFAP in 10-day-old *Ctsd* ko retinas. Expression of GFAP in retinal astrocytes was elevated in *Ctsd* ko retinas at P10 (b) when compared with age-matched control retinas (a). In addition, some Müller cell processes were GFAP-positive in mutant retinas at this age (b). cn, control; gcl, ganglion cell layer; GFAP, glial fibrillary acidic protein; inl, inner nuclear layer; ko, knock-out; onl, outer nuclear layer; P, postnatal day. Scale bar: 50 μ m.

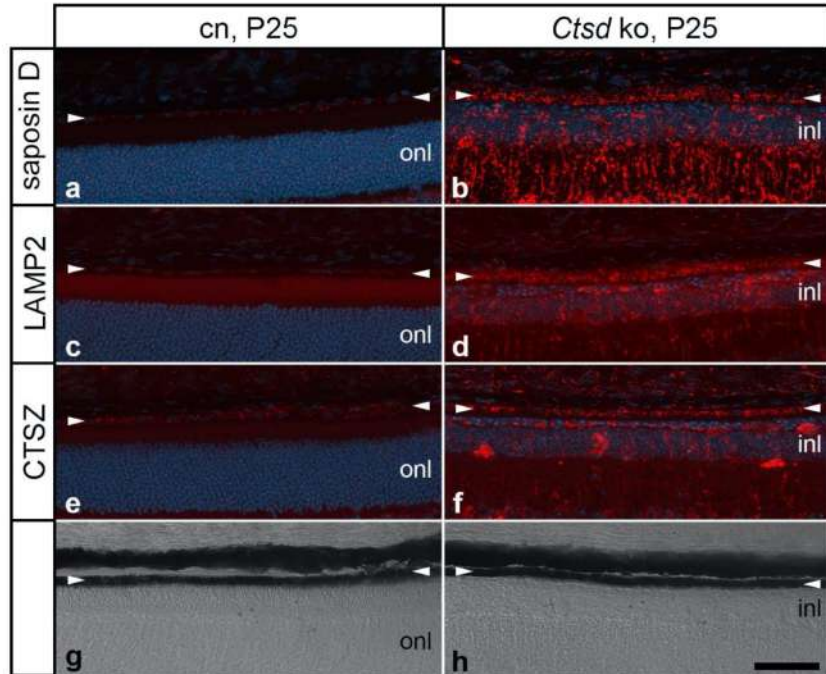


Figure S2. The retinal pigment epithelium of the degenerated *Ctsd* ko retina. Levels of saposin D (b), LAMP2 (d) and CTSZ (f) were significantly elevated in the RPE (marked with arrowheads in a-h) of *Ctsd* ko mice at P25 when compared with age-matched control animals (a, c and e, respectively). The morphological organization of the RPE at this age was indistinguishable between mutant (h) and control (g) retinas. cn, control; CTSZ, cathepsin X/Z/P; inl, inner nuclear layer; ko, knock-out; LAMP2, lysosomal-associated membrane protein 2; onl, outer nuclear layer; P, postnatal day. Scale bar: 50 μ m.

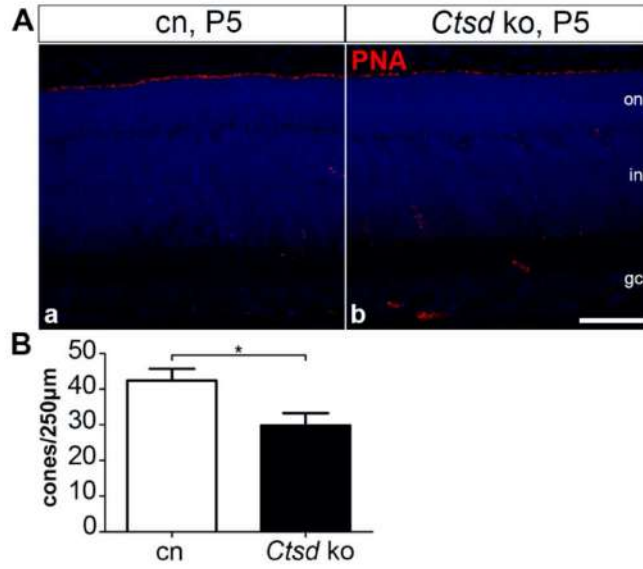


Figure S3. Reduced number of cone photoreceptor cells in 5 days old *CtSD* ko mice. A) A markedly reduced number of PNA-labelled cones was detected in *CtSD* ko retinas as early as at P5 (b) when compared to age-matched control retinas (a). B) Quantitative analyses confirmed a significantly reduced number of cones in the mutant retina. Each bar represents the mean value (\pm SEM) of 4 animals. *: $p < 0.05$, Student's t-test. cn, control; gcl, ganglion cell layer; inl, inner nuclear layer; ko, knock-out; onl, outer nuclear layer; P, postnatal day; PNA, peanut agglutinin. Scale bar: 50 μ m.

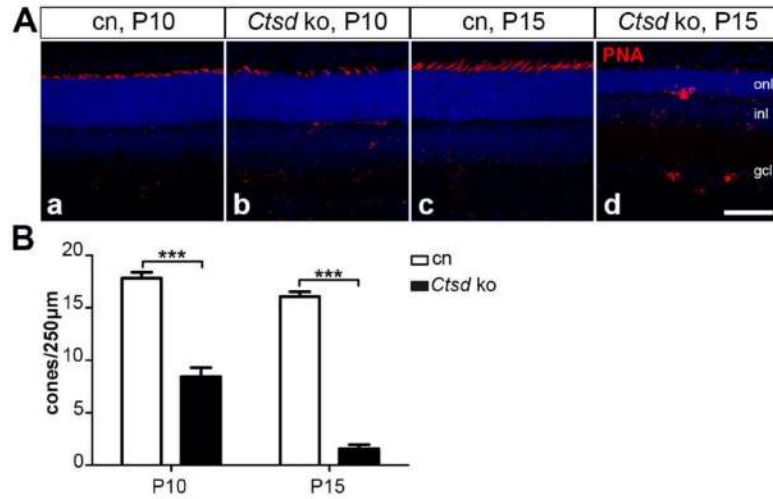


Figure S4. Degeneration of PNA-labelled cones. A) The number of PNA-labelled cones in *Ctsd ko* retinas was markedly reduced at P10 (Ab) when compared to control retinas (Aa). P15 mutant retinas were almost devoid of PNA-labelled cones (Ad). B) Quantitative analysis confirmed a pronounced and rapidly progressing loss of cones in mutant retinas. Each bar represents the mean value (\pm SEM) of 6 animals. ***, $p < 0.001$, two-way ANOVA. cn, control; gcl, ganglion cell layer; inl, inner nuclear layer; ko, knock-out; onl, outer nuclear layer; P, postnatal day; PNA, peanut agglutinin. Scale bar: 100 μ m.

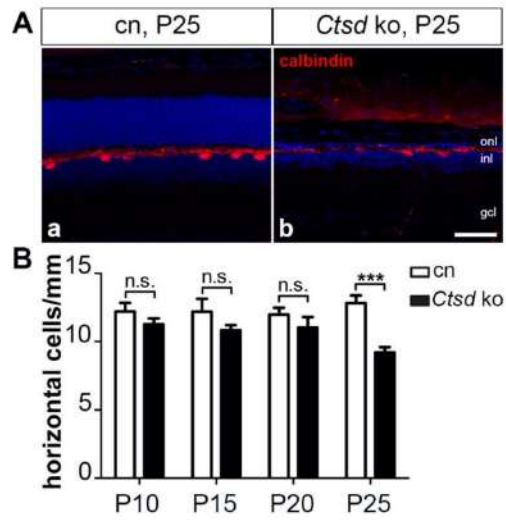


Figure S5. Degeneration of horizontal cells. A) The density of calbindin-positive horizontal cells was markedly decreased in *Ctsd* ko retinas at P25 when compared to age-matched control retinas. B) Quantitative analyses revealed that the number of horizontal cells was similar in mutant (filled bars) and control retinas (open bars) until P20, but significantly reduced in *Ctsd* ko retinas at P25. Each bar in (B) represents the mean value (\pm SEM) of 6 animals. n.s., not significant; ***, $p < 0.001$, two-way ANOVA. cn, control; gcl, ganglion cell layer; inl, inner nuclear layer; ko, knock-out; onl, outer nuclear layer; P, postnatal day. Scale bar: 100 μ m.



Experimentelle Therapieansätze für die Behandlung retinaler Dystrophien bei neuronalen Ceroid-Lipofuszinosen

Die neuronalen Ceroid-Lipofuszinosen (NCLs) sind eine Gruppe von seltenen lysosomalen Speicherkrankungen, die durch eine progrediente Neurodegeneration im Gehirn und der Netzhaut charakterisiert sind. Bei der CLN2-Krankheit konnte durch eine inzwischen zugelassene Enzymersatztherapie am Gehirn das Fortschreiten der neurologischen Symptome verzögert werden. Behandlungsmöglichkeiten für die retinalen Dystrophien bei NCL-Patienten existieren dagegen bisher nicht. In diesem Beitrag werden präklinische Studien zusammengefasst, in denen Behandlungsmöglichkeiten für die retinalen Dystrophien bei verschiedenen NCL-Formen untersucht wurden.

Ein fortschreitender Sehverlust aufgrund einer retinalen Degeneration gehört zu den charakteristischen klinischen Symptomen bei fast allen der 13 genetisch distinkten Formen der neuronalen Ceroid-Lipofuszinose (NCL; s. Beitrag von Atiskova et al.). Die häufige Beteiligung der Netzhaut zusammen mit der Identifizierung von Patienten mit nichtsyndromalen Netzhautdystrophien bei bestimmten NCL-Formen zeigt, dass die Retina besonders empfindlich auf lysosomale Dysfunktionen reagiert. Bisher existieren keine Behandlungsmöglichkeiten für diese retinalen Dystrophien. Für NCL-Formen, die durch Dysfunktionen lysosomaler Enzyme verursacht werden,

stellen Enzymersatzstrategien eine vielversprechende Therapieoption dar. Für NCL-Formen, die durch Dysfunktionen transmembraner Proteine in Lysosomen oder dem endoplasmatischen Retikulum verursacht werden, stellt der Aufbau von möglichen Therapien eine ungleich größere Herausforderung dar. In zahlreichen Studien an Tiermodellen für verschiedene NCL-Formen werden Therapiemöglichkeiten entwickelt, um die Neurodegeneration im Gehirn zu verlangsamen oder aufzuhalten. Für eine dieser fatalen Erkrankungen – die CLN2-Krankheit – konnten in einer klinischen Studie mit einer Enzymersatztherapie am Gehirn der Patienten signifikante Therapieerfolge erzielt werden. Bisher verfügbare Daten zeigen jedoch, dass spezifisch für das Gehirn etablierte Therapiestrategien keinen therapeutischen Effekt auf die Netzhaut haben. Es ist daher erforderlich, spezifische Behandlungsmöglichkeiten für das Auge zu etablieren. In diesem Beitrag geben wir eine Übersicht über präklinische Arbeiten, in denen die Effektivität verschiedener Therapiestrategien für die Behandlung retinaler Dystrophien an Tiermodellen für die CLN1-, CLN2-, CLN6- und CLN10-Krankheit untersucht wurde (siehe **Tab. 1**).

Tiermodelle für neuronale Ceroid-Lipofuszinosen

Die neuronale Ceroid-Lipofuszinose wird in 13 genetisch distinkte Erkrankungen unterteilt, bei denen es aufgrund

lysosomaler Dysfunktionen zu einer intrazellulären Ansammlung von autofluoreszierendem Speichermaterial und einer Neurodegeneration im Gehirn und in der Netzhaut kommt. Je nach NCL-Form entwickeln sich schwere neurologische Symptome in unterschiedlicher Abfolge, und betroffene Patienten versterben vorzeitig an diesen fatalen Erkrankungen [1, 14]. Für die verschiedenen NCL-Formen existieren spontan entstandene oder transgene Tiermodelle wie Mäuse, Zebrafische, Hunde oder Schafe, die viele charakteristische Krankheitsmerkmale der jeweiligen Erkrankungen rekapitulieren [4, 7]. Diese Tiermodelle werden genutzt, um die Pathophysiologie der Erkrankungen aufzuklären und um Therapiestrategien zu etablieren. So wurden an diesen Tiermodellen in den letzten Jahren verschiedene Therapiestrategien für die Behandlung der Neurodegeneration im Gehirn (z. B. Enzymersatztherapie, Gentherapie, Stammzelltherapie oder Small-molecule-Therapie) mit zum Teil beeindruckenden Erfolgen entwickelt [11, 14].

Am Gehirn eines Hundemodells für die CLN2-Krankheit, die durch Dysfunktionen des lysosomalen Enzyms Tripeptidyl-Peptidase 1 (TPP1) verursacht wird, wurde beispielsweise die Effektivität einer Enzymersatztherapie gezeigt. Durch 2-wöchentliche Infusionen eines rekombinant hergestellten TPP1-Enzyms in die Zerebrospinalflüssigkeit konnte das Fortschreiten der Erkrankung deutlich verzögert und die Lebenserwartung der

Tab. 1 Experimentelle Therapieansätze für die Behandlung retinaler Dystrophien an Tiermodellen für NCL (neuronalen Ceroid-Lipofuszinosen)-Erkrankungen

Erkrankung	Protein	Tiermodell	Therapiestrategie	Therapieeffekt	Literatur
CLN1	PPT1	Maus („knock-out“)	Intravitreale Injektionen von AAV-PPT1	Verbesserte retinale Funktion (ERG)	Griffey et al. [8]
CLN2	TPP1	Hund (spontane Mutation)	Intravitreale Injektionen von autologen MSCs mit einer Überexpression von TPP1	Verbesserte retinale Funktion (ERG), Verzögerung der retinalen Degeneration	Tracy et al. [21]
CLN2	TPP1	Hund (spontane Mutation)	Intravitreale Injektionen von rekombinantem TPP1	Verbesserte retinale Funktion (ERG), Verzögerung der retinalen Degeneration	Whiting et al. [23, 24]
CLN6	CLN6	Maus (spontane Mutation)	Intravitreale Injektionen von NSCs mit einer Überexpression von CNTF	Verbesserte Überlebensrate der Photorezeptoren	Jankowiak et al. [10]
CLN6	CLN6	Maus (spontane Mutation)	Intravitreale Injektionen von AAV-CLN6	Verbesserte retinale Funktion (ERG), verbesserte Überlebensrate der Photorezeptoren und Bipolarzellen	Kleine Holthaus et al. [13]
CLN10	CTSD	Maus („knock-out“)	Intravitreale Injektionen von rekombinantem CTSD	Partielle Korrektur der Dysregulation von lysosomalen Proteinen, abgeschwächte reaktive Mikroglie	Marques et al. [15]

AAV adenoassoziierter Virus, CNTF „ciliary neurotrophic factor“, CTSD Cathepsin D, ERG Elektroretinogramm, MSCs mesenchymale Stammzellen, NSCs neurale Stammzellen, PPT1 Palmitoyl-Protein Thioesterase 1, TPP1 Tripeptidyl-Peptidase 1

Tiere signifikant verlängert werden [12]. Bemerkenswerterweise wurde dieser auf das Gehirn ausgerichtete Therapieansatz in einer kürzlich publizierten klinischen Studie erfolgreich an CLN2-Patienten angewandt [19]. Eindrucksvolle Therapieeffekte konnten auch an einem Mausmodell für die CLN10-Krankheit erzielt werden, die durch Dysfunktionen des lysosomalen Enzyms Cathepsin D (CTSD) verursacht wird. Durch einen adenoassozierten Virus(AAV)-Vektorvermittelten *Ctsd*-Gentransfer in das Gehirn einer *Ctsd*-Knock-out(ko)-Maus konnten die neuropathologischen Veränderungen deutlich abgeschwächt und die Lebensspanne der Tiere signifikant verlängert werden [20]. Allerdings konnten trotz dieser Behandlungserfolge mit den am Gehirn angewandten Enzyersatzstrategien weder bei CLN2-Patienten noch im CLN2-Hundmodell oder in der *Ctsd*-ko-Maus positive Therapieeffekte in der Netzhaut nachgewiesen werden [20–22, 24].

» Die Netzhaut profitiert nicht von Therapiestrategien, die spezifisch am Gehirn angewendet werden

Diese Ergebnisse zeigen, dass für die Behandlung retinaler Dystrophien netz-

hautspezifische Therapiestrategien entwickelt werden müssen. Im Folgenden werden präklinische Arbeiten diskutiert, die die Effektivität verschiedener Therapiestrategien (Enzyersatzstrategien, Neuroprotektion und korrelative Genterapie) für die Behandlung retinaler Dystrophien an Tiermodellen für verschiedene NCL-Formen untersucht haben (Tab. 1). Die Rolle des Immunsystems und die Wirksamkeit immunmodulatorischer Therapieansätze für die Behandlung dieser Dystrophien werden in dem Beitrag von Verena Behnke und Thomas Langmann diskutiert.

Therapieansätze für NCL-Formen: dysfunktionale lysosomale Enzyme

Wie bereits für die CLN2- und die CLN10-Krankheit diskutiert, stellt das Einschleusen von funktionalen Enzymen in erkrankte Gewebe einen vielversprechenden Therapieansatz für NCL-Formen dar, die durch Dysfunktionen von lysosomalen Enzymen verursacht werden. Die Effektivität dieser Strategie beruht darauf, dass die Mannose-6-Phosphat(M6P)-modifizierten Enzyme von erkrankten Zellen über eine M6P-Rezeptor-vermittelte Endozytose aufgenommen und anschließend zu den Lysosomen transportiert werden können, wo sie dann die lysosomale Dys-

funktion korrigieren. Bei lysosomalen Speichererkrankungen mit überwiegend neurologischen Symptomen sind systemische Applikationen von funktionellen Enzymen in das erkrankte Nervengewebe aufgrund der Blut-Hirn-Schranke und der Blut-Retina-Schranke nicht möglich. Vielmehr müssen die Enzyme lokal appliziert werden. Dieses Ziel kann erreicht werden durch

- wiederholte Injektionen rekombinant hergestellter Enzyme,
- einen virusvermittelten Gentransfer oder
- Transplantationen von Zellen mit einer Überexpression des jeweiligen Enzyms.

Enzyersatzstrategie bei der CLN1-Krankheit: Genterapie

Die CLN1-Krankheit wird durch Mutationen im Gen verursacht, das für das lysosomale Enzym Palmitoyl-Protein Thioesterase 1 (PPT1) kodiert. Transgene Mausmodelle für diese NCL-Form entwickeln alle wesentlichen Krankheitsmerkmale, die auch CLN1-Patienten aufweisen. Dazu gehört eine fortschreitende retinale Degeneration. Wir haben kürzlich gezeigt, dass nahezu alle retinalen Nervenzelltypen in einer *Ppt1*-ko-Maus [9] vom Zelltod betroffen sind. So findet man im Spätstadium der Erkrankung einen signifikanten Verlust von Stäb-

Zusammenfassung · Abstract

chen- und Zapfenphotorezeptoren, von Stäbchen- und Zapfenbipolarzellen und von retinalen Ganglienzellen [2]. In diese Mausmutante haben Griffey et al. vor Beginn der retinalen Degeneration intravitreal einen für humanes PPT1 kodierenden AAV-Vektor (Serotyp 2; AAV2-PPT1) injiziert [8]. AAVs vom Serotyp 2 zeigen einen Tropismus für retinale Ganglienzellen. Entsprechend konnte in den behandelten Augen der *Ppt1*-ko-Mäuse in einem Großteil der Ganglienzellen eine starke Expression des Enzyms nachgewiesen werden. Bemerkenswerterweise war die enzymatische Aktivität von PPT1 in den behandelten *Ppt1*-ko-Netzhäuten sogar deutlich höher als in Netzhäuten gesunder Wildtypiere. Im Vergleich zu Kontrollaugen waren in den behandelten Augen die Antworten im skotopischen und photopischen Elektrotretinogramm signifikant verbessert. Eine signifikant verbesserte Überlebensrate der Photorezeptoren konnte jedoch nicht nachgewiesen werden, und mögliche Therapieeffekte auf andere retinale Nervenzelltypen wurden nicht untersucht. Zu den möglichen Gründen für diesen nur begrenzten Therapieerfolg gehören

- eine unzureichende Sezernierung des transgenen PPT1 durch die transduzierten Ganglienzellen und/oder
- eine unzureichende Verteilung des Enzyms in der *Ppt1*-ko-Retina [8].

Enzymersatzstrategie bei der CLN2-Krankheit: genetisch modifizierte Zellen und rekombinantes TPP1-Enzym

Wie oben diskutiert, verzögern repetitive Infusionen von rekombinantem humanem TPP1 in die Zerebrospinalflüssigkeit eines CLN2-Hundemodells das Auftreten der für diese Erkrankung charakteristischen schweren neurologischen Symptome [12]. Positive Effekte auf die Morphologie oder Funktion der Netzhaut konnten in den behandelten Tieren jedoch nicht nachgewiesen werden. Um die Effekte einer kontinuierlichen intraokulären Applikation des Enzyms auf die retinale Pathologie in diesem Tiermodell zu untersuchen,

Ophthalmologe <https://doi.org/10.1007/s00347-020-01237-9>
© Springer Medizin Verlag GmbH, ein Teil von Springer Nature 2020

S. Bartsch · J. Liu · M. Bassal · W. Jankowiak · M. S. Spitzer · U. Bartsch

Experimentelle Therapieansätze für die Behandlung retinaler Dystrophien bei neuronalen Ceroid-Lipofuszinosen

Zusammenfassung

Hintergrund. Neuronale Ceroid-Lipofuszinosen (NCLs) sind seltene neurodegenerative lysosomale Speichererkrankungen mit einem fatalen Verlauf. Eine fortschreitende retinale Degeneration und ein Visusverlust gehören zum typischen Krankheitsbild betroffener Patienten. Das Auftreten neurologischer Symptome bei CLN2-Patienten kann durch eine inzwischen zugelassene Enzymersatztherapie am Gehirn signifikant verzögert werden. Für die retinalen Dystrophien bei diesen Erkrankungen existieren dagegen gegenwärtig keine Behandlungsmöglichkeiten. **Ziel.** Der Beitrag soll einen Überblick über verschiedene präklinische Arbeiten geben, in denen Therapiestrategien für die Behandlung der retinalen Degeneration an Tiermodellen für verschiedene NCL-Formen entwickelt und evaluiert wurden.

Material und Methoden. Die wichtigsten Ergebnisse von Studien, in denen

therapeutische Effekte verschiedener Behandlungsstrategien auf die retinale Morphologie und/oder Funktion nachgewiesen werden konnten, wurden zusammengefasst und diskutiert.

Ergebnisse und Diskussion. Die bisher publizierten präklinischen Arbeiten zeigen, dass die retinale Degeneration und der damit verbundene Funktionsverlust in Tiermodellen für verschiedene NCL-Formen über unterschiedliche Therapiestrategien signifikant verzögert werden konnte. Es ist zu hoffen, dass die zum Teil beeindruckenden Therapieerfolge in zukünftigen klinischen Studien bestätigt werden können.

Schlüsselwörter

Enzymersatztherapie · Gentherapie · Neuroprotektion · Tiermodelle · Retinale Degeneration

Experimental therapeutic approaches for the treatment of retinal dystrophy in neuronal ceroid lipofuscinosis

Abstract

Background. Neuronal ceroid lipofuscinosis (NCL) is a group of rare and fatal neurodegenerative lysosomal storage diseases. Progressive retinal degeneration and loss of vision are among the characteristic symptoms of affected patients. A brain-directed enzyme replacement therapy has been shown to significantly attenuate the neurological symptoms in CLN2 patients and is currently the only approved therapy for NCL; however, there is presently no treatment option for retinal dystrophy in NCL.

Objective. This short review aims to give an overview of preclinical studies that have developed and evaluated therapeutic strategies for the treatment of retinal dystrophy in animal models of different NCL forms.

Material and methods. The key findings of preclinical studies that have achieved positive therapeutic effects on retinal structure and/or function using different treatment strategies are summarized and discussed.

Results and conclusion. The published data on preclinical studies demonstrate the efficacy of different therapeutic strategies to attenuate retinal degeneration and vision loss in animal models for different NCL forms. It remains to be seen whether these promising results can be confirmed in future clinical studies.

Keywords

Enzyme replacement therapy · Gene therapy · Neuroprotection · Animal models · Retinal degeneration

wurde humanes TPP1 in autologen mesenchymalen Stammzellen mittels AAV-Vektoren überexprimiert [21]. Durch eine einmalige intravitreale Injektion dieser modifizierten Stammzellen zu Beginn der retinalen Dystrophie konnte die Entstehung der normalerweise vor-

handenen lokal begrenzten Netzhautablösungen verhindert oder deutlich reduziert werden. Zudem war in Spätstadien der Erkrankung die Atrophie der Netzhautschichten in den behandelten Augen deutlich geringer ausgeprägt als in den Kontrollaugen. Schließlich konnte

über Elektretinogramm(ERG)-Ableitungen ein therapeutischer Effekt der zellbasierten kontinuierlichen intraokulären Applikation des Enzyms auf die retinale Funktion gezeigt werden [21]. Wie unten diskutiert (s. Abschn. „Neuroprotektion bei der CLN6-Krankheit“), ist es denkbar, zellbasierte Therapiestrategien für die Behandlung retinaler Erkrankungen in eine klinische Anwendung zu bringen.

In einer weiteren Studie wurde vor Beginn der retinalen Pathologie in immunsupprimierte TPP1-defiziente Hunde in Abständen von wenigen Wochen in 1 Auge intravitreal rekombinantes humanes TPP1 (rhTPP1) injiziert [23]. In die jeweils kontralateralen Augen wurde als Kontrolle die Vehikellösung injiziert. In den behandelten Augen war die normalerweise zu beobachtende fortschreitende Reduktion der ERG-Antworten erheblich verzögert. Außerdem konnte durch die Behandlung die Degeneration von Zellen in der inneren nukleären Schicht – nicht aber von Photorezeptoren – signifikant verzögert sowie die Ausbildung der lokal begrenzten Netzhautablösungen verhindert werden. Als Komplikation der intravitrealen rhTPP1-Injektionen wurden allerdings deutliche intraokuläre Entzündungen beobachtet [23]. Ähnliche Therapieeffekte wurden erzielt, wenn mit der Enzyersatztherapie erst nach Beginn der retinalen Pathologie begonnen wurde [24].

Enzyersatzstrategie bei der CLN10-Krankheit: rekombinantes CTSD-Enzym

Die *Ctsd*-ko-Maus ist ein Tiermodell für die CLN10-Krankheit, die aufgrund von schweren pathologischen Veränderungen im zentralen Nervensystem und in den inneren Organen lediglich eine Lebenserwartung von weniger als 4 Wochen hat [18]. Im Endstadium der Erkrankung am postnatalen Tag 25 sind die Photorezeptoren fast vollständig und andere retinale Zelltypen in einem erheblichen Umfang degeneriert (Abb. 1). Um die Effektivität einer Enzyersatztherapie für die Behandlung dieser massiven retinalen Degeneration zu untersuchen, wurde zu Beginn und

ein zweites Mal im Verlauf der retinalen Degeneration in 1 Auge intravitreal rekombinantes humanes CTSD (rhCTSD) injiziert. In das kontralaterale Auge wurde als Kontrolle die Vehikellösung injiziert [15]. Immunhistochemische Untersuchungen zeigten, dass das intravitreal injizierte Enzym in die Netzhaut diffundiert war und von verschiedenen retinalen Zelltypen aufgenommen wurde (Abb. 1). Interessanterweise war in den behandelten Augen im Vergleich zu den kontralateralen Kontrollaugen die Dysregulation verschiedener lysosomaler Proteine teilweise korrigiert und die reaktive Mikrogliose signifikant abgeschwächt (Abb. 1). Diese Daten zeigen, dass mit der Enzyersatztherapie die lysosomale Dysfunktion in der *Ctsd*-ko-Retina zumindest partiell korrigiert werden konnte. Eine signifikante Verzögerung der retinalen Degeneration war allerdings nicht nachweisbar [15].

» Enzyersatzstrategien sind vielversprechende Behandlungsmöglichkeiten für retinale Dystrophien

Ähnlich wie bei den Experimenten an dem CLN1-Mausmodell sind auch bei diesen Versuchen eine unzureichende Menge und/oder eine unzureichende Verteilung des Enzyms innerhalb der Netzhaut eine mögliche Erklärung für die begrenzten Therapieeffekte.

Therapieansätze für NCL-Formen: transmembrane Proteine

Wie oben diskutiert, beruht die Effektivität von Enzyersatzstrategien auf der Tatsache, dass erkrankte Zellen über eine M6P-Rezeptor-vermittelte Endozytose funktionale lysosomale Enzyme aus ihrer Umgebung aufnehmen und so die lysosomale Dysfunktion zumindest teilweise korrigieren können. Für diese kausalen Therapieansätze ist es daher „lediglich“ erforderlich, genügend funktionales Enzym in das erkrankte Gewebe einzuschleusen, z.B. durch einen virusvermittelten Gentransfer in – im Prin-

zip – beliebige Zelltypen innerhalb dieses Gewebes. Die Etablierung kausaler Therapiestrategien für die Behandlung von NCL-Formen, die durch Dysfunktionen von transmembranen Proteinen verursacht werden, stellt dagegen eine ungleich größere Herausforderung dar. Bei diesen NCL-Formen ist es nötig, z. B. über einen virusvermittelten Gentransfer möglichst viele der erkrankten Zellen so zu modifizieren, dass sie eine funktionale Variante des Proteins exprimieren. Um bei diesen NCL-Formen die Neurodegeneration im Gehirn zu verlangsamen oder aufzuhalten, werden auch hier in präklinischen Studien verschiedene Therapiestrategien verfolgt, von denen einige bereits in klinischen Studien evaluiert werden [11, 14, 17]. An der Netzhaut wurde für diese NCL-Formen das therapeutische Potenzial einer zellbasierten Neuroprotektion [10] und einer korrekiven Genterapie [13] untersucht (Tab. 1). Die Wirksamkeit beider Therapieansätze wurde an einem Mausmodell für die CLN6-Krankheit durchgeführt.

Neuroprotektion bei der CLN6-Krankheit

Neuroprotektive Therapieansätze haben zum Ziel, das Fortschreiten einer Neurodegeneration zu verlangsamen oder aufzuhalten. Es handelt sich zwar nicht um eine kausale Therapiestrategie, sie kann aber potenziell bei verschiedenen neurodegenerativen Erkrankungen unabhängig von der jeweiligen spezifischen Ursache angewandt werden. Die *nelf*-Maus ist ein Mausmodell für die CLN6-Krankheit mit einer spontan aufgetretenen Mutation im *Cln6*-Gen [5], das für ein transmembranes Protein im endoplasmatischen Retikulum mit noch unbekannter Funktion kodiert. Ähnlich wie bei CLN6-Patienten findet man bei dieser Mutante eine retinale Degeneration, die durch einen früh einsetzenden Verlust von Photorezeptoren und einen später einsetzenden Verlust von Bipolarzellen charakterisiert ist [3, 13, 16].

Um signifikante neuroprotektive Effekte in der Netzhaut zu erreichen, ist es aufgrund der kurzen Halbwertszeiten von neurotrophen Faktoren und der Blut-Retina-Schranke erforderlich, die Fakto-

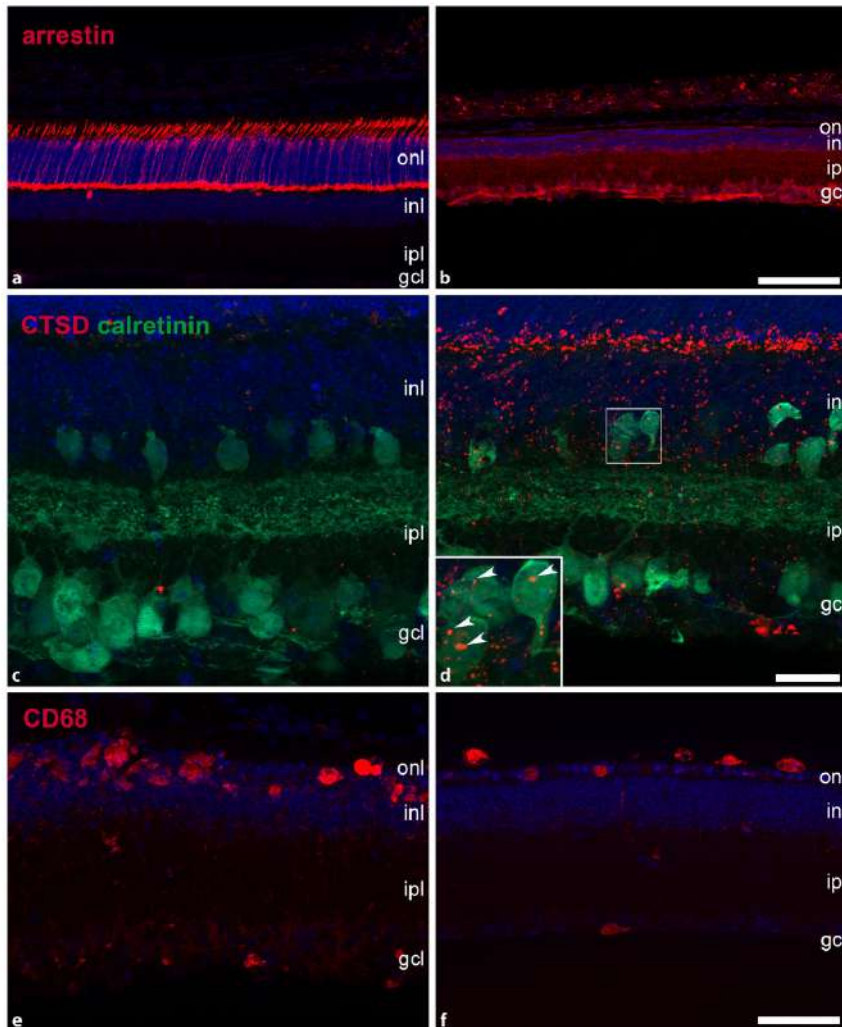


Abb. 1 ▲ Die *Ctsd*-ko-Maus ist ein Tiermodell für die CLN10-Krankheit mit einer extrem schnell fortschreitenden retinalen Degeneration. Im Endstadium der Erkrankung am postnatalen Tag 25 sind die äußere (*onl*) und innere nukleäre Schicht (*inl*) massiv atrophiert (**b**). Zapfen sind in diesem Alter nicht mehr nachweisbar (**b**). Zum Vergleich ist die Netzhaut einer altersgleichen gesunden Maus gezeigt (**a**). Nach intravitrealen Injektionen von rekombinatem humanen Cathepsin D findet man das Enzym in verschiedenen retinalen Zelltypen, wie beispielsweise Calretinin-positiven Amakrinzellen und Ganglienzellen (**d**). In unbehandelten Netzhäuten der *Ctsd*-ko-Maus ist CTSD wie erwartet nicht nachweisbar (**c**). Durch die intravitrealen Injektionen des Enzyms werden verschiedene pathologische Veränderungen in der *Ctsd*-ko-Retina abgemildert. So ist beispielsweise die Zahl von CD68-positiven Mikrogliazellen/Makrophagen in behandelten Netzhäuten (**f**) im Vergleich zu Kontrollnetzhäuten (**e**) signifikant reduziert. Ein signifikanter Effekt der Enzyersatztherapie auf die retinale Morphologie ist jedoch nicht nachweisbar (vergleiche **e** mit **f**). *CD68*, „cluster of differentiation 68“, *CTSD* Cathepsin D, *gcl* Ganglienzellschicht, *ipl* innere plexiforme Schicht, *ko* „knock-out“. Balken in **b** für **a** und **b**: 100 µm; in **d** für **c** und **d**: 25 µm; in **f** für **e** und **f**: 50 µm

ren kontinuierlich und lokal zu applizieren. Um dieses Ziel zu erreichen, wurden neurale Stammzelllinien mit einer stabilen Überexpression des neurotrophen Faktors „ciliary neurotrophic factor“ (CNTF) etabliert [10]. CNTF ist ein Zytokin, das eine ausgeprägte neuroprotektive Wirkung auf Photorezeptoren hat. Die CNTF exprimierenden Stammzellen wurden intravitreal in 1 Auge und Kontrollzellen in das kontralaterale Auge von *ncf*-Mutanten zu Beginn der retinalen Degeneration injiziert. Die Zellen überlebten für mindestens 6 Wochen, exprimierten stabil den neurotrophen Faktor und bewirkten eine signifikante Verzögerung der Photorezeptordegeneration. Allerdings wurde die Degeneration der Photorezeptoren nur verlangsamt, nicht aber aufgehalten [10]. Prinzipiell können zellbasierte neuroprotektive Therapieansätze in die Klinik gebracht werden. So wird das therapeutische Potenzial von intravitreal implantierten CNTF überexprimierenden Zellen mittels der sog. „encapsulated cell technology“ bei Patienten mit makulärer Teleangiectasie Typ 2 [6] oder Glaukom (www.clinicaltrials.gov, NCT02862938) untersucht.

Korrektive Gentherapie bei der CLN6-Krankheit

An der Netzhaut der *ncf*-Maus wurde außerdem das therapeutische Potenzial einer korrektiven Gentherapie untersucht. Überraschenderweise konnte durch eine AAV-Vektor-vermittelte Expression von humanem CLN6 spezifisch in Photorezeptoren weder die fortschreitende Degeneration der Photorezeptoren noch die fortschreitende Verschlechterung der retinalen Funktion verzögert oder aufgehalten werden [13]. Basierend auf der Beobachtung, dass Bipolarzellen eine hohe Expression von CLN6 aufweisen, wurde das Protein außerdem mittels AAV-Vektoren unter Kontrolle geeigneter Promotoren spezifisch in diesen Interneuronen exprimiert. Obwohl Bipolarzellen in der *ncf*-Netzhaut deutlich später als Photorezeptoren degenerieren, resultierte die bipolarzellspezifische Expression von CLN6 in einer signifikant verbesserten Überlebensrate der Photorezeptoren

und in signifikant verbesserten Antworten in skotopischen ERGs [13]. Außerdem wurde in den behandelten Netzhäuten eine deutlich verzögerte Degeneration der Bipolarzellen selber beobachtet [13]. Insgesamt deuten diese Daten an, dass Defekte in Bipolarzellen die Ursache für die Photorezeptordegeneration in der *ncf*-Netzhaut sind. Die Daten zeigen zudem, dass eine korrektive Gentherapie ein vielversprechender Therapieansatz ist, um Behandlungen für retinale Degenerationen bei NCL-Formen zu entwickeln, die durch Dysfunktionen transmembraner Proteine verursacht werden.

Fazit für die Praxis

- Eine fortschreitende retinale Degeneration ist ein charakteristisches Symptom der meisten NCL (neuronalen Ceroid-Lipofuszinosen)-Formen.
- Wirksame Behandlungsmöglichkeiten für diese retinalen Dystrophien existieren bisher nicht.
- Es werden verschiedene Therapiestrategien verfolgt, um den Verlauf der Neurodegeneration im Gehirn abzumildern. Bei CLN2-Patienten ist man inzwischen in der Lage, das Fortschreiten des neurologischen Krankheitsbildes durch eine zugelassene Enzymersatztherapie zu verzögern.
- Es ist zu hoffen, dass in verschiedenen, aktuell laufenden klinischen Therapiestudien am Gehirn ähnliche Erfolge bei anderen NCL-Formen erzielt werden können.
- Eine retinale Degeneration ist bei einigen NCL-Formen das Initialsymptom, und NCL-Patienten können in seltenen Fällen nichtsyndromale Netzhautdystrophien aufweisen.
- Insgesamt erscheint damit ein Aufbau retinaspezifischer Behandlungsmöglichkeiten für verschiedene NCL-Formen nicht nur sinnvoll, sondern dringend erforderlich.

Korrespondenzadresse



Prof. Dr. Udo Bartsch
Klinik und Poliklinik für
Augenheilkunde, Experimentelle
Ophthalmologie,
Universitätsklinikum
Hamburg-Eppendorf
Martinistr. 52, 20246 Hamburg,
Deutschland
ubartsch@uke.de

Einhaltung ethischer Richtlinien

Interessenkonflikt. S. Bartsch, J. Liu, M. Bassal, W. Jankowiak, M.S. Spitzer und U. Bartsch geben an, dass kein Interessenkonflikt besteht.

Für diesen Beitrag wurden von den Autoren keine Studien an Menschen oder Tieren durchgeführt. Für die aufgeführten Studien gelten die jeweils dort angegebenen ethischen Richtlinien.

Literatur

1. Anderson GW, Goebel HH, Simonati A (2013) Human pathology in NCL. *Biochim Biophys Acta* 1832:1807–1826
2. Atiskova Y, Bartsch S, Danyukova T et al (2019) Mice deficient in the lysosomal enzyme palmitoyl-protein thioesterase 1 (PPT1) display a complex retinal phenotype. *Sci Rep* 9:14185
3. Bartsch U, Galliciotti G, Jofre GF et al (2013) Apoptotic photoreceptor loss and altered expression of lysosomal proteins in the *ncf* mouse model of neuronal ceroid lipofuscinosis. *Invest Ophthalmol Vis Sci* 54:6952–6959
4. Bond M, Holthaus SM, Tammen I et al (2013) Use of model organisms for the study of neuronal ceroid lipofuscinosis. *Biochim Biophys Acta* 1832:1842–1865
5. Bronson RT, Donahue LR, Johnson KR et al (1998) Neuronal ceroid lipofuscinosis (*ncf*), a new disorder of the mouse linked to chromosome 9. *Am J Med Genet* 77:289–297
6. Chew EY, Clemons TE, Jaffe GJ et al (2019) Effect of ciliary neurotrophic factor on retinal neurodegeneration in patients with macular telangiectasia type 2: a randomized clinical trial. *Ophthalmology* 126:540–549
7. Faller KM, Gutierrez-Quintana R, Mohammed A et al (2015) The neuronal ceroid lipofuscinoses: opportunities from model systems. *Biochim Biophys Acta* 1852:2267–2278
8. Griffey M, Macauley SL, Oglivie JM et al (2005) AAV2-mediated ocular gene therapy for infantile neuronal ceroid lipofuscinosis. *Mol Ther* 12:413–421
9. Gupta P, Soyombo AA, Atashband A et al (2001) Disruption of PPT1 or PPT2 causes neuronal ceroid lipofuscinosis in knockout mice. *Proc Natl Acad Sci U S A* 98:13566–13571
10. Jankowiak W, Kruszewski K, Flachsbarth K et al (2015) Sustained neural stem cell-based intraocular delivery of CNTF attenuates photoreceptor loss in the *ncf* mouse model of neuronal ceroid lipofuscinosis. *PLoS ONE* 10:e127204

-
11. Johnson TB, Cain JT, White KA et al (2019) Therapeutic landscape for Batten disease: current treatments and future prospects. *Nat Rev Neurol* 15:161–178
 12. Katz ML, Coates JR, Sibigroth CM et al (2014) Enzyme replacement therapy attenuates disease progression in a canine model of late-infantile neuronal ceroid lipofuscinosis (CLN2 disease). *J Neurosci Res* 92:1591–1598
 13. Kleine Holthaus SM, Ribeiro J, Abelleira-Hervas L et al (2018) Prevention of photoreceptor cell loss in a CLN6(ncf) mouse model of batten disease requires CLN6 gene transfer to bipolar cells. *Mol Ther* 26:1343–1353
 14. Kohlschütter A, Schulz A, Bartsch U et al (2019) Current and emerging treatment strategies for neuronal ceroid lipofuscinoses. *CNS Drugs* 33:315–325
 15. Marques ARA, Di Spiezio A, Thiessen N et al (2019) Enzyme replacement therapy with recombinant pro-CTSD (cathepsin D) corrects defective proteolysis and autophagy in neuronal ceroid lipofuscinosis. *Autophagy*. <https://doi.org/10.1080/15548627.2019.1637200>
 16. Mirza M, Volz C, Karlstetter M et al (2013) Progressive retinal degeneration and glial activation in the CLN6 (ncf) mouse model of neuronal ceroid lipofuscinosis: a beneficial effect of DHA and curcumin supplementation. *PlosOne* 8:e75963
 17. Mole SE, Anderson G, Band HA et al (2019) Clinical challenges and future therapeutic approaches for neuronal ceroid lipofuscinosis. *Lancet Neurol* 18:107–116
 18. Saftig P, Hetman M, Schmahl W et al (1995) Mice deficient for the lysosomal proteinase cathepsin D exhibit progressive atrophy of the intestinal mucosa and profound destruction of lymphoid cells. *EMBO J* 14:3599–3608
 19. Schulz A, Ajayi T, Specchio N et al (2018) Study of Intravitreal cerliponase alfa for CLN2 disease. *N Engl J Med* 378:1898–1907
 20. Shevtsova Z, Garrido M, Weishaupt J et al (2010) CNS-expressed cathepsin D prevents lymphopenia in a murine model of congenital neuronal ceroid lipofuscinosis. *Am J Pathol* 177:271–279
 21. Tracy CJ, Whiting RE, Pearce JW et al (2016) Intravitreal implantation of TPP1-transduced stem cells delays retinal degeneration in canine CLN2 neuronal ceroid lipofuscinosis. *Exp Eye Res* 152:77–87
 22. Whiting RE, Narfstrom K, Yao G et al (2014) Enzyme replacement therapy delays pupillary light reflex deficits in a canine model of late infantile neuronal ceroid lipofuscinosis. *Exp Eye Res* 125:164–172
 23. Whiting REH, Pearce JW, Vansteenkiste DP et al (2020) Intravitreal enzyme replacement preserves retinal structure and function in canine CLN2 neuronal ceroid lipofuscinosis. *Exp Eye Res*. <https://doi.org/10.1016/j.exer.2020.108130>
 24. Whiting REH, Robinson GO, Ota-Kuroki J et al (2020) Intravitreal enzyme replacement inhibits progression of retinal degeneration in canine CLN2 neuronal ceroid lipofuscinosis. *Exp Eye Res*. <https://doi.org/10.1016/j.exer.2020.108135>

11 Declaration of personal contribution to the thesis and publications

11.1 Personal contribution in the main project of the thesis:

Title: Comparative evaluation of the efficacy of two enzyme replacement strategies for the treatment of the retinal dystrophy in a mouse model of CLN10 disease.

Description of personal contribution:

Tissue preparation, neural stem cell culture, primary retinal culture, immunocytochemistry, immunohistochemistry, western blot, immunocytochemistry analysis, immunohistochemistry analysis, western blot analysis, fluorescence microscopy, figures preparation, statistic analysis, writing thesis and manuscript.

11.2 Personal contribution in Publication 1:

Title: Rapid and Progressive Loss of Multiple Retinal Cell Types in Cathepsin D-Deficient Mice—An Animal Model of CLN10 Disease.

Authors: Mahmoud Bassal,‡, Junling Liu,‡, Wanda Jankowiak, Paul Saftig and Udo Bartsch (‡ These authors contributed equally to this work).

Journal: Cells.

Publication status: published (2021)

Description of personal contribution:

Methodology, validation, investigation, writing—original draft preparation, writing—review and editing and funding acquisition.

11.3 Personal contribution in Publication 2:

Title: Experimentelle Therapieansätze für die Behandlung retinaler Dystrophien bei neuronalen Ceroid-Lipofuszinosen.

Authors: Susanne Bartsch, Junling Liu, Mahmoud Bassal, Wanda Jankowiak, Martin S. Spitzer, Udo Bartsch

Journal: Der Ophthalmologe

Publication status: published (2020)

Description of personal contribution:

Participated in data collection, figure preparation, and conceptualization of manuscript.

12 Acknowledgements

First of all, I would like to express my gratitude to my supervisor, Professor Dr. Udo Bartsch for giving me a chance to study in the lab. He always has the door of his office open, patiently listens to my questions and problems, gives me advice and encourages me, and helps me to solve scientific problems and private issues. Thank him for his great enthusiasm for science, letting me go from a person who knows nothing about scientific research to a person who is now full of interest in research and enjoys discovering and solving scientific problems.

I am also deeply indebted to my colleagues Stefanie Schlichting, Elke Becker, and Sabine Helbing for patiently teaching me all the experimental methods and for the excellent technical assistance on the present thesis. Thank Mahmoud Bassal who helped me with imaging and analysis.

For the successful collaborations, I would like to thank Dr. Ingke Braren for virus preparation, Alessandro Di Spiezio and Prof. Dr. Director Saftig Paul for enzyme activity assay, Ali Derin and Susanne Conrad for excellent animal care, and Prof. Stephan Storch for helping me solve western blot problems.

Special thanks should go to the China Scholarship Council offering me the opportunity and the scholarship for my doctoral study in Germany. In addition, I would like to thank the Chinese Embassy in Germany for giving me care and support during Corona time.

I would also like to thank Mr. Lei Chen and Mr. Ya Cao, for their kind support when I applied for my scholarship.

I am especially grateful for Mr. Jiang from TCM Shanghai, who gave me treasured support and encouragement, and helped me keep healthy.

I also appreciated Dr. Wanda Jankowiak who kindly helped me a lot in my private life especially during the time when I first came to Germany.

Many thanks to all my friends in China and Germany. I am very fortunate to have all of you these years. Our friendship makes me feel not alone no matter how far away we are.

I would like to offer my sincere thanks to Shen Zhou, whose songs always comfort and encourage me during the last years.

Finally, I would like to thank my beloved family for their loving considerations all through these years. They support me whenever needed regardless of the time difference and the distance between China and Germany, especially my mother who gives me endless love and company all the time.

13 Curriculum vitae

Lebenslauf wurde aus datenschutzrechtlichen Gründen entfernt.

14 Eidesstattliche Versicherung

Ich versichere ausdrücklich, dass ich die Arbeit selbständig und ohne fremde Hilfe verfasst, andere als die von mir angegebenen Quellen und Hilfsmittel nicht benutzt und die aus den benutzten Werken wörtlich oder inhaltlich entnommenen Stellen einzeln nach Ausgabe (Auflage und Jahr des Erscheinens), Band und Seite des benutzten Werkes kenntlich gemacht habe. Ferner versichere ich, dass ich die Dissertation bisher nicht einem Fachvertreter an einer anderen Hochschule zur Überprüfung vorgelegt oder mich anderweitig um Zulassung zur Promotion beworben habe.

Ich erkläre mich einverstanden, dass meine Dissertation vom Dekanat der Medizinischen Fakultät mit einer gängigen Software zur Erkennung von Plagiaten überprüft werden kann.

Hamburg, 23.06.2021

Place, Date

Junting Lin

Signature